FEB 0 1 1999

GRADUATE AERONAUTICAL LABORATORIES
CALIFORNIA INSTITUTE OF TECHNOLOGY

GALCIT Report FM 98-10

INTERACTION OF CHEMISTRY, TURBULENCE, AND SHOCK WAVES IN HYPERVELOCITY FLOW

G. V. Candler*, P. E. Dimotakis, H. G. Hornung, A. Leonard, D. I. Meiron, B. V. McKoy, D. I. Pullin, and B. Sturtevant

*University of Minnesota

19990209 048

Final Technical Report

Approved for public release; distribution is unlimited

Prepared for

AIR FORCE OFFICE OF SCIENTIFIC RESEARCH

110 Duncan Avenue, Suite B115, Bolling AFB DC 20332-0001

Firestone Flight Sciences Laboratory

Guggenheim Aeronautical Laboratory

Karman Laboratory of Fluid Mechanics and Jet Propulsion

DTIC QUALITY INSPECTED 2

Pasadena

REPORT DOCUMENTATION PAGE

AFRL-SR-BL-TR-99-

0029

Public reporting burden for this collection of information is estimated to average 1 hour per response, in gathering and maintaining the data needed, and completing and reviewing the collection of information collection of information, including suggestions for reducing this burden, to Washington Headquarters S Davis Highway, Suite 1204, Arlington, VA 22202-4302, and to the Office of Management and Budget, Pap

1. AGENCY USE ONLY (Leave blank)	2. REPORT DATE	3. REPORT TYPE AND DATES COVERED
	January 25, 1999	Final Technical Report

4. TITLE AND SUBTITLE
(U) Interaction of chemistry, turbulence, and shock waves in hypervelocity flow

5. FUNDING NUMBERS
PE - 61103D
PR - 3484
SA - AS
G - F49620-93-1-0338

6. AUTHOR(S)
G. Candler, P. Dimotakis, H. Hornung, A. Leonard, D. Meiron, B. V. McKoy, D. Pullin and B. Sturtevant
(Compiled by H. Hornung)

7. PERFORMING ORGANIZATION NAME(S) AND ADDRESS(ES)
California Institute of Technology
1200 E. California Blvd.
Pasadena, CA 91125

8. PERFORMING ORGANIZATION REPORT NUMBER
GALCIT FM 98-10

9. SPONSORING/MONITORING AGENCY NAME(S) AND ADDRESS(ES)
AFOSR/NA
110 Duncan Avenue, Suite B115
Bolling AFB DC 20332-0001

10. SPONSORING/MONITORING AGENCY REPORT NUMBER

11. SUPPLEMENTARY NOTES

12a. DISTRIBUTION/AVAILABILITY STATEMENT
Approved for public release; distribution is unlimited

12b. DISTRIBUTION CODE

13. ABSTRACT (Maximum 200 words)

Significant contributions were made in a four-year interdisciplinary experimental, numerical and theoretical program to extend the state of knowledge and understanding of the effects of chemical reactions in hypervelocity flows. The program addressed the key problems in aerothermochemistry that arise from the interaction between the three strongly nonlinear effects: Compressibility; vorticity; and chemistry. Results included:

- Discovery of dramatic damping effects of nonequilibrium vibration and chemistry on transition in hypervelocity flows
- Proper formulation of parameters for reacting blunt-body flows.
- Effects of nonequilibrium chemistry in shock-on-shock interaction
- New experiments on, and correlation with theory of high-enthalpy flap-induced separation
- Computations of interaction of a shock wave with density interfaces and with compressible Hill's spherical vortex
- Extensive clarification of phenomena in supersonic shear flows using new diagnostic and computational tools
- New experiments and computations of hypervelocity double-cone flow yielded insights into vibration-dissociation coupling
- First-principles computations of electron collision cross-sections with diatomic molecules and CO_2
- Development of new diagnostic technique LITA for accurate non-intrusive point measurement of gas properties.

14. SUBJECT TERMS	15. NUMBER OF PAGES
chemical reaction, shock wave, vorticity, hypervelocity, shock-vortex interaction, heat transfer gauges, laser scattering, laser-induced thermal acoustics, vibration-dissociation coupling.	89
	16. PRICE CODE

17. SECURITY CLASSIFICATION OF REPORT	18. SECURITY CLASSIFICATION OF THIS PAGE	19. SECURITY CLASSIFICATION OF ABSTRACT	20. LIMITATION OF ABSTRACT
Unclassified	Unclassified	Unclassified	UL

Contents

Background

At the outset of this report it is pertinent to quote three of the opening paragraphs of the proposal that led to the current URI Grant:

"Transport to or from space, aero-assisted orbital transfer operations and other hypervelocity flight maneuvers necessarily occur at such high (near orbital) speeds, that the bow-shock heating of the components of air causes them to be dissociated, to react with each other, and, at particularly high speeds, to be ionized. Efficient air-breathing propulsion of such high-speed vehicles also requires supersonic combustion of the fuel. To a large degree, these applications have motivated the interest in the field of study that has been named aerothermochemistry by von Karman.

The character of the dynamics of reacting gases is changed relative to perfect-gas dynamics in two important ways: First, the equilibrium behavior is much more complicated, and second, characteristic times are introduced by the fact that the reactions proceed at finite rates. These two types of highly nonlinear gas imperfections, interacting with the classical nonlinear manifestations of gasdynamics, namely shock waves and turbulence, produce many new flow structures and phenomena. Some of these are known and qualitatively understood, a few are quantitatively predictable by computation, all are of scientific, and most of practical importance to the operations listed above. The experimental data in this field are very limited, because of the difficulties associated with laboratory simulation. This constitutes the most important need in aerothermochemistry.

The proposed research work may be grouped under the following major headings:

supersonic turbulent mixing and combustion
effects of chemical reactions in external hypervelocity flows
reaction rate models

The philosophy of this proposal is to concentrate interdisciplinary effort on particular problems in the first two categories. The main thrust of the proposed research is to use the two new facilities (T5 hypervelocity shock tunnel and Supersonic Shear-Layer Facility) for an experimental program to study and understand the effects introduced by chemical reactions. A parallel theoretical and computational effort will help design the experiments and test models and mechanisms of the gas behavior. The third category pervades the whole program and represents research in theoretical and computational chemistry and fluid dynamics, as well as comparison with experiment."

The program was then subdivided into the following four parts

I. Reaction-rate controlled shear flows
II. Shock-vorticity interactions
III. Supersonic mixing and combustion
IV. Chemistry in non-uniform flow,

all of which involve complicated and non-linear interaction between *vorticity, chemistry* and *compressibility.* By focusing the available facilities and expertise on the main problems in the field, sub-projects were determined as shown in Fig. 1 together with the PI's and the main interactions between them.

A brief outline of the objectives was then formulated in the following statement of work. The numbering of these sub-projects corresponds to that of the sections in this report under which the progress is described in more detail.

Statement of Work

- I.1 Obtain qualitative information on the structure of transitional and turbulent boundary layers at high enthalpy. Determine the response of a laminar boundary layer to disturbances at the most strongly amplified frequency for the second mode instability. Perform T5 experiments on a sharp slender cone, using differential interferometry, laser-induced fluorescence and surface instruments.

- I.2 Design experiments for testing the limits of binary scaling by making a numerical study of blunt body flows in nitrogen and air. Carry out T5 experiments on spheres using surface instrumentation, differential interferometry and degenerate four-wave mixing (DFWM). Extend the experiments to study the high-vorticity layer downstream of a bow shock associated with the large density rise caused by dissociation.

- II.1 Perform ultra-high resolution numerical experiments combined with nonlinear analysis and numerics to establish appropriate initial conditions to elucidate the generic mechanisms of shock-vortex interactions, namely, (1) interaction of a shock with a vorticity field in the presence of nonequilibrium chemistry, and (2) vorticity generation in shock focusing with chemistry.

- II.2 Determine the effects of chemical relaxation on the shock-on-shock problem. Demonstrate the magnitude of nonequilibrium effects on shock impingement heating. Carry out experiments with a 2-dimensional model in T5, supported by local shock-polar analysis and numerical calculations of an ideal dissociating gas.

- III Carry out Supersonic Shear Layer experiments with chemically reacting and non-reacting flows, using schlieren, spectroscopy, Rayleigh scattering, chemical effects and new diagnostic methods, to gain understanding of the mechanisms of mixing when a shock interacts with a supersonic turbulent shear layer, and in the flow downstream of an expansion wave. Develop new related diagnostics and computational capabilities.

- IV.1 Design and carry out an experiment in T5 to provide data to test chemical reaction models for flows with vibrational nonequilibrium. Use a previously developed computational technique to simulate the flow over proposed experimental configurations. Identify a configuration that exhibits significant effects of vibrational nonequilibrium on the reaction rates.

- IV.2 Exploit computational methodologies and high-performance and cost-effective computing provided by highly parallel and scalable supercomputers to solve the complex equations which govern electron-molecule collision processes needed for robust modeling of the chemical and physical properties of hypervelocity flows.
- IV.3 Demonstrate the effect of chemistry on the leeward shock-vortex separation region of hypervelocity flow about slender bodies using high-resolution CFD on the Intel Touchstone-Delta computer, combined with dimensional analysis and physical scaling.
- V.2 Develop DFWM for measuring species concentration and temperature in hypervelocity flows. concentrate on NO-concentrations because of their importance in air flows. Buy the remaining equipment to complete the set of components, assemble the instrumentation, debug and apply it to T5 flows.

Layout

The following chapters present summaries of the results of the work, in the order shown above. Each subproject then lists the personnel, publications, transitions and interactions separately.

Chapter I: REACTION-RATE CONTROLLED SHEAR FLOW

I.1 TRANSITIONAL AND TURBULENT BOUNDARY LAYERS

Accomplishments

During the course of this sub-project, the experimental study of hypervelocity flow over a slender cone yielded the following main results:

1. Air and nitrogen flows up to reservoir specific enthalpies h_0 of 20 MJ/kg could be established in T5. Laminar, transitional and turbulent boundary layers and their demarcation could be visualized by resonantly enhanced interferometry and measured by surface heat flux records. These experiments extended the h_0 range of transition data from the previous highest value of 3 MJ/kg.

2. Evaluating the transition Reynolds number at the reference temperature T^* in the boundary layer, which is logically more meaningful than the edge Reynolds number in the context of transition, correlates the data in a plot against h_0. This relation shows a massive stabilizing effect of h_0, and a marked difference between air and nitrogen flows.

3. Further measurements in carbon dioxide show a strongly increased stabilizing effect of enthalpy, confirming that the damping is related to the influence of nonequilibrium processes in the boundary layer.

4. The carbon dioxide measurements were extended and further laminar boundary layer computations and comparisons with free-flight data were made.

5. New computations by Seipp (1997), a student of Candler, on the stability of chemically reacting boundary layers at the conditions of the T5 experiments confirmed the trends and provided valuable insight.

The main findings of the project are presented here with the aid of some plots. Fig. I.1 shows a plot of the transition Reynolds number evaluated at the reference condition for air flow over the 5° half–angle cone, including T5 measurements as well as data from the free–flight measurements reported by Wright and Zoby (1977). When these data are plotted in the form of transition Reynolds number evaluated at the boundary–layer edge conditions,

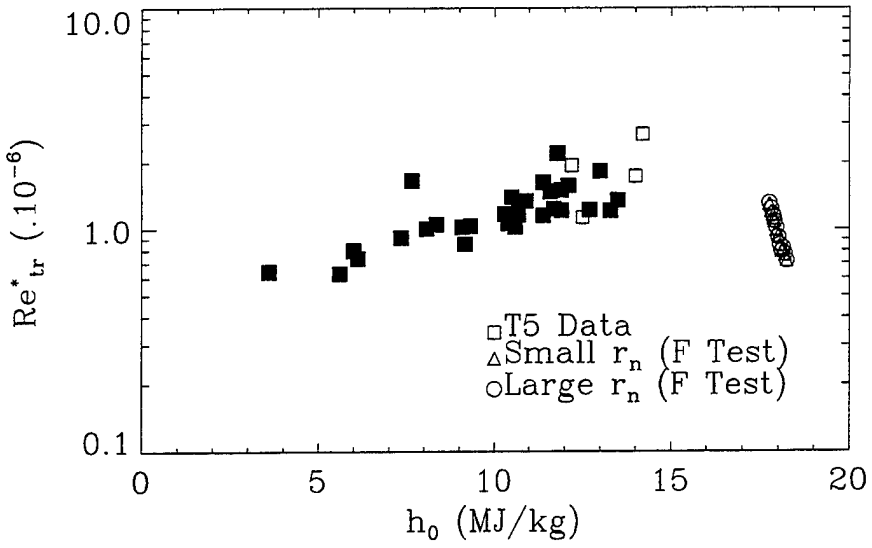

Figure I.1. Comparison of free flight reference transition Reynolds numbers and all T5 air data

the free–flight data give values approximately 50 times higher than the tunnel data. It is argued here, however, that the values of viscosity, density and sound speed that matter to the growth of instabilities in the boundary layer are not those at the edge of the boundary layer, but those within it. In the shock tunnel simulation, the temperature distribution in the inner part of the boundary layer is quite faithfully simulated, while the values at the edge temperatures differ by a factor of 4, see Fig. I.2.

Fig I.3 shows the T5–data on reference Reynolds number as measured in the three test gases. This brings out the dramatic departure of the CO_2 data from those in air and nitrogen. A further attempt at correlating the data in a dimensionless form is afforded by the BLIMPK computations which yield the maximum enthalpy in the boundary layer. Using this value to normalize the specific reservoir enthalpy, the fairly smooth correlation shown in Fig I.4 results.

In an attempt to check the T5 transition results from stability theory, Seipp (1997) made linear stability computations at the conditions of the experiments in air and nitrogen. These made the parallel flow assumption, but considered vibrational and chemical nonequilibrium. The results indicate that the most strongly amplified modes are the second (Mack) modes in the range 1–5 MHz, and that the stability does indeed increase with increasing h_0. In order to make a comparison with the experimental results Seipp made an e^N estimate of the transition Reynolds number using the results of the stability calculation. The results with $N = 10$ are shown in Fig I.5. While the computed results lie consistently above the experimental ones by a factor of about 3, the different trends in the two test gases are evidently confirmed. If N is chosen as 9, the results are almost congruent with the experimental data.

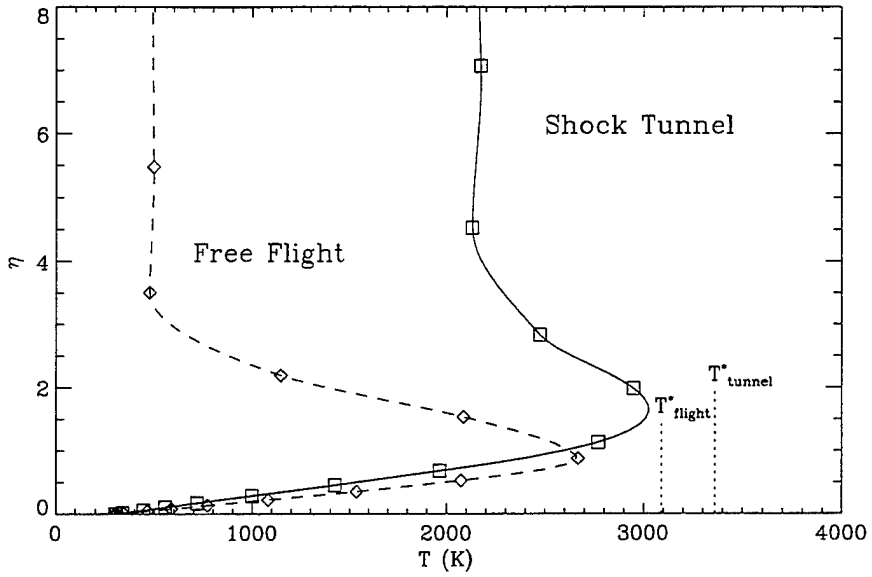

Figure I.2. Typical tunnel and flight boundary layer temperature profiles in boundary layer coordinates ($h_0 \approx 14$ MJ/kg). BLIMPK computations.

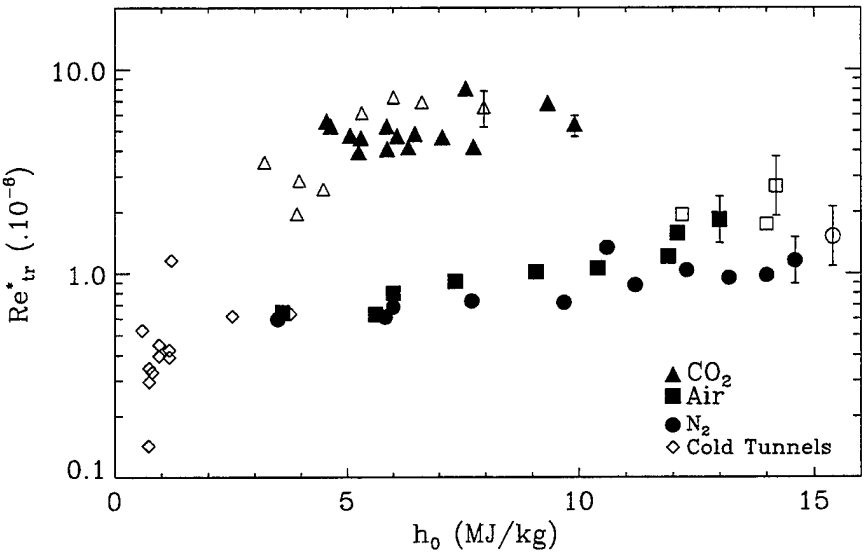

Figure I.3. Reference transition Reynolds number correlation with stagnation enthalpy. Open symbols indicate flows that were almost fully laminar with a hint of transition. Error bars are approximate measures of the error in Re^*_{tr}

.

This extensive study of high–enthalpy boundary layers and transition has yielded unique experimental data that have uncovered the previously unknown, important phenomenon of

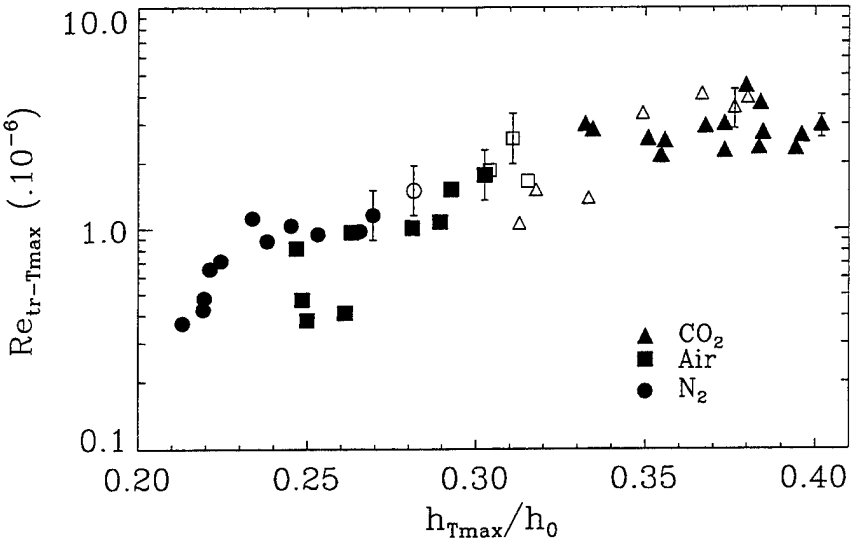

Figure I.4. Transition Reynolds number evaluated at reference conditions plotted versus normalized reservoir enthalpy.

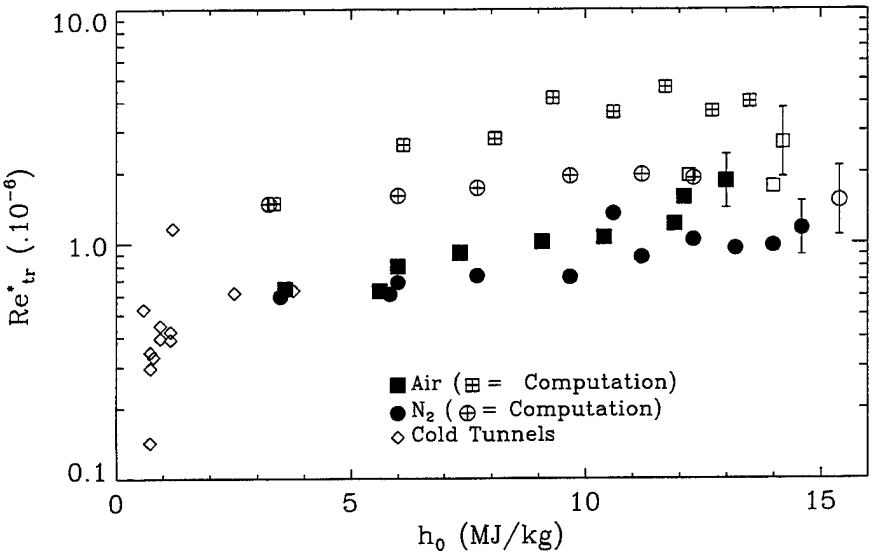

Figure I.5. Experimental and e^N reference transition Reynolds numbers. Calculations were performed by Seipp (1997) with a thermochemical nonequilibrium linear stability code and an e^N transition criterion.

the stabilizing effect of non–equilibrium phenomena in boundary layers. The obvious next step in the exploration of these phenomena is to perform stability experiments which will permit a more direct comparison with theory.

References

Seipp T. G., 1997, The Effect of Freestream Enthalpy on Hypersonic Boundary Layer Stability, M.Sc. thesis, Graduate School, University of Minnesota.

Wright R. L. and Zoby E. V., 1977, Flight boundary layer transition measurements on a slender cone at Mach 20. AIAA Paper 77-719.

Personnel Supported

1. Hans G. Hornung, Kelly Johnson Professor of Aeronautics, Director, GALCIT
2. Patrick Germain, Graduate Research Assistant, Ph.D graduation June 1994
3. Philippe Adam, Graduate Research Assistant, Ph.D. graduation June 1997
4. Bahram Valiferdowsi, Associate Engineer

Publications Resulting from Research

1. Hornung H. G., Cummings E. B., Germain P., Sanderson S. R., Sturtevant B., and Wen C.-Y. (1994) "Recent results from hypervelocity research in T5," AIAA 94-2523, Colorado Springs.
2. Hornung, H.G., Wen, C.Y. and Germain, P., "Hypervelocity Flow Simulation,", 1994, in *Mechanics USA 1994*, ed. A. S. Kobayashi, Appl. Mech. Rev. **47** pp. S14-S19.
3. Germain, P. and Hornung, H. G. "The boundary layer on a sharp cone in hypervelocity flow" in *Shock Waves @ Marseille*, ed. R. Brun, L. Z. Dumitrescu, Springer Verlag, 1995, pp. 63-68.
4. Germain, P. and Hornung, H. G. "Transition on a slender cone in hypervelocity flow", submitted to Phys. Fluids A.
5. Adam P. H. Enthalpy effects on hypervelocity boundary layers. Ph.D. thesis, California Institute of Technology.
6. Adam P. H. and Hornung H. G. Enthalpy effects on hypervelocity boundary–layer transition: Ground tests and flight data. J. Spacecraft and Rockets, Vol. 35, No. 5, 1997.
7. Adam P. H. and Hornung H. G. Hypervelocity boundary layers: transition normalization and enthalpy effects, 21st Int. Symp. on Shock Waves, 1997.

8. Adam P. H. and Hornung H. G. Enthalpy effects on hypervelocity boundary layer transition: experiments and free–flight data. AIAA Paper 97-0764.

Transitions, Interactions

AEDC high enthalpy facility, Dr. Jim Maus. H. G. Hornung, consultant.

Planning of T5 experiments for effects of ionization on transition and drag. Rockwell Science Center, Dr. N. Malmuth. H. G. Hornung, consultant.

Application of new operation of T5 operation and heat flux sensor technology, Raytheon, Mr. Leo Paradis.

Transfer of short-duration hydrogen injection technology to APRI, Dr. Tom Sobota.

Conference presentations at AIAA Reno 1993 1995 1997, AIAA Colorado Springs, Int'l Shock Wave Symposia at Marseille, Pasadena, and Great Keppel Island, Pacific International Conference on Aeronautical Science and Technology, Taiwan, US National Congress on Applied Mechanics, IUTAM Transition Conference Sendai, 4th Int'l Workshop on Shock Tube Technology.

Seminar presentations at Princeton University, University of Minnesota, University of Michigan, DLR Göttingen, Purdue University, Tohoku University, AEDC hypersonics workshop, University of Arizona, Mississippi State University.

New Discoveries, Inventions, Patents

None.

Honors/Awards

H. G. Hornung: ICAS von Karman Award for Int'l. Cooperation in Aeronautics
Scientific member of the Board of the DLR, Germany
Foreign member, Royal Swedish Academy for Engineering Sciences
Foreign Associate, National Academy of Engineering

I.2 NONEQUILIBRIUM AND VORTICITY DOWNSTREAM OF BOW SHOCKS

Accomplishments

In the course of this sub–project, the following main results have been obtained.

1. The theoretical framework of binary scaling for blunt–body flows and its limitations were formulated by using hypervelocity experiments and computation, see Wen and Hornung (1995).
2. The role of recombination reactions and the flow regimes and geometrical locations where they become important were determined, see Wen and Hornung (1993).
3. A new technique for visualizing streaklines in hypervelocity shock–tunnel flows was developed.
4. The instability of the shear-layer generated by a curved bow shock was demonstrated experimentally using the streak-line method and interferometry.

The main findings of this sub–project are illustrated here with some plots.

By considering the flow along the stagnation streamline of a blunt body,it was possible to find an expression for the shock stand–off distance in terms of two parameters: a generalized reaction rate parameter suitable for gases in which many reactions can occur, and the equilibrium density ratio. The analysis permits a closed solution to be obtained for the shock stand-off distance in two regimes: where the equilibrium density ratio does not influence the result, and where, therefore, binary scaling works,

$$\tilde{\Delta} = \frac{1}{\tilde{\Omega}} \left[-1 + \left(1 + 2L\tilde{\Omega} \right)^{\frac{1}{2}} \right] , \tag{1}$$

with $L = 0.41$ and $\tilde{\Delta} = \Delta\rho_\infty/\rho_s d$. At $\tilde{\Omega} = 0$, this goes to the correct limit L, as can be seen by expanding the square root. This is valid when the density at the stagnation point, $\rho_b < \rho_e$.

When $\rho_b = \rho_e$, binary scaling breaks down, and the appropriate formula is

$$\tilde{\Delta} = \frac{\rho_s}{\rho_e} \left[L + \frac{1}{2\tilde{\Omega}} \left(\frac{\rho_e}{\rho_s} - 1 \right)^2 \right] . \tag{2}$$

Again, this may be seen to have the correct limiting value $L\rho_s/\rho_e$ when $\tilde{\Omega} = \infty$. Equations 1 and 2 are plotted in Fig. I.6.

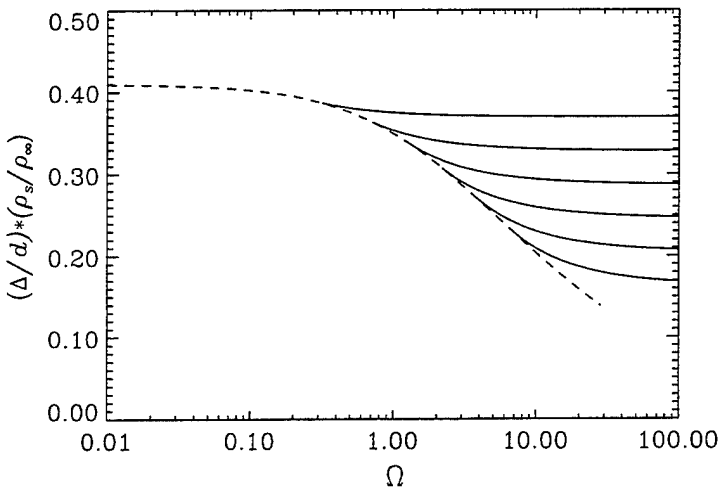

Figure I.6. Plot of equations 1 (dashed line), and 2 (full lines) for selected values of specific reservoir enthalpy h_0 resulting in values of ρ_s/ρ_e =0.4, 0.5, 0.6, 0.7, 0.8 and 0.9.

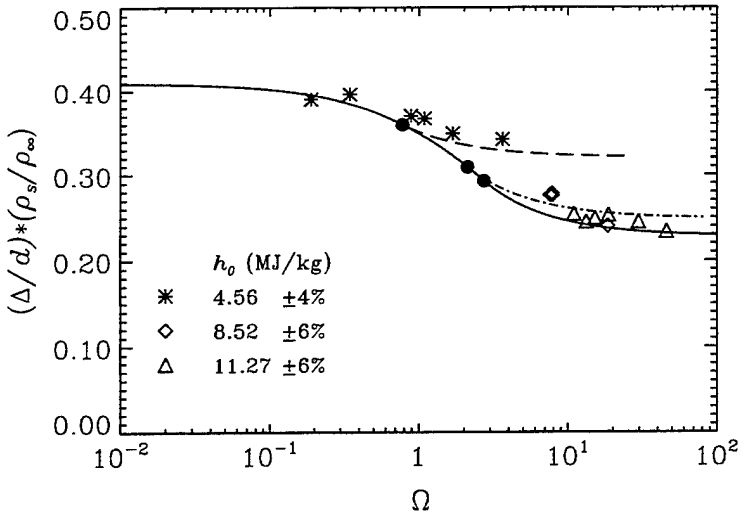

Figure I.7. Plot of equations 1 (dashed line), and 2 (full lines) for selected values of specific reservoir enthalpy h_0. The symbols represent experimental results for CO_2. The full circles are the junction points of equation 1 and equation 2. Note that the theory underestimates the stand-off distance slightly, consistently with the overestimate of the average density.

The theory is in good agreement with experimental results obtained over large ranges of enthalpy in different gases from differential interferograms, as well as with numerically computed flows (see Wen and Hornung, 1995). An example is shown in Fig I.7. The correlation in terms of these two parameters applies not only to the stand–off distance, but also to the other features of inviscid blunt–body flows.

In a second part of the project the instability of the shear layer generated by a curved bow shock was investigated. Computations were used to design a model (a cylindrically blunted wedge) with which a suitable curved shock wave was to be generated, in such a way as to optimize the chances of being able to observe instability of the high–vorticity layer and to distinguish it from boundary–layer vorticity. The model was constructed, and a first series of tests were conducted with it in T5. The measurements performed in the flow over the model included surface heat transfer and pressure distributions, holographic interferometry, and streakline visualization with a method developed further from that applied in the previous year.

The vorticity at a curved shock is given by

$$\omega = -U_\infty \kappa \cos\beta (1 - \rho_1/\rho_2)^2 \rho_2/\rho_1 \tag{1}$$

where ω is the vorticity, and U_∞, κ, and β are free–stream speed, shock curvature and shock angle, and the ρ's are densities before and after the shock. Thus it is easy to see that a convex shock will produce a maximum density between the normal–shock point and the asymptotic straight shock on a wedge, a cone or a blunt body. An example is shown in Fig. I.8 for the shock shape in the flow of Fig. I.9.

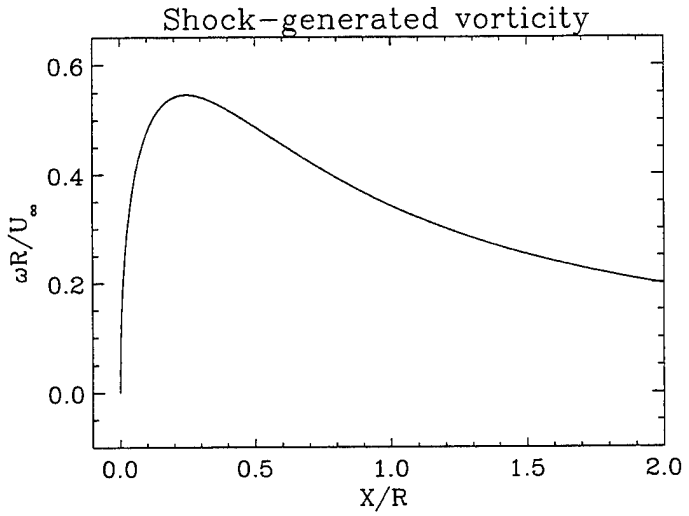

Figure I.8. Vorticity distribution along a shock of the shape obtained in the flow of Fig. I.9. Here, X is axial distance measured from the normal–shock point, and R is the radius of curvature of the shock at the normal shock point.

In two–dimensional flows the vorticity changes along a streamline in accordance with the product of density and temperature, which is approximately proportional to pressure. We impose the requirements that a vorticity maximum be achieved sufficiently far from the boundary layer to avoid confusion, and that a high value be maintained to a sufficiently

large downstream distance to give it a chance to become unstable. These requirements determine the model to be a wedge (pressure not decreasing to low value) with a sufficiently large bluntness radius to move the layer away from the boundary layer sufficiently, but a small enough radius to make κ large. Because the nose radius is therefore clearly a compromise, several different interchangeable noses were made.

An example of the use of the streakline visualization method is shown in Fig. I.9. The wire is painted with an aqueous solution of sodium chloride at discrete spots. The high–enthalpy flow causes the salt to ablate and dissociate so that atomic sodium is present in the wire wakes behind the spots. The picture is formed by transmitting a collimated beam of light through the flow, at a wavelength just slightly different from that at the center of one of the D–lines of sodium. Where sodium is present in the flow, this light is absorbed, so that a qualitative image of the sodium distribution is produced, which is therefore also an image of the streaks.

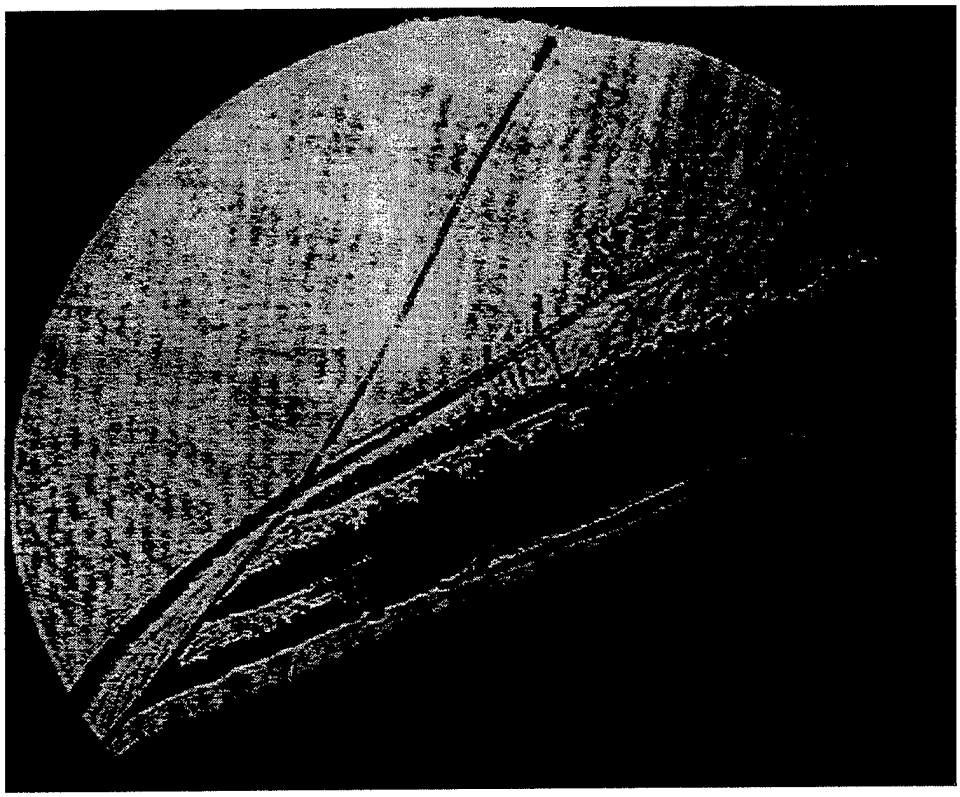

Figure I.9. Streakline visualization in the flow over the hemispherically blunted wedge, with oblique wire passing through the shock layer.

The picture shows that the central streak, which is approximately in the region of maximum vorticity, apparently develops an instability at a short distance downstream of the wire, while the other two streaks appear to be more stable. Though estimates of the eddy–shedding frequency of the wire indicate that the associated structure would be significantly finer than that observed, a control experiment with a sharp wedge, *i. e.* with zero vorticity, was

performed. This enabled us to distinguish effects caused by the wire in an irrotational shock layer from the effects of the vorticity in the shock layer. Placing the wire inside the shock layer is more successful than an arrangement with upstream wire, because the temperature and density in the shock layer are higher.

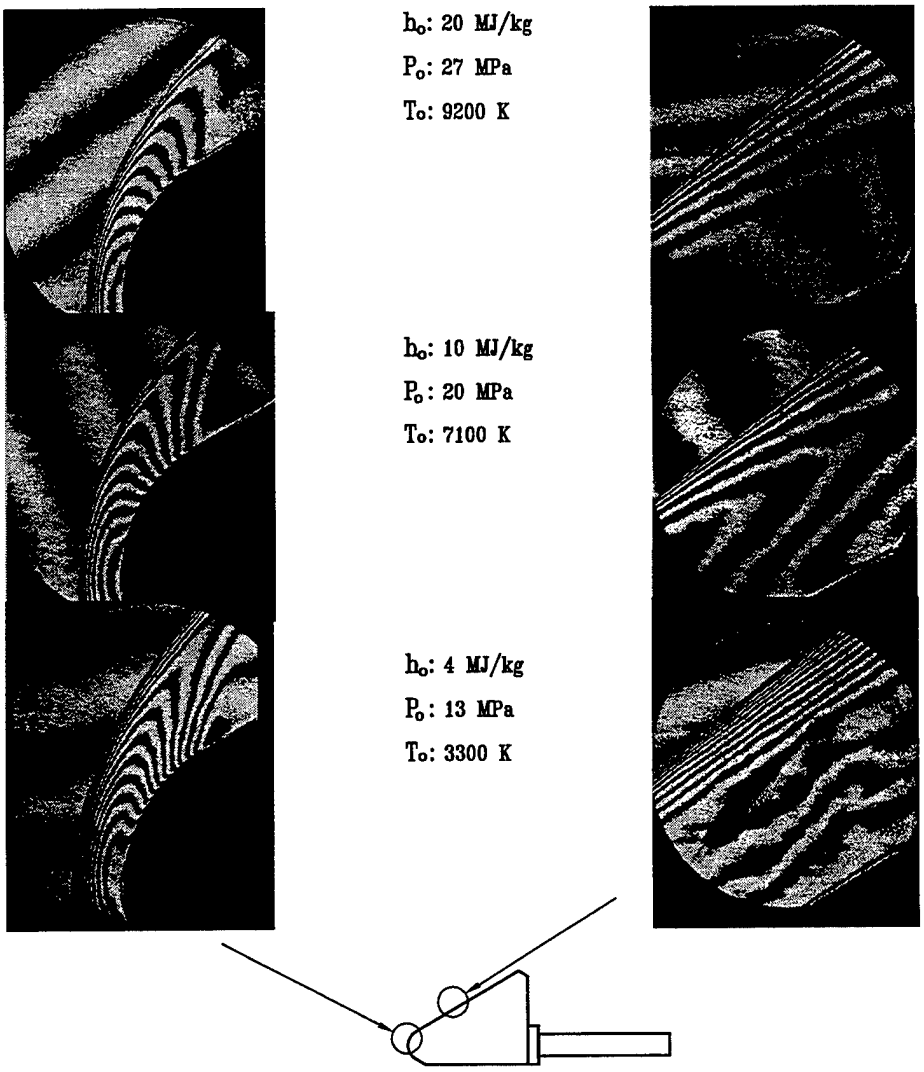

Figure I.10. Holographic interferograms of flow over hemispherically blunted wedge. The inset shows the locations of the photos relative to the model.

To supplement the streakline visualization, holographic interferometry was also applied to these flows. The field of view of the holographic interferometer is only 3 in. in diameter, so that the flow field on the large wedge can be covered only in several shots. Fig. I.10 shows three pairs of images taken at high, intermediate and low enthalpy. Each pair consists of one interferogram of the nose region, and one far downstream. In the downstream images, only the low enthalpy image shows any sign of instability. However, interferometry only shows features which manifest themselves in the density field, and integrate along the line of sight,

so that this visualization method is much less suitable for detecting shear layer instability than streak visualization. Nevertheless, the dramatic dependence of the fringe pattern at the downstream location on enthalpy, which may be understood in terms of the theoretical work of Hornung (1997), is of general interest and will be compared with computational interferograms in the near future.

References

Hornung H. G. 1997 Gradients at a curved shock in reacting flow. Shock Waves, **8** 11–21, 1998.

Personnel Supported

1. Hans G. Hornung, Kelly Johnson Professor of Aeronautics, Director, GALCIT
2. Patrick Lemieux, Graduate Research Assistant
3. Chih-yung Wen, Graduate Research Assistant, Ph. D. graduation June 1994
4. Bahram Valiferdowsi, Associate Engineer

Publications Resulting from Research

1. Wen C. Y. and Hornung H. G. 1993 Non–equilibrium recombination after a curved shock wave, Proceedings, 1st Pacific Int. Conf. Aerosp. Sc. and Techn., 639–646.
2. Wen C. Y. and Hornung H. G. 1995 Nonequilibrium dissociating flow over spheres. J. Fluid Mech. **299**, 389–405.
3. Lemieux P. and Hornung H. G. Visualizing the vorticity produced by curved shocks. 21st Int. Symp. on Shock Waves, 1997.
4. Hornung H. G. Curved shocks and chemical reactions. Paul Vieille Memorial Lecture, 21st Int. Symp. on Shock Waves, 1997.

Transitions, Interactions: See section I.1

New Discoveries, Inventions, Patents: None.

Honors, Awards: See section I.1

Chapter II: SHOCK-VORTICITY INTERACTION

II.1 NONEQUILIBRIUM CHEMISTRY IN SHOCK-VORTEX INTERACTION

II.1.1 Steady compressible vortex structures

Our approach to shock-vortex interactions required first the computation of steady compressible vortex solutions. These solutions are used as initial conditions to examine the shock-vortex interaction. The main idea is to continue to finite Mach number M_∞, well-known solutions of the incompressible Euler equations representing steady vortex states. This results in generic mathematical equations of the form

$$-\frac{1}{h_1 h_2 h_3 \rho}\left[\frac{\partial}{\partial x_1}\left(\frac{h_2}{h_1 h_3 \rho}\frac{\partial \psi}{\partial x_1}\right)+\frac{\partial}{\partial x_2}\left(\frac{h_1}{h_2 h_3 \rho}\frac{\partial \psi}{\partial x_2}\right)\right]=V(\psi), \tag{1}$$

$$\frac{M_\infty^2}{2}\left[\frac{1}{h_1^2}\left(\frac{\partial \psi}{\partial x_1}\right)^2+\frac{1}{h_2^2}\left(\frac{\partial \psi}{\partial x_2}\right)^2\right]+\frac{\rho^{\gamma+1}}{\gamma-1}=\rho^2 h_3^2 H(\psi). \tag{2}$$

being the vorticity and energy equations respectively, where ψ is the stream function, ρ is the density, $H = H_0 - \int_0^\psi V(\psi')d\psi'$ is the enthalpy and $V(\psi)$ is a function chosen to allow continuation from $M_\infty = 0$ and h_1, h_2, h_3 are scale-factors in generalized co-ordinates x_1, x_2, x_3. Several different flows were studied in detail. These are ;

1. Compressible hollow-core vortices (Ardalan *et al* 1995). These are a row of hollow-core, constant-pressure vortices. The basic equations were transformed from the physical plane to the hodograph plane, which results in a linear problem that was solved numerically. The numerical solution was checked via a Rayleigh-Janzen expansion. It was observed that for an appropriate choice of the parameters M_∞ and the speed ratio, $a = q_\infty/q_v$, where q_v is the speed on the vortex boundary, transonic shock-free flow exists. In the limit of an evacuated vortex core, we found that all such solutions exhibit cuspidal behavior corresponding to the onset of limit lines.

2. Compressible Hill's Spherical Vortex (CHSV, Moore & Pullin, 1998). These flows represent the continuation of the incompressible Hill's spherical-vortex along a branch representing homentropic flow at finite M_∞. In spherical coordinates r, θ this corresponds to the choice $V(\psi) = -15/2, \quad \psi < 0, \; V(\psi) = 0, \quad \psi > 0$. The flow is rotational for $r < 1$ and irrotational for $r > 1$. We solved the nonlinear PDE's using finite differences and by the Rayleigh-Jansen method. It was found that the vortex boundary, which is a sphere when $M = 0$ becomes a prolate spheroid elongated along

the direction of the free stream when $M > 0$. Also, the flow becomes sonic at the origin at $M_\infty = 0.589$ at which Mach number the branch terminates in a singularity. Thus we do not find transonic flow states for the CHSV.

3. Compressible Stuart (1967) vortices. These are compressible analogs of the classical incompressible solution first discussed by Stuart. The Stuart vortices can be continued to finite M_∞ using $V(\psi) = \exp(-2\psi)$. These solutions can be used as a model of the non-linear phase of a compressible shear layer. These structures were first investigated by Ardalan (1995) and subsequently by Moore *et al.* (1998).

II.1.2 Shock-vortex interaction

The successful use of statistical ensembles of HSV's to calculate the properties of homogeneous isotropic turbulence (Synge & Lin 1943) suggests the utility of the HSV as a model of a representative large eddy in turbulent flow in the context of a shock-vortex interaction. High resolution computations were performed on the Caltech *Paragon* of the impingement of a shock on a CHSV. A second-order Godunov Euler code was used with a grid of size 1536×768 (Samtaney & Pullin 1997). The shock moves initially along the vortex axis with the plane of the shock normal to this axis. The main parameters of interest were the strength of the incident shock (characterized by the non-dimensional pressure jump across the shock $p_{ratio}(p_0, p_1) = 1 - p_0/p_1$ where $p_0(p_1)$ is the pressure ahead (behind) the shock, and the Mach number at infinity for the CHSV, M_v. Several cases were studied including incident shocks with strengths $p_{ratio} = 0.19, 0.59, 0.95$.

A time sequence of greyscale images of $|\nabla\rho|$ of an axisymmetric shock-CHSV interaction is shown on the left of Fig. II.1, with $p_{ratio} = 0.59$, $M_v = 0.5$. The shock moves left to right. Time is scaled by the time t_s, which denotes the time taken by the shock to traverse the vortex in the axial direction and we set $t = 0$ as the time when the shock first strikes the vortex boundary. The shock diffracts as it interacts with the vortex, and we observe a distortion (bending) of the shock in a localized region. The shock within the vortex lags behind the incident shock front because the gas velocity in that part of vortex near the axis is in the opposite direction to the shock velocity. A complex structure is generated by the interaction characterized by a pair of triple points connected by a slip surface and the accompanying growth of a mach disc, a reflected shock and a near-conical slip line, or shear layer, bounding axial flow. This axial flow undergos an expansion that ends at a second shocklet disk embedded within the remnants of the vortex. The incident shock recovers its planar shape at a later time, leaving behind an asymmetrical vortex ring–like structure containing a weak shock.

The initial circulation in the CHSV is $\Gamma_0 = -6.147$. Fig. II.2 shows the total circulation $\Gamma(t)$ scaled by Γ_0, as a function of time scaled by t_s for shocks of varying strengths. For the relatively weaker shocks $\Gamma(t)$ remains nearly constant $t < 0$. For $t > 0$ we observe a rapid decrease in $|\Gamma(t)|$. The mechanisms via which the passage of the shock through the vortex either modifies the vorticity already present in the vortex, or creates additional vorticity can be understood from examination of the magnitude of the various terms in the

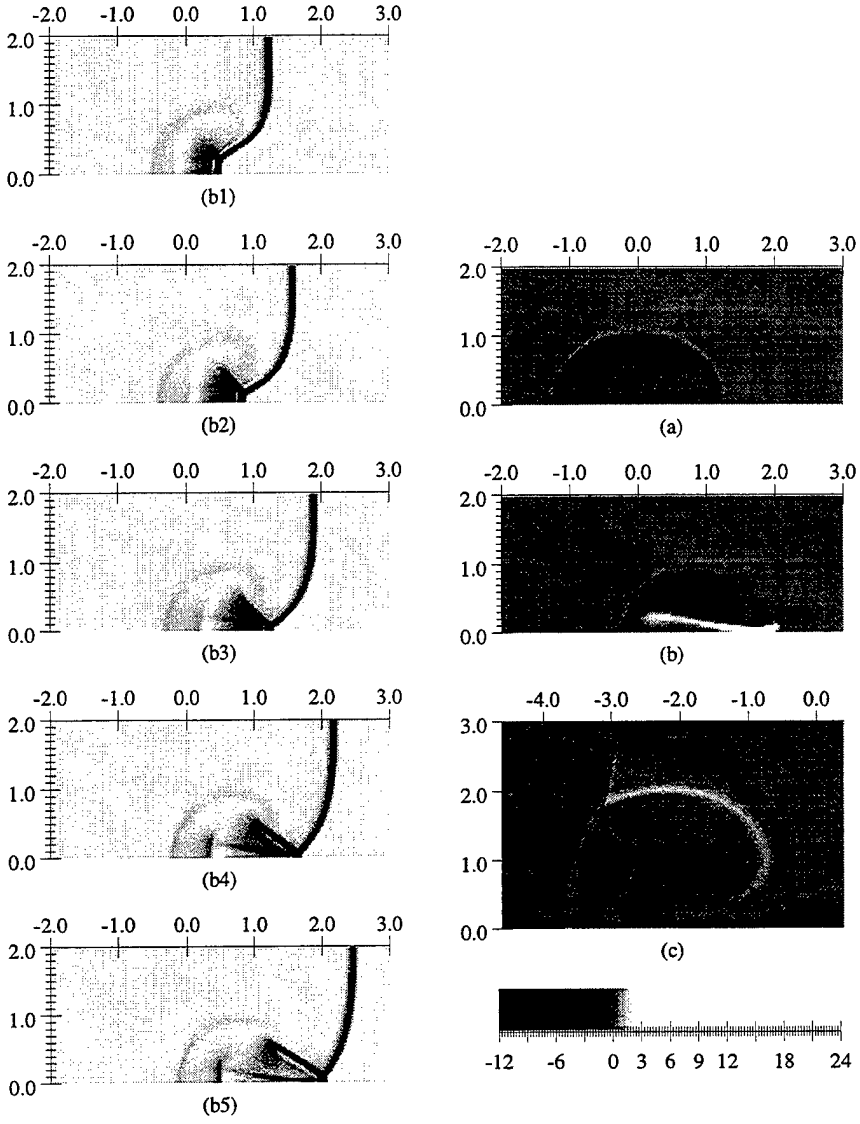

Figure II.1. Left; time sequence plots showing $|\nabla\rho|$ for a shock-CHSV interaction. Non-dimensional pressure ratio across the shock is $p_{ratio} = 0.59$. Times shown are (b1)$t/t_s = 1.00$, (b2)$t/t_s = 1.15$, (b3)$t/t_s = 1.27$, (b4)$t/t_s = 1.39$ and (b5) $t/t_s = 1.51$. Right; Vorticity distribution in the CSHV. (a) $t/t_s = -3.15$, (b) $t/t_s = 1.51$ for the case of the shock moving from left to right, and (c) $t/t_s = 1.66$ for the case of the shock moving from right to left.

vorticity equation. For $t < 0$, just before the shock reaches the boundary of the vortex it encounters a favorable density gradient which makes the baroclinic term in the vorticity equation negative. This leads to a slight increase in $|\Gamma(t)|$ (which is seen clearly for the strong shock case with $p_{ratio} = 0.95$). For $t > 0$, when the shock begins to move through the velocity field of the vortex, the baroclinic source term changes sign owing to a change in sign of the density gradient within the vortex. This leads to vorticity generation of opposite sign to that present in the CHSV. The net result is to decrease $\Gamma(t)$ inside the vortex. On the right of

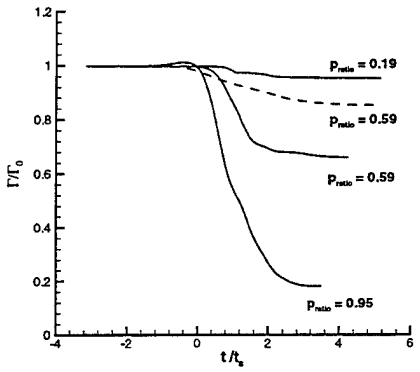

Figure II.2. Scaled circulation Γ/Γ_0 versus scaled time t/t_s. The dashed line is for a shock of strength $p_{ratio} = 0.59$ moving from right to left.

Fig. II.1 we plot the vorticity distribution at the start of the simulation and at a time after the shock-diffraction. The shocked vortex is asymmetric and exhibits a substantial increase in the maximum of the local vorticity magnitude, owing to the dilatational effect. The white layer clearly visible is the shear layer arising at the triple point. This also contains very strong vorticity of opposite sign to that initially present in the vortex leading to a further decrease in $\Gamma(t)$. Thus although $\Gamma(t)$ decreases, we would expect that the total enstrophy, or area integral of the square of the vorticity, would increase substantially as a result of the shock-vortex interaction.

II.1.3 Self-similar solutions of the compressible Euler equations

We have developed an iterative technique for computation of conically self-similar solutions of the two-dimensional unsteady Euler equations (Samtaney & Pullin, 1996, Samtaney 1997). The idea is to search for solutions to the Euler equations of the form

$$U(x,y,t) = (\rho(\xi,\eta), u(\xi,\eta), v(\xi,\eta), E(\xi,\eta)), \qquad \xi = x/t \qquad \eta = y/t. \tag{3}$$

Using this similarity transformation on the Euler equations leads to the nonlinear system

$$2\tilde{U} + \tilde{F}_\xi + \tilde{G}_\eta = 0, \tag{4}$$

where

$$\tilde{F} = \{\rho(u-\xi), \rho u(u-\xi) + p, \rho v(u-\xi), E(u-\xi) + pu\}^T, \tag{5a}$$

$$\tilde{G} = \{\rho(v-\eta), \rho u(v-\eta), \rho v(v-\eta) + p, E(v-\eta) + pv\}^T. \tag{5b}$$

This approach can be applied to a fairly wide variety of two dimensional flows which include the diffraction of a plane shock wave by an oblique interface. This gives a similarity solution corresponding to the initial-value problem with initial condition as shown in Fig. II.3. We solved the above boundary value problem directly by an approximate Newton method. The numerical method is based on direct evaluation and iterative inversion of the Jacobian for both the implicit Godunov and implicit EFM methods. A striking feature of the solutions is

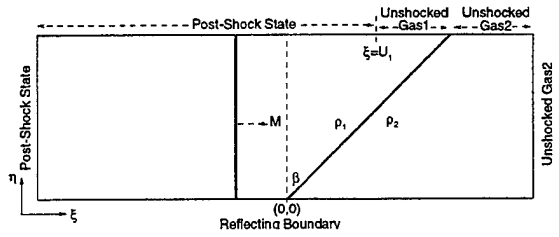

Figure II.3. Shock impinging on an inclined density interface.

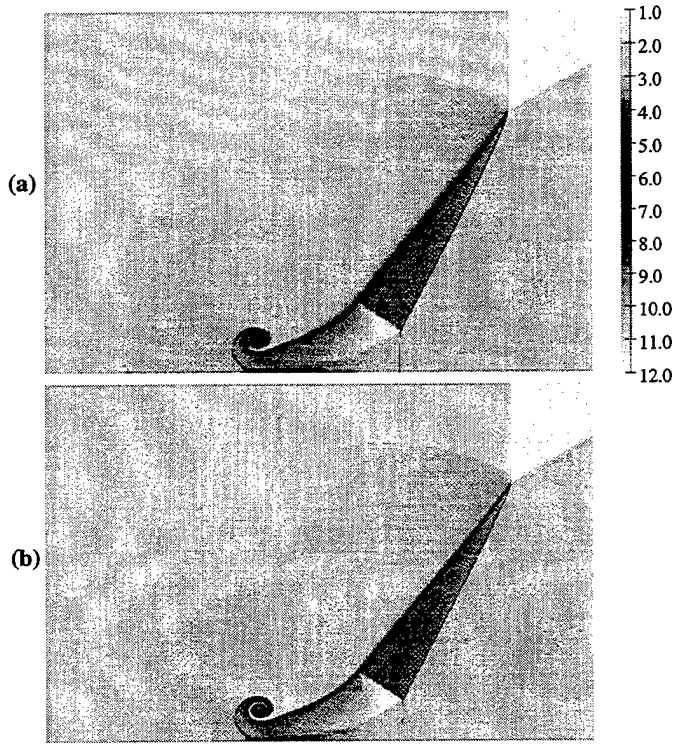

Figure II.4. Density images for the self-similar solution for a shock with $M = 2.02$ impinging on a density interface. Grid sizes; (A) 768×392, (B) 1536×768.

that flow discontinuities are resolved much more sharply than for the solution of the equivalent initial-value problem. In addition, the technique computes reliably the self-similar roll-up of the contact discontinuity, which becomes a vortex sheet after the shock has interacted with the interface. Shown in Fig. II.4 is the refraction of a Mach 2.02 shock wave at a gaseous interface separating gases of density $\rho_1 = 1$, $\rho_2 = 3$ inclined at an angle of $\alpha = 60°$ to the plane of the shock. The interface is initially in thermal and mechanical equilibrium. The spiral associated with the rollup of the vortex sheet is clearly seen, and, in contrast to solutions obtained using the initial value problem, it is completely reproducible without the artifacts normally seen in initial value calculations. Further, the similarity calculations exhibit convergence with respect to grid refinement, unlike initial-value calculations.

We have extended these ideas and investigated the self-similar interaction of a strong shock, including the effects of equilibrium dissociation chemistry (Samtaney & Pullin 1998). We have observed that the transition from regular to irregular refraction is slightly delayed by equilibrium chemistry effects in most cases. We employed the Lighthill (1957) ideal dissociating gas (IDG) model. Comparison between the frozen and equilibrium limits, both of which are self-similar, indicates large changes in peak density and temperatures. Significant differences in the overall flow pattern between the frozen and equilibrium limits are observed for low negative Atwood ratio, $\Delta\rho/(\rho_1 + \rho_2)$, and high positive Atwood ratio interfaces. A local analysis was also developed for the case when the shock refraction is regular. The critical angle at which the transition from regular to irregular refraction occurs is slightly larger for the equilibrium chemistry case.

We present results for a $M = 15$ incident shock interaction with an argon-oxygen interface inclined at an angle $\beta = 60°$. This case is rather unusual because, even though the density ratio is less than one (as well as the fact that the shock moves from a gas of high acoustic impedance to one with a low acoustic impedance), the refraction is *fast-slow* rather than slow-fast, as one might expect. The reflected wave is a rarefaction. However, note that the centered rarefaction eventually curves around and interacts with the lower part of the shocked interface. The resulting wave structure is clearly seen in the density plots in Fig. II.5, where I, R, T indicate the incident shock, reflected rarefaction, and transmitted shock, respectively. The contact discontinuity separating argon and oxygen is indicated by cd_1 while cd_2 is a contact discontinuity in oxygen emanating from the kinked transmitted shock. The kink in the transmitted shock results from the refraction of the rarefaction that curves back to meet cd_1. The presence of equilibrium chemistry shifts the kink on the transmitted shock by a significant distance towards the lower boundary. Note that cd_1 and cd_2 are vortex sheets (actually vortex layers due to numerical diffusion) that roll up at the lower boundary. The vorticity is of negative (positive) sign for $cd_1(cd_2)$. It is quite apparent that at the lower boundary, cd_2 is stronger and, in fact, entrains cd_1 for the frozen chemistry case so that the roll up of cd_1 is in the counter-clockwise sense. For the equilibrium chemistry case, the roll up cd_1 is in the clockwise sense.

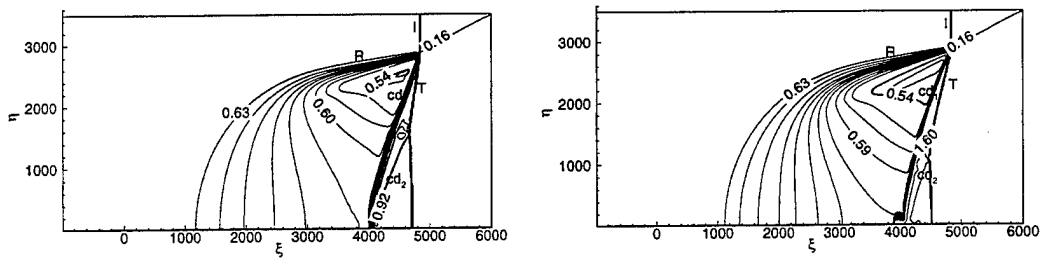

Figure II.5. Density contours for a $M = 15$ shock interaction with an argon-oxygen interface inclined at $\beta = 60°$. Frozen (equilibrium) chemistry on the left (right)

An examination of the baroclinic source term ($\nabla\rho \times \nabla p$) ($\nabla p$ applied across the incident shock, $\nabla\rho$ applied across the interface) indicates that the baroclinic vorticity generation

should be positive, while we observe a negative vorticity generation for this particular case (this was also seen as part of the local analysis). In this case the maximum dissociation level of oxygen was $\alpha = 0.36$. The maximum density for the frozen (equilibrium) case was 1.04 (1.8) kg/m^3. The peak temperature in oxygen is 10,700 K in the frozen case and reduces to 4500K in the equilibrium case.

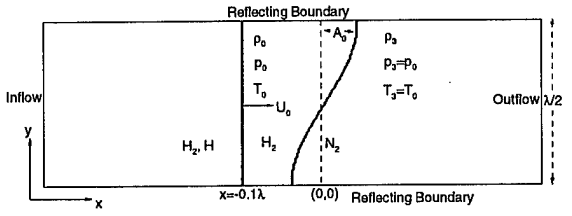

Figure II.6. Schematic of a shock interaction with single harmonic perturbed density interface. Boundary conditions are inflow/outflow in the x-direction and reflecting in the y-direction.

II.1.4 Hypervelocity Richtmyer-Meshkov Instability

The Richtmyer-Meshkov instability has been numerically investigated for strong shocks i.e. for hypervelocity cases (Samtaney & Meiron 1997). The EFM finite-volume method was used for a series of two-dimensional numerical simulations of the impingement of a plane shock with Mach number $M = U_0/c_0$ onto a sinusoidal perturbed density interface, with Atwood ratio $At = (\eta - 1)/(\eta + 1)$ where η is the density ratio, and with ratio of initial amplitude to wavelength A_0/λ. The initial configuration is shown in Fig. II.6. To model the interaction of the flow with non-equilibrium chemical effects typical of high-enthalpy flows, the Lighthill (1957) -Freeman(1958) ideal dissociating gas model is employed. Several gas combinations were considered: hydrogen - nitrogen (H_2-N_2), nitrogen - hydrogen (N_2-H_2), nitrogen - oxygen (N_2-O_2) and oxygen - nitrogen (O_2-N_2). The effects of At, A_0, λ and gas chemsitry, characterized by the Damköhler number $\Omega = d\alpha/dt\lambda/c_0$, where α is the dissociation fraction, were investigated. Calculations were performed on the Caltech Intel Paragon using MPI. Also, a local analysis has been developed to investigate the mechanism of baroclinic circulation generation at the interface, and Richtmyer's linear theory and the impulse model have been extended to include equilibrium dissociation chemistry.

Here, we present results for a $M = 10$ shock interaction with a H_2-N_2 interface perturbed sinusoidally with $A_0/\lambda = 0.1$. The physical domain extent in the x-direction is $[x_l, x_r] \equiv [-0.2\lambda, 4.8\lambda]$. In Figs. II.7 and II.8 density images for frozen and equilibrium chemistry respectively are shown at various times during the simulations. The first interaction between the shock and the interface is the very rapid shock refraction process. In this case the transmitted and the reflected waves are both shock waves. The transmitted shock moves at a slower speed relative to the incident shock, while the reflected shock moves to the right in the laboratory frame of reference. The mean velocities in the x-direction of the primary waves (the reflected shock, the transmitted shock and the contact discontinuity) are larger

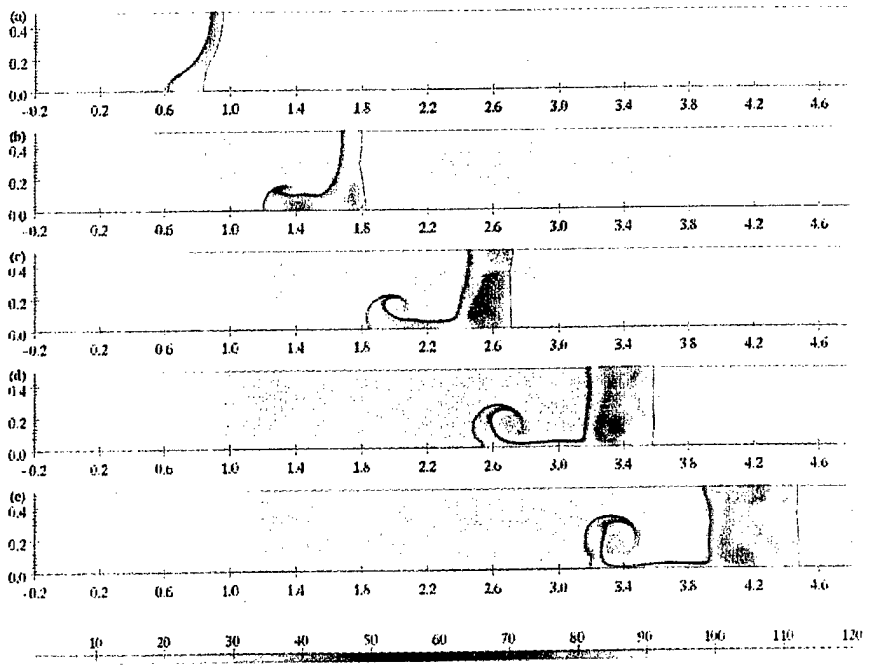

Figure II.7. Time sequence of density images for a M=10 shock interaction with a $A_0/\lambda = 0.1$ H_2-N_2 interface. Frozen chemistry. Times shown are: (a) 0.166, (b) 0.345, (c) 0.523 (d) 0.700 and (e) 0.878.

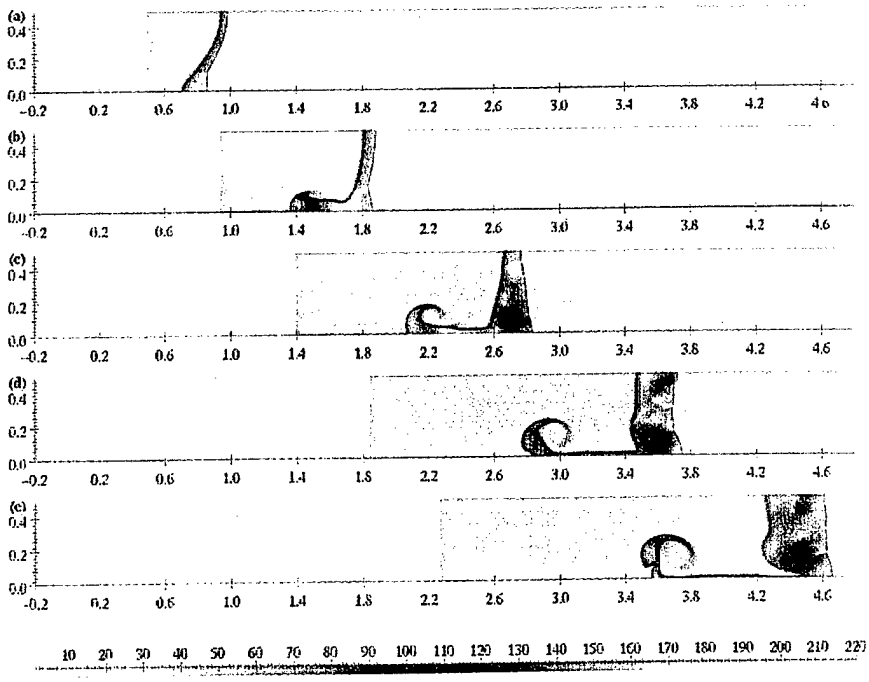

Figure II.8. Time sequence of density images for a M=10 shock interaction with a $A_0/\lambda = 0.1$ H_2-N_2 interface. Equilibrium chemistry. Times shown are: (a) 0.167, (b) 0.346, (c) 0.524 (d) 0.703 and (e) 0.881.

for the equilibrium case than the frozen case. However, for the equilibrium chemistry case, the transmitted and the reflected shocks lie closer to the interface than the frozen case. This effect is due to the larger compression of the gases for the equilibrium case than the frozen case. The contact discontinuity rolls up and gives rise to the familiar mushroom shape of the interface. Nitrogen penetrates into hydrogen as a strong spike. The hydrogen penetration into nitrogen is in the form of a bubble that assumes a vertically flat shape in a short time, and the bubble velocity approaches the velocity of the contact from a one-dimensional shock-contact interaction. Thus, the growth of the perturbation is mostly due to the relative velocity of the strong spike, and the evolution of the interface is very asymmetric, unlike the near-symmetric evolution for very weak shocks.

Aside from differences in the speed of the waves and local magnitudes of the density and temperature, the geometry of the interface is similar for equilibrium and for frozen flow. The growth rate of the amplitude is plotted in Fig. II.9. At any instant the frozen and equilibrium limits exhibit different growth rates. The circulation on the interface (interfacial circulation), Γ_i is an important parameter governing the mixing. Γ_i is defined here as the total vorticity for those computational cells containing a mixture of hydrogen and nitrogen. The total circulation in the domain Γ and the interfacial circulation Γ_i is plotted as a function of time on the right in Fig. II.9. The shear layers in either hydrogen or nitrogen far from the interface, are relatively unimportant in the mixing process. It is observed that chemical reactions reduce the interfacial circulation only slightly. The horizontal lines are theoretical predictions of the primary baroclinic circulation Γ_1 at the end of the shock refraction process . In this case, fortuitously, the total interfacial circulation is close to the theoretical predictions during the entire simulation.

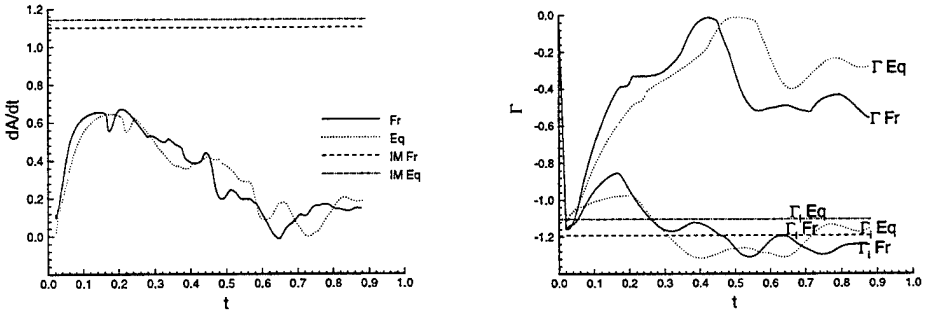

Figure II.9. M=10 shock interaction with a $A_0/\lambda = 0.1$ H_2-N_2 interface. Left; growth rate of the perturbation. The horizontal dotted lines are the impulse model (IM) growth rates. Right; Total circulation. The interfacial circulation is Γ_i and the initial baroclinic circulation from local analysis if Γ_l.

II.1.5 Conclusions

In summary, it was found that mechanisms of vorticity generation for the shock-vortex interaction discussed presently are reminiscent of, but differ somewhat from, those active

in the interaction of a shock with a density interface. In the latter case the main site(s) of vorticity generation lie at the intersection of shocks with the sharp density interface at the bubble boundary whereas in the shock-vortex interaction, owing to the continuous variation of density within the vortex, the baroclinic generation of vorticity is broadly distributed along the curved shock. A further notable difference between the shock density interface and the shock vortex interaction is the way in which the triple point forms. In the former case, the triple point is produced as a result of shock refraction at the density interface whilst in the shock-vortex interaction, the triple point is generated following extreme shock deformation by the velocity shear inside the vortex.

The influence of chemistry on the self-similar interaction of a shock with a density interface was examined for various interfaces. For high Mach numbers, and at equilibrium, the influence of chemistry occurs for the following cases (in decreasing order of importance): low negative Atwood ratio, high positive Atwood ratio, low positive Atwood ratio and high negative Atwood ratio interfaces. For self-similar interaction of a strong shock at an interface separating an inert gas from a chemically active gas we found that the transition from regular to irregular refraction is slightly delayed by equilibrium chemistry for most cases. For low Atwood number interfaces (argon-oxygen, helium-hydrogen) the transition occurs when the flow behind the incident shock becomes sonic and thus is not influenced by chemistry.

Numerical simulations of the compressible Euler equations for hypervelocity Richtmeyer-Meshkov instability indicate no period of linear growth even for amplitude to wavelength ratios as small as one percent. For large Atwood numbers, dissociation causes significant changes in density and temperature, but the change in growth of the perturbations is small. A Mach number scaling for strong shocks has been inferred, which holds for frozen chemistry at high Mach numbers. A local analysis has been used to determine the initial baroclinic circulation generation for interfaces corresponding to both positive and negative Atwood ratios.

References

Freeman, 1958, N.C.Non-equilibrium flow of an ideal dissociating gas, *J.Fluid Mech.*, **4**, 407.

Lighthill, M.J., 1957, Dynamics of a dissociating gas. Part 1. Equilibrium flow, *J.Fluid Mech.*, **2** 1.

Stuart, J.T. 1967, On finite-amplitude oscillations in laminar mixing layers, *J.F.M* , **29**, 417.

Synge J.L. and Lin C.C. 1943, "On a statistical model of isotropic turbulence". *Trans. Roy. Soc. Canada*, **37**, 45-79.

Publications Resulting from Research

Ardalan,K., Meiron, D.I.& Pullin, D.I., 1995, "Steady compressible vortex flows- the hollow-core vortex array". *J. Fluid Mech.*, **301**, pp1-17.

Moore, D.W.& Pullin, D.I., 1998, "On steady compressible flows with compact vorticity; the compressible Hill's spherical vortex". *J. Fluid Mech.*, In press.

Moore, D.W., Pullin, D.I. & Meiron, D.I., 1998, "The effect of compressibility on the Stuart-vortex array". In preparation.

Samtaney, R. 1997, "Computational methods for self-similar solutions of the compressible Euler Equations.". *J. Comp. Phys.* , **132**, 327-345

Samtaney, R., & Meiron, D. I. 1997. "Hypervelocity Richtmyer-Meshkov Instability". *Phys. Fluids* , **9**, 1783-1803.

Samtaney, R. & Pullin, D. I. 1996, "On similarity and initial-value solutions of the compressible Euler Equations". *Physics of Fluids* **8**, 2650-2655.

Samtaney, R. & Pullin, D. I. 1997, "Shock interactions with a compressible Hill's spherical vortex" in *Proceedings of the 21st International Symposium on Shock Waves. Great Keppel Island, Australia, July 1997*, Ed. A. Paull.

Samtaney, R. & Pullin, D. I. 1998, "Hypervelocity shock interactions with oblique contact discontinuities" , *Shock Waves*, In press .

Personnel Associated with Research

Prof. D. Pullin, Professor of Aeronautics.

Prof. D.I. Meiron, Professor of Applied Mathematics.

Dr . Ravi Samtaney, Postdoctoral and Senior Postdoctoral Fellow.

Kavan Ardalan, Postgraduate student.

Mark Meloon, Postgraduate student.

Interactions/Transitions

(a) Participations/presentations at meetings etc.

Meiron, D., Meloon. M. & Samtaney, R. , "Models for vorticity generation in Richtmeyer-Meshkov instability". *Presented at the SIAM annual meeing, October 1995.*

Samtaney, R. & Pullin, D. I., "On self-similar solutions of the compressible Euler Equations". *Presented at the APS meeting, November 1995, Irvine CA.*

Samtaney, R. & Pullin, D. I. 1997, "Shock interactions with a compressible Hill's spherical vortex" in Presented at the 21st International Symposium on Shock Waves. Great Keppel

Island, Australia, July 1997.

(b) Consultative and advisory functions etc.

None.

(c) Transitions

Presentations on the high Mach number Richtmyer-Meshkov instability were made to the staff of A Division at Lawrence Livermore National Lab interested in Richtmyer-Meshkov mixing. Interest was expressed in the use of the Samtaney Zabusky model and its extension to dissociating flows.

New discoveries, inventions, patents None.

Honors/Awards etc.

None.

II.2 SHOCK WAVE INTERACTIONS IN HYPERVELOCITY FLOW

In Project II.2 we have studied two fundamental problems in hypervelocity flow in which shear layers resulting from shock wave interactions impinge on bodies and cause elevated heat transfer. They are the shock-on-shock problem and shock-wave boundary-layer interaction on a flat plate with a deflected flap. Experiments in the T5 free piston shock tunnel have permitted for the first time the study of the effects of dissociation/recombination on these impingement processes. In the first case an unexpected negative result with significant implications was obtained, while, in the second, significant effects of recombination are deduced. Both effects are of sufficient magnitude to influence the design of future aerospace vehicles.

The interaction of oblique shock waves with bow shocks on bluff bodies

The interaction of a weak oblique shock with the strong bow shock ahead of a blunt body in supersonic flow produces extreme heat transfer rates and surface pressures. Although the problem had been studied extensively in low enthalpy flows, until now the influence of high enthalpy real gas effects remained unknown. Perfect-gas models from earlier work predicted greatly increased heating with increasing Mach number and decreasing ratio of specific heats.

We conducted experiments in T5 to determine the effects of thermochemistry on the problem at high enthalpy. The flow topology was simplified by studying the nominally two dimensional flow about a cylinder with a coplanar impinging shock wave. High resolution holographic interferometry was used to investigate changes in the flow structure as the location of the impinging shock wave was varied. Fast response heat transfer gauges were developed to provide time–resolved measurements of the model surface temperature. The data that were obtained do not support the existing predictions of greatly increased heat transfer at high enthalpy.

A model was formulated to study the thermo-chemical processes occurring in the interaction region. The phenomenon arises because the stagnation streamline is forced to pass through a system of oblique shock waves that produce less entropy than the undisturbed bow shock. Peak heating was shown to result from a balancing of the strengths of the oblique shock waves. This condition was demonstrated to simultaneously minimize the influence of thermochemistry on the flow. Real gas effects were shown to become important at lower Mach numbers (< 7.5) and for shock angles weaker or stronger than that which produces maximum heating. The model successfully reconciled the experimental observations.

A nonequilibrium approximation was introduced that applies when the oblique waves are weak with respect to the undisturbed bow shock. Within the scope of the approximation, non-monotonic behavior with the reaction rate was predicted. The reaction rate was not

varied as an independent parameter in the current experiments.

New instrumentation developed for this project has allowed critical assessment of the flow quality produced by the T5 facility. In addition, the high bandwidth of the heat flux gauges developed here permitted examination of the temporal characteristics of the heat transfer signals. Observations of coherent unsteady fluctuations of the type IV jet are consistent with oscillations observed in recent numerical simulations by Gaitonde and Zhong.

The conclusion of the experimental and theoretical investigations was that a subtle balance of shock waves in the shock layer near the shear layer reduces the influence of thermochemistry on the flow, so previously anticipated enhanced heating at shock impingement does not occur. This result can have a profound effect on the design of aerospace vehicles of the future.

High-enthalpy shock/boundary-layer interaction on a double wedge

Interaction between a shock wave and a boundary layer at a compression corner can produce a region of separated flow, the size of which is important in determining aerodynamic forces. This point was graphically impressed on the hypersonics community during the first STS reentry, when it was discovered that the flap effectiveness was less than had been predicted based on the understanding of that day. Until the present work, real gas effects (e.g., in a high-enthalpy dissociating flow) on the length of the separated region had remained unknown. Experiments to measure separation length were performed in the T5 Hypervelocity Shock Tunnel on a double wedge configuration with nitrogen test gas. The double wedge geometry allows greater control over local flow conditions at separation and, at high incidence angle, may produce real gas effects due to dissociation behind the leading shock. Local flow conditions at separation are found by computational reconstruction of the external nonequilibrium flow field.

Analysis of separation length for a laminar non-reacting boundary layer leads to a new scaling based on triple-deck theory, extending a previous result to an arbitrary viscosity law and a non-adiabatic wall. A classification is introduced which divides mechanisms for real gas effects into mechanisms acting internal and external to viscous regions of the flow (the boundary layer and separated region). External mechanisms are shown to decrease the separation length in high-enthalpy dissociating flows. Internal mechanisms are considered qualitatively. A limited numerical study of reacting boundary layers shows that internal mechanisms for real gas effects entering via the incoming boundary layer are relatively unimportant in the present experiments.

Correlations were obtained of experimentally measured separation length as a function of reattachment pressure ratio and Reynolds number using the new scaling law (which includes external mechanisms for real gas effects). The scaled separation length, with external effects accounted for theoretically, is found, on average, to increase by a factor of two as

the stagnation enthalpy increases by a factor of three or four, thus providing a possible high-enthalpy-based explanation of reduced flap effectiveness on re-entering hypervelocity vehicles. This behavior must be due to internal mechanisms for real gas effects entering via the separated region, and is attributed to recombination occuring there. The implication for aerodynamic forces is that for flight at high angle of attack with significant dissociation behind the leading shock, recombination in the separated region will cause a large increase in size of the separation zone and hence reduce control flap effectiveness.

Personnel Supported

1. B. Sturtevant, Professor of Aeronautics.
2. Jean-Paul Davis, then a graduate student.
3. Simon R. Sanderson, then a graduate student.

Degrees Earned

1. Simon R. Sanderson, Ph.D., 1995
2. Jean-Paul Davis, Ph.D., 1998

Publications

Hornung, H. G., Cummings, E. B., Germain, P., Sanderson, S. R., Sturtevant, B. and Wen, C.-Y. 1994 Recent results from hypervelocity research in T5, Presented at 18th AIAA Aerospace Ground Testing Conference, 6/20-23, 1994, AIAA 94-2523, Colorado Springs, CO.

Davis, J. P. 1994 Tests on the HALIS axisymmetric configuration in the T5 hypervelocity shock tunnel, FM 94-4, Caltech Galcit, Pasadena, CA.

Sanderson, S. R. 1995 Shock wave interaction in hypervelocity flow. Ph.D. Thesis, California Institute of Technology.

Sanderson, S. R. and Sturtevant, B. 1995 Shock wave interactions in hypervelocity flow, in "Shock Waves @ Marseille", *Proc. 19th Intl. Symp. Shock Waves*, Eds. R. Brun and L. Z. Dumitrescu, 69-74, Springer Verlag, Berlin.

Davis, J.-P. 1996 Further tests on the HALIS axisymmetric configuration in the T5 hypervelocity shock tunnel, FM 96-2, Caltech Galcit, Pasadena, CA.

Sanderson, S.R. and Sturtevant, B., 1996, Shock-interference heating in hypervelocity flow, in "Shock Waves", *Proc. 20th Symp. on Shock Waves*, Eds. B. Sturtevant, J. E. Shepherd and H. Hornung, 209, World Scientific, Singapore.

Davis, J.-P., Sturtevant, B. and Muylaert, J. 1996 Experiments on the Halis axisymmetric configuration in the T5 shock tunnel, in "Shock Waves", *Proc. 20th Symp. on Shock Waves*, Eds. B. Sturtevant, J. E. Shepherd and H. Hornung, 191-196, World Scientific, Singapore.

Davis, J.-P., and Sturtevant, B. 1997 High-enthalpy shock/boundary-layer interaction on a double wedge: Separation length, in "Shock Waves", *Proc. 21st Intl. Symp. Shock Waves*, Ed. A. F. P. Houwing, 1970, Univ. Queensland, Brisbane.

Davis, J.P., 1998 High-enthalpy shock/boundary-layer interaction on a double wedge Ph.D. Thesis, California Institute of Technology.

Interactions

1. Attended 19th International Symposium on Shock Waves, Marseille, July, 1993.
2. Attended 3rd International Workshop on Shock Tube Technology, Brisbane, December 1992.
3. Organized and participated in the 20th Symposium on Shock Waves, Pasadena, CA, July, 1995.
4. Collaboration with ESA-ESTEC on shock-wave boundary-layer interaction in hypervelocity flow. Ref: GALCIT Reports FM 94-4 and FM 96-2.
5. Attended 21st Symposium on Shock Waves, Queensland, July, 1997.

Inventions

1. None.

Honors/Awards received during grant

1. J.-P. Davis: Awarded prize for the best paper presented by a student, 21st Symposium on Shock Waves, Queensland, July, 1997.
2. B. Sturtevant: Fellow, American Physical Society

Chapter III: SUPERSONIC SHEAR-FLOW MIXING AND COMBUSTION

This part of the program focused on investigations of mixing in high Reynolds number subsonic, and supersonic free-shear flows. Specifically, the effects of inflow/initial conditions, compressibility, and Reynolds number were experimentally investigated and, to a large extent, clarified. A test-section insert to permit investigations of shear layers and aspirating walls following an expansion turn was designed and fabricated for the GALCIT Supersonic Shear Layer facility. The computational effort has added further developments in Riemann-Invariant-Manifold gasdynamic simulation techniques and their application to chemically-reacting flows and unsteady detonation phenomena. On the diagnostic front, developments in digital imaging and Image Correlation Velocimetry have continued. They have been used to investigate turbulent-jet mixing, the unsteady flow over an accelerating airfoil, to mitigate aliasing problems in the computer reconstruction of (2+1)-dimensional isosurface data, and in other applications.

III.1 Introduction

This part of the work was focused on investigations of mixing processes, in high Reynolds number turbulent, subsonic, and supersonic free-shear flows. The program was comprised of:

- an experimental effort, in
  - chemically-reacting and non-reacting, subsonic and supersonic turbulent free-shear layers;
  - preliminary work on transverse jets in a cross-flow, and
  - a study of the flow field over accelerating airfoils;
- an analytical, modeling, and computational effort, focusing on the behavior of hyperbolic systems with strong fronts (shocks/detonations);

and

- a diagnostics, instrumentation, and data-acquisition-development effort.

Parts of this effort were cosponsored by the Air-Breathing Propulsion core-program AFOSR Grant F49620–94–1–0353, on "Chemical Reactions in Turbulent Mixing Flows," with some instrumentation support derived from the imaging efforts under AFOSR/DURIP Grant No. F49620–95–1–0199.

III.2 Supersonic Shear Layer Facility

The GALCIT Supersonic Shear Layer (S^3L) Facility was upgraded and utilized for the supersonic-mixing and chemical reaction experiments conducted as part of this effort. The material below is derived from the Slessor (1998) Ph.D. thesis and is included for completeness.

III.2.1 Facility overview

The S^3L facility is a two-stream, blowdown, wind tunnel, capable of attaining freestream Mach numbers ranging from incompressible to highly-compressible gas-phase flow, in both chemically-reacting and non-reacting configurations. A brief overview of this facility is included here for completeness. Additional details can be found in Hall & Dimotakis (1989), Hall (1991), and Bond (1998). Two major upgrades were undertaken as part of this work: an upgrade extending the operating envelope to bi-supersonic flow and a replacement of the original surge tank by a larger and higher-pressure vessel. These will be documented below.

The facility, shown schematically in Fig. III.1, operates with a run time of $t_{\rm run} > t_{\rm dat} \simeq 2 - 4\,{\rm s}$, where $t_{\rm dat}$ is the data-recording time interval. Gas for the two freestreams is supplied by independent (high- and low-pressure, usually corresponding to high- and low-speed, respectively) flow systems charged by standard bottled-gas supplies prior to a run. The facility can accommodate flows with fast-kinetic reactants, whose chemical reaction and associated temperature rise can yield quantitative measurements of molecular-scale mixing in the shear-layer region. In such experiments, a dilute mixture of H_2 and NO is typically carried in the high-speed stream and a dilute concentration of F_2 is carried in the low-speed stream. The remaining diluent components are selected to control freestream thermodynamic properties, *e.g.*, densities, speeds-of-sound, *etc.*

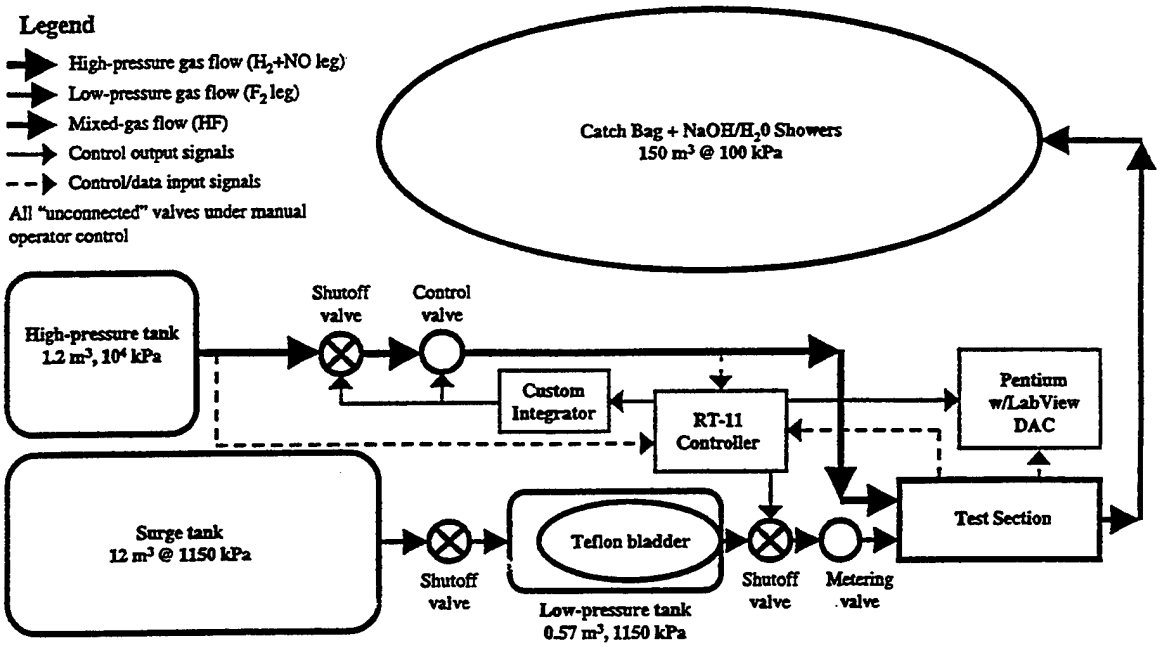

FIG. III.1 Overall facility gas-flow schematic.

To provide the molecular number densities required for "fast" chemical reactions, large (unit) Reynolds numbers, and high optical-image cross sections, the test section operates at nominally-atmospheric static pressure. This sets it apart from most other supersonic-flow facilities, in which test sections operate at lower-pressure conditions to ease demands on upstream flow-supply systems.

For the shear-layer flows investigated in these experiments, the high-pressure freestream speed is maintained by plenum-pressure control, operated in either an open-loop (program-control) configuration at low mass-flux, subsonic conditions, or in a closed-loop (nonlinear-feedback-control) configuration, at moderate-to-high mass-flux, typically supersonic, conditions. Gas is supplied to this plenum from a $1.2\,\mathrm{m}^3$ pressure vessel, at a maximum pressure of $10^4\,\mathrm{kPa}$. During blowdown, vessel pressure can drop by as much as 50%, necessitating an active-control system. The gas in the vessel is maintained at a nearly-constant temperature, by rolled aluminum screen (large heat capacity) throughout the pressure-vessel interior, displacing a total of, approximately, 15% of its volume.

The mass flux through the low-pressure plenum is set by a choked metering valve kept fixed during each run. Gas to this plenum is supplied from a $0.57\,\mathrm{m}^3$ vessel that encloses a bladder bag containing the F_2-laden charge. This vessel is

pressurized, in turn, by a N_2-filled, large-volume surge tank whose pressure falls by $3-5\%$ during a run, and less during actual data-recording time. This nearly-isobaric arrangement obviates the need for a low-pressure-side active control system, greatly simplifying the flow-control process, assuring control stability, as well as providing a relatively-safe (teflon-buffered) method for handling the extremely-corrosive/toxic fluorine gas.

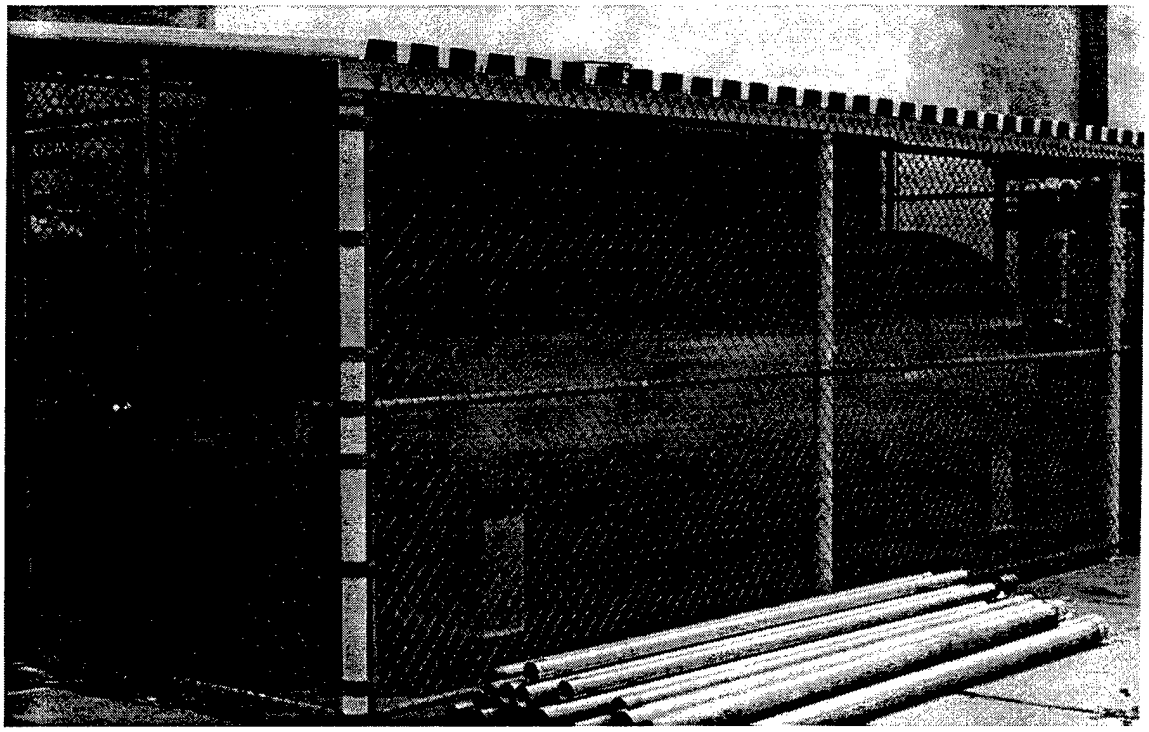

FIG. III.2 Northeast view of the upgraded surge tank installation.

The upgrade of the original (ca., 1940), $12.7\,m^3$ surge tank used in the first implementation of the supersonic shear-layer facility represents a major engineering task undertaken under sponsorship of this grant. The original system had a maximum working pressure of 700 kPa, limited by the tank pressure rating. The impetus for this significant upgrade was provided by the planned demolition of the GALCIT 10-Foot Wind Tunnel during the summer of 1997, since the original surge tank resided adjacent to this tunnel, at both basement and sub-basement levels, in the center of the Guggenheim Building. The replacement surge tank, a custom $14.2\,m^3$ unit with a (maximum) working pressure of 1150 kPa, was installed in the Karman/Guggenheim courtyard (Fig. III.2) and connected to the low-pressure supply system in July 1997. The upgraded system has since been successfully tested over a range of pressures and flowrates.

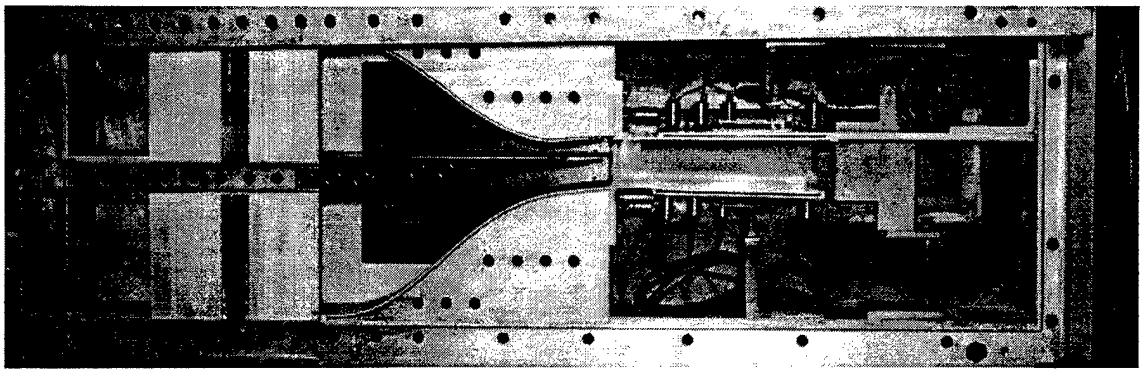

FIG. III.3 Photograph of shear-layer flow-management and test-section regions. Gases flow from left to right. Test section is approximately 2 m in length.

A photograph of the flow-management and test-section regions is shown in Fig. III.3. Coarse-mesh-screen, honeycomb, and a series of fine-mesh-screen sections are used for turbulence management in the region upstream of the contractions. The two streams are separated in their respective plena by a splitter plate, which is flat on the top (high-speed) surface and curved on the bottom (low-speed) surface, as shown in Fig. III.3. The splitter plate has a trailing-edge thickness of 0.13 mm, an included angle of 5°, and is estimated (using General Electric gauges) to have an average surface roughness of 0.4 μm.

For subsonic freestream flows, the modular "nozzle blocks" are configured as specially-machined contraction sections. Their shapes are described by 6^{th}-degree polynomials, which are iteratively optimized using a potential-flow solver (Pepin & Dimotakis 1989) to obtain the inviscid outer-flow solution, and the method of Thwaites (*e.g.*, White 1974) to obtain the boundary-layer thickness(es). The optimization endeavors to maximize flow uniformity and minimize boundary-layer momentum thicknesses at the contraction exit, while ensuring suppression of any flow separation and three-dimensional Taylor-Görtler instabilities. This flow instability can occur in the boundary layers on the concave surfaces of both nozzle walls, as well as on the concave part of the lower splitter-plate surface. The design-iteration process minimizes the potential for this instability in all susceptible regions. For supersonic freestream flows, these nozzle blocks are configured as converging-diverging (Laval) nozzles, which employ similar contraction sections to the throat, mated to supersonic-expansion contours designed using the characteristic-capturing method of Sivells (1978). As seen in Fig. III.3, the 5° included angle of the splitter plate is matched on the bottom nozzle block, *i.e.*, the bottom-freestream flow enters the test section at a 5° angle relative to the top-freestream flow. Flow in the test

section, downstream of the contractions/nozzles, is confined by top and bottom guidewalls, with optical windows serving as sidewalls, with a span, $b = 15.3\,\mathrm{cm}$. In these experiments, the upper guidewall is maintained horizontal (parallel to the top splitter-plate surface), with the lower guidewall adjusted, as necessary in each flow, to remove any mean streamwise pressure gradients.

Upon exiting the test section, the flow encounters a shower-tunnel and catch-bag containment, handling, and neutralization system. A set of shower heads inside the tunnel spray a H_2O/NaOH mixture into the exiting flow, simultaneously neutralizing and cooling the exhaust gases. The neutralization process transforms the exhaust into a mixture of non-toxic gases, more H_2O, and NaF, the active ingredient in many toothpastes. The $150\,\mathrm{m}^3$-volume, atmospheric-pressure catch bag collects and contains the exhaust mixture downstream of the shower tunnel. An additional set of shower heads, within the bag, provides further neutralization and cooling of the exhaust products. Finally, in preparation for eventual venting, the catch bag allows for controlled dilution of any potentially-flammable gas mixtures to concentrations comfortably below ignition limits.

III.2.2 Upgrade to bi-supersonic flow

The original low-pressure freestream of the S^3L facility was limited in Mach number to subsonic flow ($M_2 \lesssim 0.5$) by the existing components. Consequently, an upgrade of these components was required to fulfill the original proposal requirements and explore the regime of bi-supersonic flow, where both freestreams are supersonic in the laboratory frame. Two major modifications were required to allow bi-supersonic operation of the facility: a new control/regulation system, and a new nozzle block designed for an appropriate Mach number. The original, low-pressure side reservoirs (supply and surge tanks) were deemed capable of supplying enough gas for adequate run times at supersonic Mach numbers, even though it was decided to upgrade them also, as documented above.

III.2.2.1 Low-pressure freestream control system

One might expect that an active-control valve, similar to the unit which regulates the high-pressure freestream flow, would be required to compensate for the anticipated stagnation-pressure drop during a run (35 kPa from the original surge-tank pressure of 700 kPa). However, since the existing high-pressure control valve can be pre-programmed, it is possible to achieve the desired pressure ratio across the splitter-plate tip throughout a run with fixed-area-valve metering of the low-pressure freestream. In order to accommodate the higher mass fluxes associated with supersonic Mach numbers, an increase in (sonic) valve-orifice area was required. To provide this increase, a new sleeve was machined by the Aeronautics Machine Shop, with approximately triple the choked-flow area of the original (subsonic) sleeve. These modular sleeves are easily interchanged, increasing the operating envelope of the S^3L facility to include bi-supersonic flow, in addition to high-mass-flux subsonic-flow conditions, as discussed in Slessor (1998).

The existing passive-blowdown method of metering the low-pressure freestream has several significant advantages over an active-control scheme. In particular, this allows continued use of the original operating procedure and control algorithm/computer, minimizing changes to a well-tested facility. Additionally, all existing low-pressure "settings" remain valid, permitting low mass-flux runs to be undertaken with a minimum of recalibration. Finally, omission of a complex valve assembly eliminates the significant safety considerations of long-term fluorine passivation and compatibility.

III.2.2.2 Supersonic nozzle

A preliminary study indicated that a Mach number of less than approximately 1.13 would be achievable using existing reservoir components. This limit is dictated if a minimum allowable run time of 2 s is desired, *e.g.*, to provide adequate data-acquisition record lengths, and a nozzle-exit height of 38 mm is desired, *e.g.*, to accommodate the shear-layer growth expected over the test-section length. Near-sonic Mach numbers, however, dictate throat-to-expansion area ratios correspondingly close to unity. Considering the uncertainties inherent in the displacement-thickness estimate of 0.35 mm,* as well as expected errors in machining a large block of alu-

---

* Estimate provided by Spalding-Chi turbulent boundary-layer model, internal to the Sivells nozzle-design code.

minum, it seemed wise to design a nozzle with a throat-to-exit expansion as large as possible, *i.e.*, a nozzle with as high a Mach number allowed by the above constraints. Consequently, a Mach 1.13 nozzle, with a throat-to-exit expansion of approximately 0.85 mm, was fabricated by Caltech Central Engineering Services and used throughout the bi-supersonic flow experiments described in Slessor (1998).

III.3 Shear-layer mixing and combustion

The experimental data discussed in this section were investigated in the GALCIT Supersonic Shear-Layer Facility described above. This facility allows the study of high-Reynolds-number, subsonic and supersonic, chemically-reacting, turbulent shear-layer flows, by employing the $(H_2 + NO)/F_2$ chemical system for "flip experiments" (Koochesfahani & Dimotakis 1986, Dimotakis 1991), in addition to color-schlieren and Rayleigh-laser imaging, for flow visualization. This effort has focused on several aspects of turbulent shear-layer behavior, spanning incompressible- to compressible-flow regimes. In particular, the results of studies on effects of inflow/initial conditions, compressibility, and Reynolds number, will be described in what follows. This part of the work was cofunded by AFOSR Grant F49620–94–1–0353.

III.3.1 Inflow/initial conditions

Experiments were performed to explore the effects of inflow conditions for incompressible shear-layer flows. The flow at the measuring station in these experiments was set at a (local) Reynolds number of,

$$Re_\delta \equiv \frac{\rho \Delta U \delta(x)}{\mu} \sim 2 \times 10^5 , \qquad (1)$$

and freestream-velocity and -density ratios of,

$$r \equiv U_2/U_1 \simeq 0.4 \qquad \text{and} \qquad s \equiv \rho_2/\rho_1 \simeq 1 , \qquad (2)$$

respectively. The data show a dramatic influence of perturbed inflow conditions on scalar mixing.

Two sets of temperature-rise data from these experiments are presented in Fig. III.4. The "flip-experiment" temperature-rise data provide a quantitative molecular probe of molecular-scale mixing when in the fast-kinetic regime.

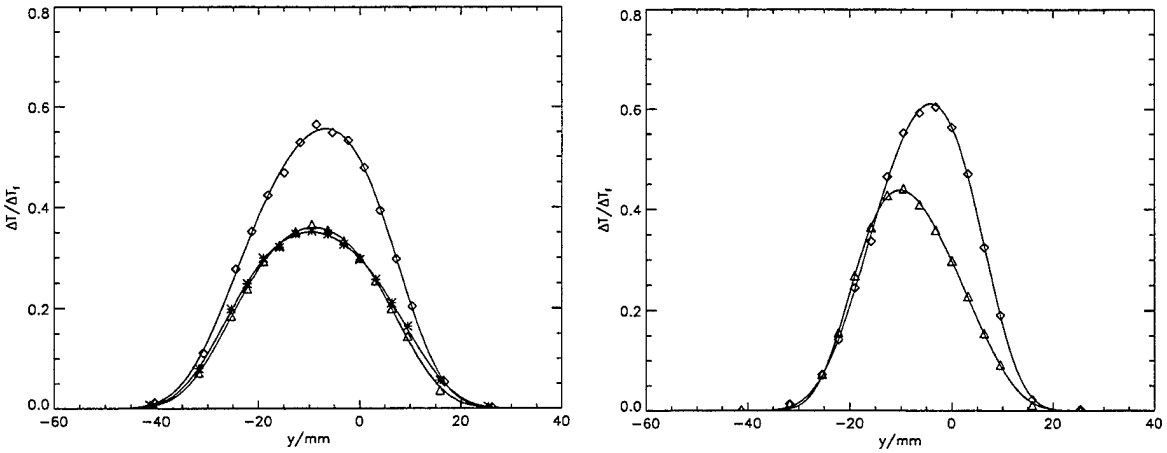

FIG. III.4 Normalized temperature-rise data. Left: untripped boundary layers. Right: tripped high-speed boundary layer. Reactant compositions - diamonds: $\phi = 8$; triangles: $\phi = 1/8$; asterisks: $\phi = 1/8$, reduced chemical-kinetic rate.

The only difference between these two flows is a 0.8 mm-diameter trip wire added on the splitter-plate high-speed side, 50 mm upstream of its trailing edge. The data are measured far downstream of separation, $x/\theta_1 \simeq 3300$, where x is the streamwise coordinate and θ_1 is the high-speed boundary-layer momentum thickness, as well as by any of a number of other measures, indicating a locally, fully-developed turbulent free-shear flow.

This change in inflow conditions has a significant effect on all scales of the flow: the shear-layer growth rate, δ_T/x, where δ_T is the temperature-rise profile 1% thickness, has decreased by 21%; the mixed-fluid fraction δ_m/δ_T, where δ_m is the mixed-fluid profile thickness (Dimotakis 1991), has increased by 11%; and the mixed-fluid composition ratio has decreased by 9%. Additionally, the data indicate a change from a non-marching scalar probability-density function (pdf), to a marching pdf when the boundary layer was tripped. These observations suggest a shear-layer behavior that depends not only on local-flow properties, but also on upstream conditions, reminiscent of results from low-dimensionality, non-linear (chaotic) systems. A complete documentation of this work can be found in Slessor, Bond, and Dimotakis (1998).

III.3.2 Compressibility and growth

Compressibility effects on turbulent shear layers are often scaled by the total convective Mach number (Papamoschou 1989),

$$M_c \equiv \frac{U_1 - U_2}{a_1 + a_2}, \tag{3}$$

where U_i and a_i are the freestream velocities (speeds) and speeds of sound, respectively.

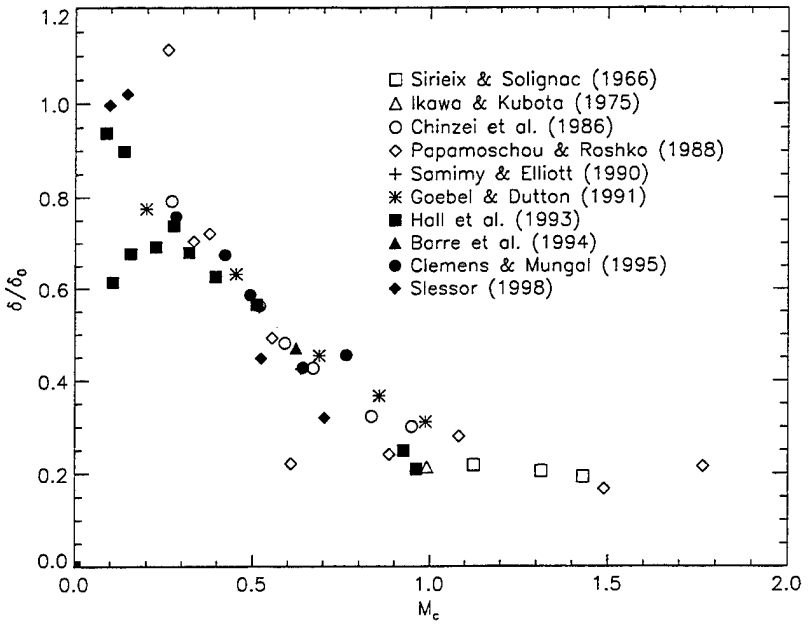

FIG. III.5 Normalized compressible shear-layer growth rates as parameterized by the total convective Mach number, M_c (Eq. 3).

Compressibility acts to decrease the outer-scale growth rate, $\delta(x)/x$, and is usually assumed to act independently of the effects of freestream-velocity and -density ratios, *i.e.*,

$$\frac{\delta/x}{\delta_0/x} \simeq \frac{\delta}{\delta_0}(M_c) \neq \text{fn}\left(r \equiv \frac{U_2}{U_1}, s \equiv \frac{\rho_2}{\rho_1}\right), \tag{4}$$

with estimates for the incompressible-flow growth rate, δ_0/x, used to normalize the (measured) compressible-flow growth rate, δ/x, provided by the spatial-growth model of Dimotakis (1986). Existing compressible-flow data are plotted in this fashion, in Fig. III.5.

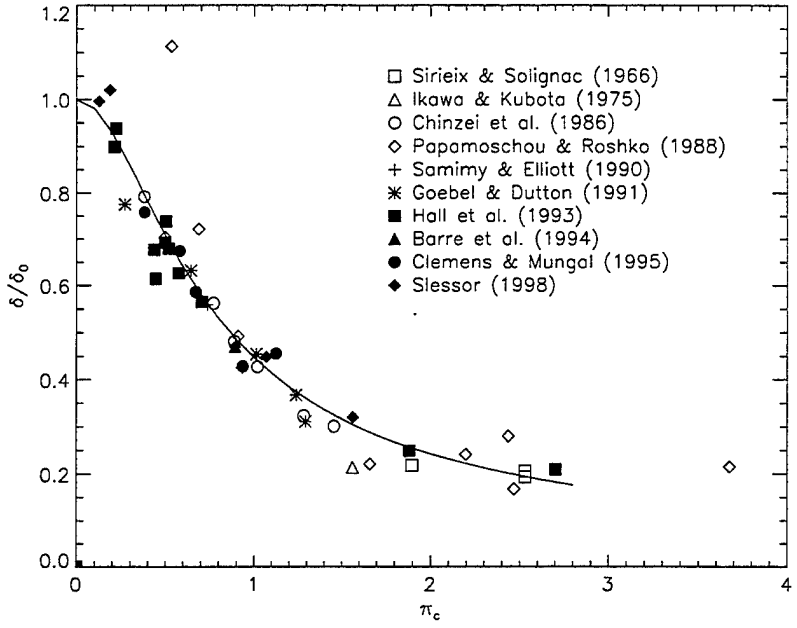

FIG. III.6 Normalized (as in Fig. III.5) compressible shear-layer growth rates parameterized by the proposed compressibility parameter Π_c (Eq. 5). Solid curve is Eq. 6.

Abnormally-low growth rates are evident in Fig. III.5, and suggest either an inaccurate representation of either the incompressible shear-layer growth rate or the flow compressibility. As observed by several authors, *e.g.*, Hall *et al.* (1993) and Lu & Lele (1994), these scaling violations are observed in flows with extreme values of the freestream density ratio, $s \equiv \rho_2/\rho_1$. Existing incompressible growth-rate data (Brown & Roshko 1974) are well-represented by the Dimotakis (1986) model, indicating that M_c provides an inadequate measure of compressibility.

As part of this work, we investigated alternate compressibility scaling, deriving a proposal given by,

$$\Pi_c \;=\; \max_i \left[\frac{\sqrt{\gamma_i - 1}}{a_i} \right] \times \Delta U \,, \tag{5}$$

derived from considerations of compressibility as a kinetic-to-thermal-energy conversion effect. The experimentally-measured growth rates, normalized as in Fig. III.5, are plotted against Π_c in Fig. III.6. The data can be seen to exhibit a near-functional dependence on this parameter, to a better extent than on M_c. The smooth solid curve is given by,

$$\frac{\delta}{\delta_0} \;\simeq\; \left(1 + \alpha \Pi_c^2\right)^{-\beta} \,, \qquad \text{with} \quad \alpha \simeq 4,\ \beta \simeq 0.5 \,. \tag{6}$$

The systematic deviations observed in flows with extreme density/speed-of-sound ratios are absent when scaled in this fashion. A more complete discussion of these results is available in Slessor, Zhuang, and Dimotakis (1998).

III.3.3 Compressibility and mixing

Experiments were performed to explore effects of compressibility on molecular mixing. Since mixed fluid can only be contained within the shear-layer mixed-fluid region, compressibility can be expected to result in a *net decrease* in the amount of molecularly-mixed fluid, at least at moderate-to-high compressibility conditions (*cf.* Eq. 4 and Fig. III.5). This expectation stems from two experimental facts (Dimotakis 1991): the large-scale growth rate, δ_T/x, is approximately 1/2 of its incompressible value by $M_c \simeq 0.5$, and the mixed-fluid fraction, δ_m/δ_T, is approximately 1/2 at incompressible-flow conditions.

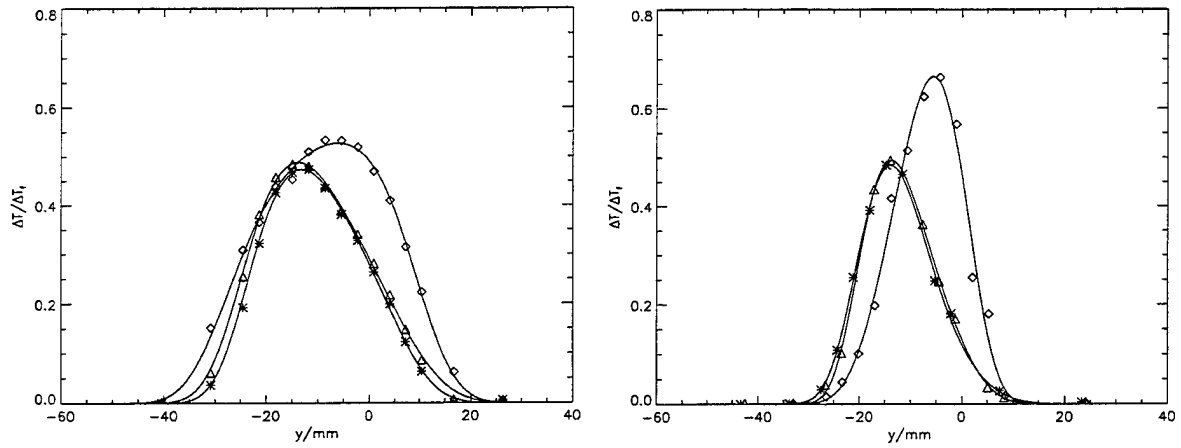

FIG. III.7 Normalized temperature-rise data. Left: $M_c \simeq 0.25$, Right: $M_c \simeq 0.47$. Reactant compositions - diamonds: $\phi = 8$; triangles: $\phi = 1/8$; asterisks: $\phi = 1/8$, reduced chemical-kinetic rate.

The experiments were conducted at nominally-constant values of the (local) Reynolds number, *i.e.*,

$$Re_\delta \equiv \frac{\rho \Delta U \delta(x)}{\mu} \sim 0.9 \times 10^6 ,$$

and freestream-velocity and -density ratios,

$$r \equiv U_2/U_1 \simeq 0.4 \qquad \text{and} \qquad s \equiv \rho_2/\rho_1 \simeq 1 ,$$

respectively, flip experiments were performed at two compressibility levels,

$$M_c \simeq 0.25 \qquad \text{and} \qquad M_c \simeq 0.47$$

(for these particular $\rho_2/\rho_1 \simeq 1$ flows, M_c- and Π_c-scaling is basically the same). Temperature-rise data from these two chemically-reacting flip experiments are presented in Fig. III.7.

Several differences, attributable solely to the increase in flow compressibility, can be noted. The shear-layer is thinner, *i.e.*, δ/x has been reduced at the higher compressibility, in quantitative agreement with previous investigations (Fig. III.5). For the H_2-rich ($\phi = 1/8$) parts of the flip experiment, the maximum normalized temperature rises are comparable in both low- and moderate-compressibility flows. However, the maximum attained in the F_2-rich ($\phi = 8$) part is significantly (25%) higher than in low-compressibility flow, reaching nearly 70% of the adiabatic flame temperature for this mixture.

These data, despite the significant increase in normalized temperature-rise at $\phi = 8$, show only a modest increase in mixed-fluid fraction, δ_m/δ_T, associated with the increase in M_c. This reflects a change in the shape of the temperature-rise profile, and consequently, the mixed-fluid structure. Changes in flow structure can also be seen in instantaneous spanwise-averaged flow visualizations. A modified flow structure is also indicated by the change in the mixed-fluid composition ratio, which is seen to increase for moderate-compressibility flow, favoring the high-speed fluid to a greater extent than in the corresponding low-compressibility flow. A complete description of these experiments is available in Slessor (1998).

III.3.4 Near-wall shear-layer combustion following an expansion turn

We had originally proposed to investigate the flow following a supersonic-expansion turn around a corner, that would be formed if the outer stream were to mix, and react, with fuel supplied by transpiration through the wall following the turn. See Fig. III.8.

A test-section insert was designed as part of this and our AFOSR F49620–94–1–0353 effort, and fabricated by TriModels, Inc., for the S^3L facility towards the end of this effort. It was designed to generate such a flow, permitting the investigation of the resulting shear layer, both with and without chemical reactions. The test-section insert is ready and we hope to explore the many flow phenomena descibed

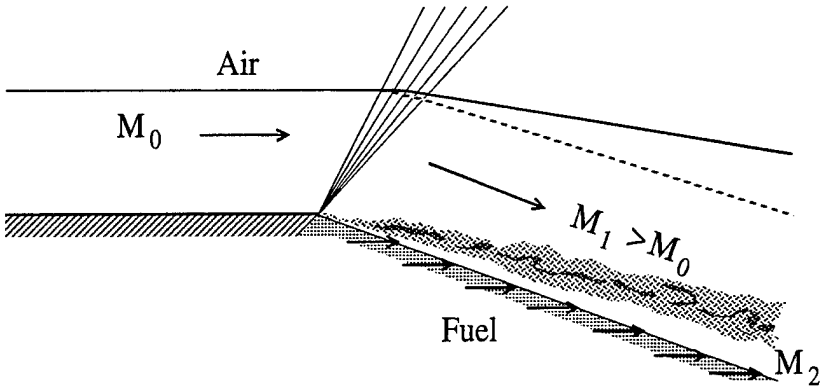

FIG. III.8 Transpiration-fueled external flow shear layer combustion zone following a supersonic-expansion turn. Dashed streamline line: no transpiration. Solid streamline: Chemically-reacting flow.

above in the next few years. Unfortunately, the deobligation of F49620–94–1–0353 funds did not permit this work to be completed as part of this effort.

III.4 Image correlation velocimetry

The Image Correlation Velocimetry (ICV) method developed as part of work sponsored by this grant and F49620–94–1–0353, is an extension of the original implementation by Tokumaru & Dimotakis (1995) developed under previous AFOSR sponsorship. The new implementation is based on the thesis work of G. Gornowicz (1997) and utilizes a hierarchical B-spline representation of the velocity (mapping) field.

Variational methods have been used to infer displacement fields in a variety of contexts, as done by Zhou *et al.* (1995), for example, who employed a multiresolution representation of the three-dimensional displacement field in the interior of a cylindrical asphalt/aggregate core, assuming a volume-preserving (divergence-free) displacement field.

Another general category of this methodology identified by Barron *et al.* (1994) are the so-called differential techniques, pioneered by Horn & Schunck (1981). These methods calculate the components of the scalar-transport equation and use additional constraints to remove ambiguities. Recent work has investigated and compared the required additional constraint(s) to the scalar transport equation proposed by various researchers after Horn & Schunck (*e.g.*, Willick & Yang 1991).

Strong proponents of the application of this technique for fluid velocimetry have been Dahm *et al.* (1991, 1992). More recently, a variational approach was offered by Su & Dahm (1995) and Dahm *et al.* (1996). Pearlstein & Carpenter (1995), however, noted that the method of Dahm and collaborators suffers from a local ambiguity problem in that the local velocity field is only defined in the direction of the imaged-scalar gradient. Pearlstein & Carpenter proposed to mitigate this ambiguity problem by simultaneously tracking multiple scalar fields. A shortcoming of these methods is that they rely on spatial and temporal derivatives of the imaged field to deduce the convecting velocity field, rendering them rather susceptible to the inevitable image noise.

The implementation and applications discussed below were developed for incompressible flows. While a (velocity-field) divergence-free condition is not imposed, per se, and the method can be just as easily applied to compressible flows, extensions that would allow shocks or flamefronts, for example, to be accommodated would need to be developed. As will be discussed, a new methodology has been incorporated in this implementation of ICV. This methodology allows embedded boundary-lines and boundary-surfaces to be accommodated, with special conditions that can be imposed on the velocity-field representation. In future work in this area, this methodology would be applied across strong fronts (shocks, flames), by including "jump" conditions across such fronts, as appropriate.

III.4.1 Continuous-field ICV method

The ICV procedure seeks the displacement field, $\boldsymbol{\xi}(\mathbf{x})$, such that the region in the neighborhood of $\mathbf{x}$, in the image $I_1(\mathbf{x})$, at time t_1, is best mapped into the region $\mathbf{x}+\boldsymbol{\xi}$ in the next image, $I_2(\mathbf{x})$, at $t_2 = t_1 + \tau$, *i.e.*, such that,

$$I_1(\mathbf{x}) \;\mapsto\; I_2(\mathbf{x}+\boldsymbol{\xi}) \;. \tag{7}$$

Specifically, the displacement field, $\boldsymbol{\xi}(\mathbf{x})$, is sought that minimizes the square of the difference of the two images, integrated over the correlation domain, Ω, *i.e.*, a cost function given by,

$$\mathcal{J}\{\boldsymbol{\xi}\} \;=\; \int_{\Omega} [\, I_2(\mathbf{x}+\boldsymbol{\xi}) - I_1(\mathbf{x}) \,]^2 \; \mathrm{d}\Omega(\mathbf{x}) \;\rightarrow\; \min \;. \tag{8}$$

Uniqueness and smoothness of the solution depend on the functional representation of the $\boldsymbol{\xi}$ mapping field and are addressed in Gornowicz (1997).

The solution of the variational problem, for small $\tau = t_2 - t_1$, leads to the requirement,

$$\tau \frac{\partial}{\partial t} I_1(\mathbf{x}, t_1) + \boldsymbol{\xi} \cdot \frac{\partial}{\partial \mathbf{x}} I_1(\mathbf{x}, t_1) \simeq 0 \ ,$$

to leading order in the space/time displacements, *i.e.*,

$$\frac{\partial}{\partial t} I_1 + \mathbf{u} \cdot \frac{\partial}{\partial \mathbf{x}} I_1 \simeq 0 \ , \qquad \text{for,} \quad \mathbf{u} = \frac{1}{\tau} \boldsymbol{\xi} \ . \tag{9a,b}$$

Equation 9 is the optical-flow equation. It is also the scalar-transport equation, provided diffusive effects are negligible, which typically translates to an upper limit on the time interval, τ, between the image pair. Since scalar diffusivity is essentially fixed by the choice of the fluid, the time interval must be chosen such that diffusion is negligible (*cf.* discussion in Tokumaru & Dimotakis 1995).

To compute an optimal mapping field, the ICV method relies on a parametric representation of the displacement field, $\boldsymbol{\xi}(\mathbf{x})$. In the ICV implementation of Tokumaru & Dimotakis (1995), the minimized cost function included terms which increased its value with the (square of the) amplitude of any discontinuities of the displacement field and its derivatives at the boundaries of the array of Taylor-expansion regions around the selected control points, $\mathbf{x}_c$. As a consequence, much of the built-in flexibility in describing spatial variations of the displacement (velocity) field was lost, with degrees of freedom gained from the Taylor-expansion coefficients, in effect, expended to minimize discontinuities of the velocity field and of its derivatives at the Taylor-expansion region boundaries.

To mitigate this difficulty, the present ICV implementation relies on a displacement field that possesses the required, $\mathcal{C}^n$, continuity properties by construction, with the order of continuity, n, chosen appropriately, as described below. The remaining (true) degrees of freedom are utilized to minimize the cost function, $\mathcal{J}\{\boldsymbol{\xi}\}$, with no added (smoothing) terms in the integrand.

Velocity- and vorticity-field solutions of the Navier-Stokes equations are continuous, with continuous derivatives to all orders, *i.e.*, are $\mathcal{C}^\infty$. In the present implementation, which was limited to two-dimensional fields, a $\mathcal{C}^2$ displacement (velocity) field was employed, *i.e.*, possessing continuous second derivatives, corresponding to inferred vorticity fields that possessed continuous first derivatives. The continuity was achieved by representing the displacement field in terms of B-splines with appropriate basis functions, whose control parameters, $\mathbf{q}_{ij}^{(r,R)} \in \Re^2$, then provided the parametric description of the displacement field, *i.e.*,

$$\boldsymbol{\xi}(\mathbf{x}) = \boldsymbol{\xi}\left[\mathbf{x};\, \mathbf{q}_{ij}^{(r,R)}\right] \ . \tag{10}$$

With the solution space of the minimization problem (Eq. 8) restricted in this fashion, the cost *functional*, $\mathcal{J}\{\boldsymbol{\xi}\}$, becomes a *function* of the control parameters, *i.e.*,

$$\mathcal{J}\{\boldsymbol{\xi}\} \rightarrow \mathcal{J}\left[\mathbf{q}_{ij}^{(r,R)}\right] , \tag{11}$$

possessing a minimum where derivatives of $\mathcal{J}$, with respect to each of the $\mathbf{q}_{ij}^{(r,R)}$, vanish. This scheme allows a global minimization over the (selected) image-correlation domain to be sought, using an iterative, multidimensional, conjugate-gradient method over *all* parameter values, with a suitable initial guess.

III.4.2 ICV algorithm implementation

The ICV implementation is comprised of a sequence of iterative, algorithmic steps:

- image-data preparation,
- image-correlation domain definition,
- cross-correlation displacement-field initialization, and
- a final, conjugate-gradient displacement-field optimization to minimize the cost function (Eq. 8).

The procedure starts by further processing individual data images, after background removal, illumination normalization, *etc.*, for shot-to-shot intensity variations of the illuminating laser sheet. A geometry file is generated, which specifies the correlation domain, Ω, within the image domain. An initial hierarchy of the B-spline resolution knot grid is specified, and any excluded regions from the correlation domain (*e.g.*, laser shadows, imaging occlusions, *etc.*) are also identified. The outer boundary of the correlation domain, Ω, is specified as a polyline (n-sided polygon). Inner boundaries can also be accommodated, allowing correlation domains to be defined that are not simply-connected, as necessary. These boundaries are defined on the first of the two images (for each pair).

The next step initializes the solution at the coarsest resolution level, usually one spline patch. The initialization is performed by cross-correlating spatially-local windows, using Fourier techniques, as in DPIV analyses (*e.g.*, Adrian 1991, Willert & Gharib 1991). The results of these correlations initialize the mapping vector field, $\boldsymbol{\xi}(\mathbf{x})$. Windows are then centered at the peak of each B-spline basis function,

and the cross-correlation results are used to determine the corresponding B-spline control parameters, $\mathbf{q}_{ij}^{(r)}$, at the resolution level r.

The initialization, $\boldsymbol{\xi}^{(0)}$, of the B-spline representation for $\boldsymbol{\xi}$ allows Eq. 7 to be applied, producing an initial mapped version of the second image, *i.e.*, $I_2(\mathbf{x}+\boldsymbol{\xi}^{(0)})$, that is "closer" to the first image, $I_1(\mathbf{x})$. Further cross-correlations are run between $I_1(\mathbf{x})$ and $I_2(\mathbf{x}+\boldsymbol{\xi})$ to produce subsequent estimates, $\boldsymbol{\xi}^{(n)}$. A similar process for determining the displacement field in DPIV, but without FFT's, is outlined in Huang (1994) and termed, "Particle Image Distortion". A fast version, termed, "Lagrangian Particle Tracking", was introduced by Sholl & Savas (1997). In these implementations, the deduced displacement field was specified in terms of local Taylor expansions, to first and second order, respectively. The ICV initialization step starts with large cross-correlation windows (up to 256×256 pixels, or $1/4 \times 1/4$ the image domain, for example) to avoid spurious correlations and to pick up any large displacements. This initialization step is particularly important if there are displacements greater than half the characteristic length of a continuous scalar used to mark the flow (equivalent to a Nyquist criterion). Small-scale features of the velocity field are determined in subsequent stages. This aspect is particularly important, in as much as the subsequent minimization stages may not correct for errors introduced at this stage, and a *local* minimum of $\mathcal{J}(\boldsymbol{\xi})$ might be found instead. Once large-scale displacements have been found with such windows, the size of the window is successively reduced by a factor of 2, cross-correlations are performed, and the corresponding B-spline parameters are computed to yield the next window-size estimates of the displacement (mapping) field. These successive halvings continue until a user-determined minimum window size is reached.

The displacement field, $\boldsymbol{\xi}$, produced by the cross-correlation sequence is used to initialize an iterative minimization procedure. The projection of the displacement field on the set of B-spline basis functions (*cf.* Eq. 10 and discussion in Gornowicz 1997) converts the integral $\mathcal{J}$ to be minimized from a functional of $\boldsymbol{\xi}$ to a function of the finite number of B-spline control parameters (*cf.* Eq. 11), as noted above. The required minimization of $\mathcal{J}$ is now performed in a finite-dimensional space.

An important part of the ICV implementation is the accommodation of appropriate boundary conditions. The inferred flow fields are typically elliptic, so the choice of appropriate boundary conditions is important. Especially important is the inference of flows in the vicinity of no-slip boundaries, an area that is typically not very well resolved by DPIV-correlation methods. The hierarchical B-spline representation allows for the appropriate definition of control points, formally exterior to

the correlation domain, such that the displacement field on the boundaries has the requisite boundary properties. This and other details are discussed in Gornowicz (1997).

III.4.3 Applications

The ICV methodology was first tested and developed on a simulated flow around a free Lamb-Oseen vortex. Specifically, a measured scalar field was convected with the analytical displacement field for this flow and ICV was employed to assess the ability to infer the flow field from the pair of images. Results were very good, permitting measurement of the velocity with a 0.4%-rms error and the vorticity, with a 0.6%-rms error.

The ability to incorporate boundary conditions was tested with a simulated laminar-boundary-layer profile. This was also used as a test case for the multiresolution hierarchical B-spline displacement field representation.

The main application study of the ICV methodology was flow around an accelerating NACA–0012 airfoil at low Reynolds numbers. Experiments were specially-designed to provide images using both nearly-neutrally-buoyant particles and fluorescent dye. This flow has not be measured to date and is very difficult to capture with conventional techniques. The results were compared to preliminary Direct Numerical Simulations (DNS) of two-dimensional flow by Ron Henderson (unpublished). The comparison with the DNS calculations indicates very good qualitative agreement with the measurements, with differences suggesting that this flow is almost impossible to maintain as a two-dimensional flow in the laboratory. ICV was also used in the study of a three-dimensional transverse jet in a cross flow and successfully employed in the construction of three-dimensional isosurfaces in turbulent jets.

III.5 Numerical simulation of flows with strong fronts

Work on the numerical simulation of flows with strong fronts continued, based on the ideas and simulation technology in terms of Riemann Invariant Manifolds (Lappas 1993, developed under a previous AFOSR grant, Lappas *et al.* 1993, and Lappas *et al.* 1998). In particular, under co-sponsorship of Grant F49620–94–1–0353, this numerical-simulation methodology was extended to flow systems with source terms in the equations of motion, as occur in chemically-reacting systems (Papalexandris 1997), for example. The new developments permitted reliable simulations of unstable (underdriven) one-dimensional detonation phenomena, using a Zeldovich-von Neuman-Doering, one-step chemical-reaction (ZND) detonation model (Papalexandris *et al.* 1997a), and, more recently, the extension to two-dimensional detonations (Papalexandris *et al.* 1997b).

A key element in these developments has been the extension of the classical theory of characteristics, permitting the numerical simulation of various strong-front phenomena without resorting to dimensional- as well as flow/chemistry-operator splitting. By way of example, this permitted the simulation of one- and two-dimensional detonation phenomena with a general, mathematically-constistent set of equations, without resorting to added numerical viscosity or other numerical-dissipation artifices.

III.6 References

ADRIAN, R. J. 1991 "Particle-Imaging Techniques for Experimental Fluid Mechanics," *Ann. Rev. Fluid Mech.* **23**, 261–304.

BARRON, J. L., FLEET, D. J. & BEAUCHEMIN, S. S. 1994 "Performance of Optical Flow Techniques," *Int. J. Comp. Vision* **12**, 43–77.

BOND, C. L. 1998 *Reynolds Number Effects on Mixing in the Turbulent Shear Layer*, Ph.D. thesis, California Institute of Technology.

BROWN, G. L. & ROSHKO, A. 1974 "On Density Effects and Large Structure in Turbulent Mixing Layers," *J. Fluid Mech.* **64**, 775–816.

DAHM, W. J. A., SOUTHERLAND, K. B. & BUCH, K. A. 1991 "Direct, high resolution, four-dimensional measurements of the fine scale structure of $Sc \gg 1$ molecular mixing in turbulent flows," *Phys. Fluids A* **3**(5, Pt. 2), 1115–1127.

DAHM, W. J. A., SU, L. K. & SOUTHERLAND, K. B. 1992 "A scalar imaging velocimetry technique for fully resolved four-dimensional vector velocity measurements in turbulent flows," *Phys. Fluids A* **4**(10), 2191–2206.

DAHM, J. A., SU, L. K. & TACINA K. M. 1996 "Four-Dimensional Measurements of Vector Fields in Turbulent Flows," (invited paper) *AIAA* 27th *Fluid Dynamics Conference*, Paper 96–1987.

DIMOTAKIS, P. E. 1986 "Two-Dimensional Shear-Layer Entrainment," *AIAA J.* **24**, 1791–1796.

DIMOTAKIS, P. E. 1991 "Turbulent Free Shear Layer Mixing and Combustion," *High Speed Flight Propulsion Systems*, in *Progress in Astronautics and Aeronautics* **137**, Ch. 5, 265–340.

GORNOWICZ, G. G. 1997 *Continuous-field Image-Correlation Velocimetry and its Application to Unsteady Flow Over an Airfoil*, California Institute of Technology, Aeronautical Engineer's thesis.

HALL, J. L. 1991 *An Experimental Investigation of Structure, Mixing and Combustion in Compressible Turbulent Shear Layers*, Ph.D. thesis, California Institute of Technology.

HALL, J. & DIMOTAKIS, P. E. 1989 "Design Overview of the Supersonic Hydrogen-Fluorine Facility (V4.0)," GALCIT Internal Report, 30 August 1989.

HALL, J. L., DIMOTAKIS, P. E. & ROSEMANN, H. 1993 "Experiments in non-reacting compressible shear layers," *AIAA J.* **31**, 2247–2254.

HORN, B. K. P. & SCHUNCK, B. G. 1981 "Determining Optical Flow," *Artificial Intelligence* **17**, 185–203.

HUANG, M.-J. 1994 "Theoretical and Computational Studies of Isotropic Homogeneous Turbulence," California Institute of Technology, Ph.D. thesis.

KOOCHESFAHANI, M. M. & DIMOTAKIS, P. E. 1986 "Mixing and chemical reactions in a turbulent liquid mixing layer," *J. Fluid Mech.* **170**, 83–112.

LAPPAS, T. 1993 *An Adaptive Lagrangian Method for Computing 1-D Reacting Flows and the Theory of Riemann Invariant manifolds for the Compressible Euler Equations*, Ph.D. thesis, California Institute of Technology.

LAPPAS, T., LEONARD, A. & DIMOTAKIS, P. E. 1993 "An Adaptive Lagrangian Method for Computing 1-D Reacting and Non-Reacting Flows," *J. Comp. Phys.* **104**, 361–376.

LAPPAS, T., LEONARD, A. & DIMOTAKIS, P. E. 1998 "Riemann invariant manifolds for the multidimensional Euler equations," *SIAM J. Sci. Comp.* (accepted).

LU, G. & LELE, S. K. 1994 "On the density ratio effect on the growth rate of a compressible mixing layer," *Phys. Fluids* **6**, 1073–1075.

PAPALEXANDRIS, M. V. 1997 *Unsplit Numerical Schemes for Hyperbolic Systems of Conservation Laws with Source Terms*, California Institute of Technology, Ph.D. thesis.

PAPALEXANDRIS, M. V., LEONARD, A., & DIMOTAKIS, P. E. 1997 "Unsplit Schemes for Hyperbolic Conservation Laws with Source Terms in One Space Dimension," *J. Comp. Phys.* **134**, 31–61.

PAPALEXANDRIS, M. V., LEONARD, A. & DIMOTAKIS, P. E. 1997 "Unsplit schemes for multi-dimensional systems of hyperbolic conservation laws with source terms," *J. Comp. Phys.* (submitted).

PAPAMOSCHOU, D. 1989 "Structure of the compressible turbulent shear layer," *AIAA* 27$^{\text{th}}$ *Aerospace Sciences Meeting*, Paper 89–0126.

PEARLSTEIN, A. J. & CARPENTER, B. N. 1995 "On the determination of solenoidal or compressible velocity fields from measurements of passive or reactive scalars," *Phys. Fluids A* **7**(4), 754–763.

PEPIN, F. E. & DIMOTAKIS, P. E. 1989 "The DUCT Solver," California Institute of Technology, Internal CADRE Report.

SHOLL, M. & SAVAS, Ö. 1997 "A Fast Lagrangian PIV Method for Study of General High-Gradient Flows," *AIAA* 35$^{\text{th}}$ *Aerospace Sciences Meeting*, Paper 97–0493.

SIVELLS, J. C. 1978 "A computer program for the aerodynamic design of axisymmetric and planar nozzles for supersonic and hypersonic wind tunnels," AEDC–TR–78–63.

SLESSOR, M. D. 1998 *Aspects of turbulent-shear-layer dynamics and mixing*, CIT, Ph.D. thesis.

SLESSOR, M. D., BOND, C. L. & DIMOTAKIS, P. E. 1998 "Turbulent shear-layer mixing at high Reynolds numbers: effects of inflow conditions," GALCIT Report FM98–1.

SLESSOR, M. D., ZHUANG, M. & DIMOTAKIS, P. E. 1998 "Turbulent shear-layer mixing: growth-rate compressibility scaling," GALCIT Report FM98–9.

SU, L. K. & DAHM, W. J. A. 1995 *Scalar Imaging Velocimetry and Its Application in Measurements of the Structure and Dynamics of the Complete Velocity Gradient Tensor in Turbulent Flows*, Ph.D. thesis, University of Michigan.

TOKUMARU, P. T. & DIMOTAKIS, P. E. 1995 "Image Correlation Velocimetry," *Exps. in Fluids* **19**(1), 1–15.

WHITE, F. M. 1974 *Viscous Fluid Flow* (McGraw-Hill, New York).

WILLERT, C.E. & GHARIB, M. 1991 "Digital particle image velocimetry," *Exps. in Fluids* **10**, 181–193.

WILLICK, D. & YANG, Y.-H. 1991 "Experimental Evaluation of Motion Constraint Equations," *CVGIP: Image Understanding* **54**(2), 206–214.

ZHOU, Z., SYNOLAKIS, C. E., LEAHY, R. M. & SONG, S. M. 1995 "Calculation of 3D internal displacement fields from 3D X-ray computer tomographic images," *Proc. Roy. Soc. London* A **449**, 537–554.

III.7 Personnel

Personnel supported by this Grant

- Bond, C. L., Graduate Research Assistant, Aeronautics, Caltech.
- Catrakis, H. J., Research Fellow, Aeronautics — presently, Assistant Professsor, U. C. Irvine.
- Chase, S. M., Undergraduate Research Assistant — through June 1997.
- Dahl, E. E., Member of the Technical Staff, Aeronautics.
- Dimotakis, P. E., John K. Northrop Professor of Aeronautics & Professor of Applied Physics (PI).
- Fourguette, D. C., Senior Research Fellow, Aeronautics — through Nov 1996. Presently with Rice Systems, Inc.
- Gornowicz, G. G., Graduate Research Assistant, Aeronautics — through June 1997. Presently with DreamWorks SKG (Glendale, CA).
- Lang, D. B., Research Engineer, Aeronautics.
- Leonard, A., Professor, Aeronautics (Co-PI).

- Papalexandris, M. V., Graduate Research Assistant, Aeronautics — presently with the Jet Propulsion Laboratory.
- Shan, J. W., Graduate Research Assistant, Aeronautics.
- Shekar, Kiran, Undergraduate Research Assistant — through June 1997.
- Slessor, M. D., Graduate Research Assistant, Aeronautics.
- Svitek, P., Staff Engineer.

Other collaborators

- Cook, A. W., Lawrence Livermore National Laboratory.
- Cook, Grant, Lawrence Livermore National Laboratory.
- Collins, S. A., JPL (digital imaging).
- Egolfopoulos, F. N., Associate Professor, Mech. Eng., USC.
- Elliot, T., JPL (digital imaging).
- Meiron, D. I., Professor Applied Mathematics, Caltech.
- Miller, P. L., Lawrence Livermore National Laboratory.
- Wadsworth, M., JPL (digital imaging).

III.8 Publications of work supported by this Grant

Publications and reports submitted, accepted, or published of work performed under sponsorship of this grant:

BOND, C. L. & DIMOTAKIS, P. E. 1996 "Molecular mixing in high Reynolds number, subsonic, free shear layers," Fall Technical Meeting, Western States Section (Combustion Institute), 28–29 October 1996 (U. So. California), Paper 96F–099.

BOND, C. L., SLESSOR, M. D. & DIMOTAKIS, P. E. 1997 "Measurements of molecular mixing in subsonic high-Reynolds-number shear layers," *Am. Phys. Soc.* 50^{th} *Annual Meeting, Division of Fluid Dynamics* (San Francisco, CA, 23–25 November 1997).

DIMOTAKIS, P. E. 1997 "Non-premixed hydrocarbon flame," *Nonlinearity* **7**, 1–2.

DIMOTAKIS, P. E., CATRAKIS, H. J. & FOURGUETTE, D. C. 1998 "Beam Propagation and Phase-Front Integrals in High Reynolds Number Shear Layers and Jets," *AIAA* 29$^{\text{th}}$ *Plasmadynamics and Lasers Conference*, Paper 98–2833.

GORNOWICZ, G. G. 1997 *Continuous-field Image-Correlation Velocimetry and its Application to Unsteady Flow Over an Airfoil*, California Institute of Technology, Aeronautical Engineer's thesis.

GORNOWICZ, G. G. & DIMOTAKIS, P. E. 1995 "Continuous-field image correlation velocimetry," *Bull. Am. Phys. Soc.* **40**(12), 2000.

LAPPAS, T., LEONARD, A. & DIMOTAKIS, P. E. 1998 "Riemann invariant manifolds for the multidimensional Euler equations," *SIAM J. Sci. Comp.* (accepted).

PAPALEXANDRIS, M. V. 1997 *Unsplit Numerical Schemes for Hyperbolic Systems of Conservation Laws with Source Terms*, California Institute of Technology, Ph.D. thesis.

PAPALEXANDRIS, M. V., LEONARD, A. & DIMOTAKIS, P. E. 1995 "An unsplit scheme for 1-D unsteady chemically-reacting flows," *SIAM Annual Meeting* (23–26 October 1995, Charlotte, NC), to appear.

PAPALEXANDRIS, M. V., LEONARD, A., & DIMOTAKIS, P. E. 1996 "Unsplit Schemes for Hyperbolic Conservation Laws with Source Terms in One Space Dimension," California Institute of Technology, GALCIT Report FM96–1.

PAPALEXANDRIS, M. V., LEONARD, A., & DIMOTAKIS, P. E. 1997 "Unsplit Schemes for Hyperbolic Conservation Laws with Source Terms in One Space Dimension," *J. Comp. Phys.* **134**, 31–61.

PAPALEXANDRIS, M. V., LEONARD, A. & DIMOTAKIS, P. E. 1997 "Unsplit schemes for multi-dimensional systems of hyperbolic conservation laws with source terms," *Am. Phys. Soc.* 50$^{\text{th}}$ *Annual Meeting, Division of Fluid Dynamics* (San Francisco, CA, 23–25 November 1997).

PAPALEXANDRIS, M. V., LEONARD, A. & DIMOTAKIS, P. E. 1997 "Unsplit schemes for multi-dimensional systems of hyperbolic conservation laws with source terms," *J. Comp. Phys.* (submitted).

SHAN, J. W., LAIDLAW, D. H., GORNOWICZ, G. G., LANG, D. B. & DIMOTAKIS,

P. E. 1997 "Three-dimensional space-time structure of turbulent jets," *Am. Phys. Soc.* 50th *Annual Meeting, Division of Fluid Dynamics* (San Francisco, CA, 23–25 November 1997).

SLESSOR, M. D. 1998 *Aspects of turbulent-shear-layer dynamics and mixing*, CIT, Ph.D. thesis.

SLESSOR, M. D., BOND, C. L. & DIMOTAKIS, P. E. 1998 "Turbulent shear-layer mixing at high Reynolds numbers: effects of inflow conditions," GALCIT Report FM98–1.

SLESSOR, M. D. & DIMOTAKIS, P. E. 1994 "Experiments on bi-supersonic turbulent shear layers," *Bull. Am. Phys. Soc.* **39**(9), 1880.

SLESSOR, M. D. & DIMOTAKIS, P. E. 1995 "Some new compressible mixing-layer experiments," *Bull. Am. Phys. Soc.* **40**(12), 1975.

SLESSOR, M. D., ZHUANG, M. & DIMOTAKIS, P. E. 1998 "Turbulent shear-layer mixing: growth-rate compressibility scaling," GALCIT Report FM98–9.

TOKUMARU, P. T. & DIMOTAKIS, P. E. 1995 "Image Correlation Velocimetry," *Exps. in Fluids* **19**(1), 1–15.

III.9 Interactions/transitions

Visits/interactions/participation/presentations at meetings, conferences, seminars:

- Stefan Deusch (ETH, Zurich): Discussions on Image Correlation Velocimetry methodology (November 1996 visit).
- P. E. Dimotakis, M. D. Slessor, A. Leonard: Attended 49th APS/DFD meeting (Syracuse, NY), 24-26 November 1996 (2 presentations of work sponsored under this Grant).
- P. Dimotakis: "Turbulent mixing in high-speed shear-layer flows," GALCIT Seminar (10 January 1997), Arizona S.U. (March 1997), and U.C. San Diego (26 August 1997).
- A. Leonard: "LES model for scalar transport." Invited talk, AIAA (Reno, NV, January 1997). Also, later, at U.C. Irvine, and U.C. Santa Barbara.

- M. V. Papalexandris: "Unsplit numerical scheme for hyperbolic systems of equations," GALCIT seminar (9 May 1997).
- A. Leonard: "Recent advances in high-resolution vortex methods for incompressible flows," invited talk, AIAA 13th CFD Conference (Snowmass, Colorado, 29 June - 2 July 1997).
- Prof. H. Lam (Princeton U.): Discussions on reduced-chemistry methods for numerical simulation of chemically-reacting flows (4–8 August 1997 visit to Caltech).
- Prof. Paul Clavin (U. Marseilles): Discussions on detonation (August 1997 visit by P. Dimotakis to UCSD).
- Prof. Amable Liñan (Spain): Discussions on turbulent mixing (August 1997 visit by P. Dimotakis to UCSD).
- Prof. Forman Williams (UCSD): Discussions on turbulent mixing, energy equation in chemically-reacting flows, detonations (August 1997 visit by P. Dimotakis to UCSD).

Consultative and advisory functions to other labs, agencies, especially AF and DoD (include institutions, locations, dates, names):

- P. E. Dimotakis: Lawrence Livermore National Laboratories. Consulting on compressible turbulence, inertial-confinement fusion, high-fluence laser-doubling crystal growth.
- P. E. Dimotakis: Member of NAS/NRC Committee that reviewed DOE's Inertial Confinement Fusion (ICF) Program and the National Ignition (NIF) Facility. Work completed August 1997.
- P. E. Dimotakis: Membership to Mitre/JASON group (July 1997 –).

Transitions (cases where knowledge resulting from this research is used or will be used in a technology application): None

New discoveries, inventions, patents: None

III.10 Honors/awards

Honors, degrees, and awards received during period, as well as, 'lifetime achievement honors such as Nobel prize, honorary doctorates, and society fellowships prior to this effort':

- Catrakis, H. J.:
  - Ph.D., California Institute of Technology (June 1996).
  - Assistant Professor, U. C. Irvine (starting July 1998).
- Chase, S. M.: B.Sc., California Institute of Technology (June 1997).
- Dimotakis, P. E.:
  - Fellow, Am. Phys. Society (November 1980).
  - Associate Fellow, AIAA (June 1989).
  - John K. Northrop Chair, Aeronautics, Caltech (February 1995).
  - Invited plenary speaker, NATO Advanced Studies Institute Series (Cargese, Corsica, July 1996).
  - Invited plenary speaker, Am. Phys. Soc., Fluid Dynamics Meeeting (San Francisco, CA, November 1997).
  - Invited plenary speaker, 2^{nd} AIAA Theoretical Fluid Mechanics Meeting (Albuquerque, NM, June 1998).
- Gornowicz, G. G.: A.E., California Institute of Technology (June 1997).
- Leonard, A.:
  - Fellow, Am. Phys. Society.
  - Vice-Chair, Am. Phys. Society, Division of Fluid Dynamics (1997).
  - Chair, Am. Phys. Society, Division of Fluid Dynamics (1998).
- Papalexandris, M. V.:
  - Ph.D., California Institute of Technology (June 1997).
  - Ballhaus Prize, California Institute of Technology (best thesis, June 1997).
- Slessor, M. D.:
  - Charles Babcock Memorial Award, Caltech (June 1994).
  - Ph.D., California Institute of Technology (June 1998).

Chapter IV: CHEMISTRY IN NONUNIFORM FLOW

IV.1 DISSOCIATION RATES WITH VIBRATIONAL NONEQUILIBRIUM

Accomplishments / New Findings

One of the primary uncertainties in the modeling of hypersonic reacting flows is how the vibrational state of a molecule affects its dissociation rate. Therefore, the main objective of this research is to test chemical reaction rate models in the presence vibrational nonequilibrium. Our initial work showed that the flow of nitrogen over spheres at typical T5 conditions is not very sensitive to the choice of several popular vibration-dissociation coupling models. Therefore, we used computational fluid dynamics to design new experiments that show strong sensitivity to the coupling model. We found that double-wedge and double-cone geometries are good candidates, and they have been tested in the Caltech Free-Piston Shock Tunnel, T5. The results have been analyzed, and we find that the numerical simulations cannot reproduce the experimental data under any conditions of interest. The possible reasons for this strong disagreement are briefly discussed here; further details may be found in our recent publications.

The experimental configurations are either double-wedge or double-cone geometries; the first cone or wedge causes an attached shock wave to form which interacts with the detached shock from the second wedge or cone. This interaction creates a complicated flow field that is very sensitive to the vibration-dissociation coupling model. Typically, the popular Park $\sqrt{TT_v}$ coupling model, see Park (1988), produces a flow field with a smaller separation zone than the Treanor and Marrone CVDV model, see Treanor and Marrone (1962). The difference in the separation zone size causes a large change in the surface pressure and convective heating rate distributions.

Two sets of experiments were performed. The first used a finite-length double-wedge geometry instrumented with pressure and heat transfer gauges, and the second used a series of double cones. As an example of the results, consider the double-cone geometry, Shot 1271. The free-stream conditions for this case are $u_\infty = 6340\,\mathrm{m/s}$, $\rho_\infty = 0.0046\,\mathrm{kg/m^3}$, $c_{\mathrm{N}\infty} = 0.196$, and $h_o = 30.8\,\mathrm{MJ/kg}$. The first cone angle is 25°, and the second cone angle is 65°. Figure 1 shows the experimental interferogram, and Fig. IV.2 is the interferogram computed using the Park $\sqrt{TT_v}$ vibration-dissociation coupling model and the standard dissociation rates for nitrogen. It should be noted that the flow fields obtained using the CVDV model or the Macheret and Rich model are not significantly different than those obtained with the Park model. The experimental and computational interferograms have the same

general features but differ in the details. The size of the computed separation zone is too small, which changes the location of the shock impingement point on the second cone. There also appears to be about half a fringe missing in the computation. We find that for this case, if we increase the nitrogen dissociation rate by an arbitrary factor of four at all temperatures, the computational interferogram agrees fairly well with the experimental data. However, the factor required to obtain reasonable agreement varies from case to case. In general, the standard dissociation rates and existing vibration-dissociation coupling models cannot reproduce the experimental flow fields.

We have made careful studies to eliminate other possible sources of error that might cause the observed differences. We have varied the free-stream conditions in the computations to make sure that uncertainties in the reservoir conditions are not the source of the differences. We have made careful sensitivity studies of the grid resolution, the mass diffusion models, and the model surface boundary conditions. The experimental interferograms were made after a large number of characteristic flow times, but before driver gas contamination; therefore the flow has had plenty of time to establish itself. Also, the Reynolds number is low enough that the shear layers in the separation zone must be laminar. It should be noted that the same numerical method is being used to study double-cone flows in the Princeton University low-enthalpy Mach 8 Tunnel. Excellent agreement between the experiments and the calculations was been obtained under these non-reacting conditions for the small separation regions. However when the separation zone is a significant fraction of the body dimension, the computations do not agree with the experiment very well. In this case, the disagreement may be due to effects of turbulence that are not modeled in the simulations.

Thus, we can identify several things that may be causing the lack of agreement between the computations and the experiment:

- Uncertainties in the equilibrium dissociation rate because the rates inferred from the shock-tube experiments are wrong.
- The vibration-dissociation effects that occur in the double-cone flows cannot be captured by the present models that implicitly assume a Boltzmann distribution of the vibrational states.
- The computational fluid dynamics method does not work for highly separated hypersonic flows. It is postulated that the numerical error that is generated in the vicinity of the shock interaction location is swept into the separation zone where it is trapped. It then causes the separation zone to increase in size, strengthening the interaction. This assertion is supported by the fact that other researchers have been unable to reproduce these flows with a wide variety of computational fluid dynamics methods.

More work is required to determine which of these difficulties is the source of the differences, and how to remedy the problem. At this point, the failure of the computational fluid dynamics method for separated flows is the primary suspect. This work shows that our current ability to predict complex hypersonic flows is still questionable at best.

Figure IV.1. Experimental interferogram for Shot 1271; only part of the second cone is visible.

Personnel Supported

Graham V. Candler, Associate Professor of Aerospace Engineering and Mechanics, University of Minnesota.

Joseph Olejniczak, Graduate Research Assistant, Department of Aerospace Engineering and Mechanics, University of Minnesota.

References

Edney, B. E., "Effects of shock impingement on the heat transfer around blunt bodies," *AIAA J*, **6**, 1968, pp. 15–21.

Park, C., "Assessment of a two–temperature kinetic model for dissociating and weakly ionizing nitrogen," *J. Thermophys. and Heat Transf.*, **2**, 1988, pp.2–4.

Treanor, C. E., and P. V. Marrone, "Effect of dissociation on the rate of vibrational relaxation," *Phys. Fluids*, **2**, 1962, p.442.

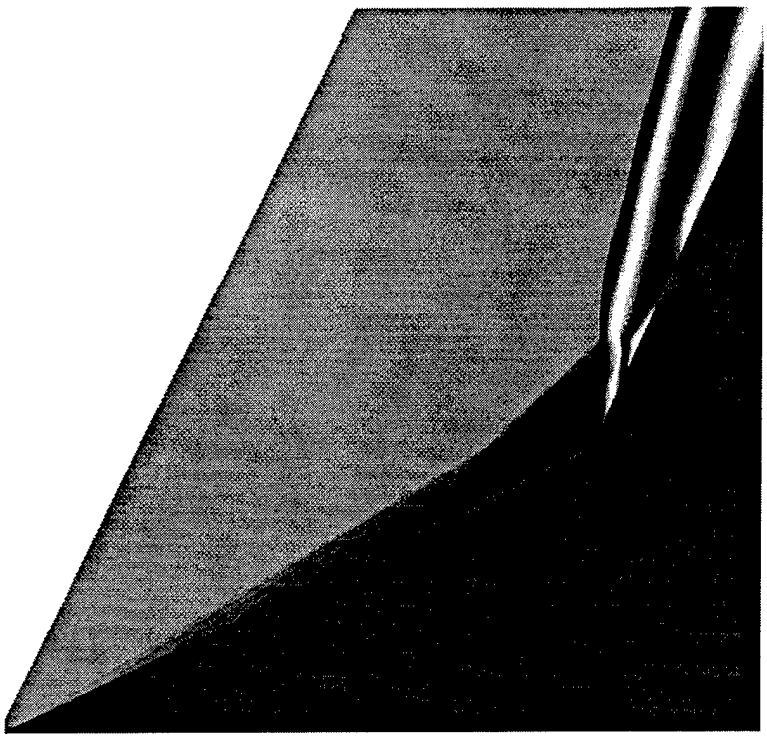

Figure IV.2. Computational interferogram for Shot 1271 with the nominal dissociation rate expression and the Park model.

Publications Resulting from Research

Olejniczak, J., G.V. Candler, H.G. Hornung, and C. Wen, "Experimental Evaluation of Vibration-Dissociation Coupling Models," *AIAA Paper No. 94-1983,* June 1994.

Olejniczak, J., and G.V. Candler, "Study of Experiments Sensitive to Vibration-Dissociation Coupling Models," 20th International Symposium on Shock Waves, July 1995.

Olejniczak, J., and G.V. Candler, "Vibrational Energy Conservation with Vibration-Dissociation Coupling: General Theory and Numerical Studies," *Physics of Fluids,* Vol. 7, No. 7, pp. 1764-1774, July 1995.

Olejniczak, J., M.J. Wright, and G.V. Candler, "Numerical Study of Shock Interactions on Double-Wedge Geometries," *AIAA Paper No. 96-0041,* Jan. 1996.

Olejniczak, J., and G.V. Candler, "High Enthalpy Double-Wedge Experiments," *AIAA Paper No. 96-2238,* June 1996.

Wright, M.J., J. Olejniczak, G.V. Candler, T. Magruder, and A. Smits, "Numerical and Experimental Investigation of Double-Cone Shock Interactions," *AIAA Paper No. 97-0063,* Jan. 1997.

Candler, G.V., and J. Olejniczak, "Nitrogen Dissociation Rates in Complex Hypersonic Flows," *AIAA Paper No. 97-2500,* June 1997.

Olejniczak, J., and G.V. Candler, "Computation of Double-Cone Experiments in High Enthalpy Nitrogen," *AIAA Paper No. 97-2529,* June 1997.

Candler, G.V., J. Olejniczak, and B. Harrold, "Detailed Simulation of Nitrogen Dissociation in Stagnation Regions," *Physics of Fluids,* Vol. 9, No. 7, pp. 2108-2117, July 1997. Also *AIAA Paper No. 96-2025,* June 1996.

Olejniczak, J., M.J. Wright, and G.V. Candler, "Numerical Study of Inviscid Shock Interactions on Double-Wedge Geometries," *Journal of Fluid Mechanics,* Vol. 352, pp. 1-25, 10 Dec. 1997.

Olejniczak, J., and G.V. Candler "Computation of High Enthalpy Shock Interaction Flow Fields," *AIAA Paper No. 98-2446,* June 1998.

Olejniczak, J., G.V. Candler, and H.G. Hornung, "An Experimental and Computational Study of High Enthalpy Double-Wedge Flow Fields," submitted to *AIAA Journal,* July 1998.

Olejniczak, J., G.V. Candler, and H.G. Hornung, "Computation of of Double-Cone Experiments in High Enthalpy Nitrogen," in preparation.

Interactions/Transitions

Presentation of papers at:

6th AIAA/ASME Joint Thermophysics and Heat Transfer Conference, Colorado Springs, CO, June 1994.

2nd European Symposium on Aerothermodynamics for Space Vehicles, Noordwijk, The Netherlands, Nov. 1994.

Von Karman Institute for Fluid Dynamics, Rhode-St. Genèse, Belgium, April, 1995.

NATO Advanced Study Institute on Molecular Physics and Hypersonic Flows, Maratea, Italy, May, 1994.

20th International Symposium on Shock Waves, Pasadena, CA, July 1995.

34th AIAA Aerospace Sciences Meeting, Reno, NV, Jan. 1996.

27th AIAA Fluid Dynamics Conference, New Orleans, LA, June 1996.

19th AIAA Advanced Measurement and Ground Testing Technology Conference, New Or-

leans, LA, June 1996.

31st AIAA Thermophysics Conference, New Orleans, LA, June 1996.

Plasma Based Hypersonic Drag Reduction Workshop, Wright-Patterson AFB, OH, May 1996.

NASA Ames Research Center, Moffett Field, CA, April 1996.

Army High Performance Computing Research Center Seminar, Minneapolis, MN, April 1996.

27th AIAA Fluid Dynamics Meeting, New Orleans, LA, June 1996.

Princeton University, Princeton, NJ, Nov. 1996.

35th AIAA Aerospace Sciences Meeting, Reno, NV, Jan. 1997.

University of Maryland, College Park, MD, Feb. 1997.

32nd AIAA Thermophysics Conference, Atlanta, GA, June 1997.

NASA Ames Research Center, Moffett Field, CA, Sept. 1997.

33rd AIAA Thermophysics Conference, Albuquerque, NM, June 1998.

Consultative Functions:

G.V. Candler discussed recent simulations of hypersonic separated flows with NASA Ames Research Center personnel. Possible ballistic range experiments are under consideration.

Transitions: None

New Discoveries

The computational work used to design the experimental configurations for vibration-dissociation model testing resulted in the discovery of a new shock-shock interaction that occurs in hypersonic flows. This interaction is similar to the Type IV interaction of Edney (1968), and results in very large surface pressure and heat transfer variations on the body surface. This effect could be important in the design of control surfaces for hypersonic vehicles.

Recent calculations indicate that standard, widely-used computational fluid dynamics (CFD) methods may break down in massively separated regions in hypersonic flows. It is postulated that this occurs because numerical error builds up in the separated region.

Honors/Awards: None.

IV.2 ELECTRON-DRIVEN REACTIONS IN HYPERSONIC FLOW

Background and Objective

Electrons produced in the bow shock of vehicles can play an important role in determining the chemical and physical properties of hypersonic flowfields. Due to non-equilibrium overshoots, electron temperatures can rise above 10,000 K in these flowfields. Furthermore, as flight velocities increase, electron collisions become more important. Electron collision data needed in simulations of these flowfields are very fragmentary and often not available. This is particularly true for near-threshold excitation processes where the incident electrons have barely enough energy to drive the excitation and for collisions with metastable species. Measurements of these cross sections at near-threshold impact energies and for low-energies in general are particularly demanding.

Calculations of electron-molecule collisions are also difficult at the low energies of interest in these flowfields. Thus, although the physical principles in low-energy electron-molecule collisions are well understood, and although several methods have been developed for numerical studies of these collisions, progress in their application has been limited. What is required is not just a method and algorithm by which the problem might be solved in principle, but an *implementation that makes relevant problems feasible.* The thrust of our effort has been to develop innovative scalable implementations of our theory of electron collisions[1] – the Schwinger multichannel variational method – with which we could harness the computational power of large parallel computers to obtain electron collision cross sections needed in modelling hypervelocity flows.

Accomplishments

At the low energies of interest in these flowfields, an accurate quantum-mechanical treatment of the full 3(N+1)-dimensional space of the Schrodinger equation that governs the collision of an electron with a molecule with N electrons is necessary; low-order approximations, such as the Born (1926) approximation, are not applicable. Furthermore, because direct integration of Schrödinger's equation in this 3(N+1)-dimensional space is not practical, most recent studies rely on the use of a variational approximation to obtain the scattering amplitudes for these collisions. Our studies are based on the Schwinger multichannel (SMC) method, a modified form of the Schwinger variational principle.[2] The SMC variational principle possesses compelling computational advantages; however, these come at the cost of evaluating a Green's operator whose matrix representation is obtainable only by numerical quadrature of a class of integrals. Indeed, evaluating the data for this quadrature is the principal computational task. This task had also been the bottleneck in previous calculations on sequential computers such as the Cray Y-MP.

We have developed scalable algorithms for the main components of this task – namely,

evaluation of a large number (typically 10^{12} to 10^{15}) of elementary integrals and subsequent linear algebraic manipulations of these integrals.[1] The first of these tasks is perfectly parallel, meaning that on a multiprocessor machine different elementary integrals can be evaluated simultaneously on different processors with effectively zero parallel overhead. Although the second step involves communication and synchronization overheads, it can be formulated in terms of multiplication of large, distributed matrices, a highly efficient procedure on parallel computers. With these scalable algorithms, we routinely achieve aggregate performance in the tens of gigaflop range. This capability, which to our knowledge is unmatched, has allowed us to carry out sophiscated first-principles calculations of electron collisions with species such as N_2, CO, OH, NO, and CO_2.

During the period of this award we have completed the following applications and enhancements of these capabilities:

- We have studied the cross sections for near-threshold excitation of the long-lived $A\,^3\Sigma_u^+$ state of N_2 by electrons. These near-threshold excitation processes are difficult to study experimentally due to the very low post-collision energy of the electron. For this system some limited cross section data based on detection of the metastable state itself is available at about 2 eVs above threshold.[3] Comparison of our calculated cross sections with this data is very encouraging.

- We have completed the first calculation of the cross sections for excitation of the $B\,^3\Pi_g$ state of N_2 by electron impact on its long-lived $A\,^3\Sigma_u^+$ state. We believe that such cross sections for electron impact on electronically excited metastable states can play an important role in modelling the chemical and physical properties of hypersonic flows. These cross sections would be generally inaccessible experimentally. Calculations of these cross sections required significant changes in our computer codes and additional calculations of these cross sections are under way.

- We have studied the cross sections for near-threshold excitation of the lowest lying excited state of OH ($A\,^2\Sigma^+$) by low-energy electrons. OH fragments are produced in flows of interest via dissociation of water vapor. No measured data is available for electron impact on the OH fragment.

- We have completed calculations of the cross sections for electron impact excitation of the $A\,^2\Sigma^+$ state of NO. This upper state is responsible for the γ-band emission which is prominent in the bow shock of flows over hardbodies. There have also been no measurements of these cross sections.

- In a joint effort with the experimental group of Professor H. Ehrhardt of Kaiserslautern University in Germany, we have completed a comprehensive study of the cross sections for electron impact excitation of the low-lying excited states of N_2 and CO from threshold to 3.7 eV above threshold. These studies should provide the most reliable estimates of these cross sections for N_2 and CO in the technically important, but experimentally challenging, near-threshold region. The availability of both differential and integral excitation cross sections offers significant opportunity for an in-depth comparison of the

measured and calculated results. Cross sections have also been calculated for impact energies beyond the threshold region.

- We continue to improve and extend our parallel computer codes for carrying out these calculations. One of the main computational tasks in these calculations is the evaluation of large numbers (trillions or more) of so-called two-electron repulsion integrals involving Cartesian Gaussians and plane-wave functions. Improving the efficiency of the integral evaluation procedure can have a major impact on the speed of these calculations, which often run for hours on large parallel computers. In the past year, a completely new set of subroutines for computing these integrals was written. A key feature of the new routines is that classes of related integrals are treated together, so that many intermediate quantities are computed only once for each class and reused. The new routines also incorporate a pre-screening technique based on rigorous upper bounds that are inexpensive to compute: integrals that would be numerically zero are not computed at all. The combined effect of these two improvements is substantial. In fact, the new routines run from 3 to 5 or more times faster than the old routines.

- To date we have used large parallel computers such as the Cray T3D and Intel Paragon in our studies. These computers consist of hundreds of computational nodes connected by a high-speed communication network to one another and to peripheral devices such as disk storage. With the dramatic improvements in PC performance, a network of mass-market processors such as the 300 MHz Intel Pentium II, interconnected with a 100 Mbits per second ethernet switch, has become a suitable compute-engine for carrying out significant calculations of electron-collision cross sections. We have been awarded an equipment grant of $200,000 from Intel that has enabled us to construct a substantial computer cluster of this kind which we now operate as a virtual parallel computer dedicated to our electron-molecule collision studies.

References

1. M. Born, Zeitschr. f. Physik, **37**, 863 (1926).

2. C. Winstead and V. McKoy, Highly Parallel Computational Techniques for Electron-Molecule Collisions, Adv. At. Mol. Opt. Phys. **36**, 183 (1996).

3. J. Schwinger, Phys. Rev. **72**, 742 (1947).

Publications resulting from research

1. Winstead, C., Lee, C-H., and McKoy, V.,*Electron-Molecule Collisions for Plasma Modelling*, in Parallel Computing for Industrial and Scientific Applications (Morgan-Kaufmann, San Francisco, 1998)

2. McKoy, V., Winstead, C., and Lee, C-H., *Parallel Computing and The Generation of Basic Plasma Data*, J. Vac. Sci. and Tech. A, **16** 324 (1998).

3. Lee, C-H., Winstead, C., and McKoy, V., *Collisions of Low-Energy Electrons with CO_2*, J. Chem. Phys. (1998).

4. Winstead, C., and McKoy, V., *Highly Parallel Computational Techniques for Electron-Molecule Collisions, Advances in Atomic, Molecular, and Optical Physics*, Edited by Bederson, B., and Walther, H. (Academic, 1996), Vol. 36, pp. 183-219.

5. Zobel, J., Mayer, U., Jung, K., Ehrhardt, H., Pritchard, H., Winstead, C., and McKoy, V., *Absolute Differential Cross Sections for Electron Impact Excitation of CO Near Threshold*, J. Phys. B **29**, 839 (1996).

6. da Paixão, F.J., Lima, M.A.P., and McKoy, V., *Elastic Electron-NO Collisions*, Phys. Rev. A **53**, 1407 (1996).

7. Winstead, C. and McKoy, V., *Electron Scattering by Small Molecules*, Advances in Chemical Physics, Edited by I. Prigogine and S.A. Rice (Wiley, 1996).

8. Winstead, C. and McKoy, V., *Studies of Electron-Molecule Collisions on Massively Parallel Computers*, Modern Electronic Structure Theory, Edited by D. Yarkony (World Scientific, 1995).

9. Winstead, C., Pritchard, H.P., and McKoy V., *Electron-Molecule Collisions for Plasma Modelling Experiences on the CRAY T3D, Cray Channels* (Cray Research, Inc., 1995).

10. Winstead, C., Pritchard, H., and McKoy, V., *Parallel Computation of Electron-Molecule Collisions*, IEEE Computational Science and Engineering, Fall Issue, **34** (1995).

Personnel Supported

Principal Investigator: Vincent McKoy, Professor of Theoretical Chemistry

Graduate Student: C-H. Lee

Research Fellow: C. Winstead

Interactions/Transitions

1. Presentation: *Parallel Computing and The Generation of Basic Plasma Data*, Invited Talk at the International Workshop on Basic Aspects of Nonequilibrium Plasmas Interacting With Surfaces, Shirahama, Japan, January 1997.

2. Presentation: *Electron-Molecule Collisions For Plasma Modelling*, Invited talk at the Conference on Multiscale Phenomena in Science and Engineering, Louisiana State University, Baton Rouge, Louisiana, February 1997.

3. Advisory: Member, Wright Laboratory Board of Visitors, Independent Strategic Assessment Group (to Gen. Richard Davis), 1996 - 1997.

4. Presentation: *High-Performance Simulation Tools for Microelectronics Fabrication*, Invited Talk at the Mardi Gras '96 Conference on Experimantal and Simulation Challenges in Nano- Structured Materials, Baton Rouge, LA, February 1996.

5. Advisory: Member, Wright Laboratory Board of Visitors: Independent Strategic Assessment Group (Col. Richard Davis), 1995 - 1996.

6. Presentation: *Some Developments in Simulations of Plasma Reactors*, Invited Talk at the Center for Cooperative Research in Advanced Science and Technology, Nagoya University, Nagoya (Japan), December 1995.

7. Presentation: *The Impact of Parallel Computers: Electron Collision Data for Plasma Modelling*, National Plasma Data Center, Nagoya (Japan), December 1995.

8. Presentation: *Studies of Electron-Molecule Collisions on Highly Parallel Computers*, Invited Talk at the Fourth Conference on Current Trends in Computational Chemistry, US Army Corps of Engineers Waterways Experimental Station, Vicksburg, MS, November, 1995.

9. Presentation: *Studies of Electron-Molecule Collisions on Parallel Computers*, Invited Talk at the 1995 Annual Meeting of the Division of Atomic, Molecular and Optical Physics, American Physical Society, May 1995, Toronto, Canada.

10. Presentation: *Data for Modelling Materials-Processing Plasmas: The Impact of Parallel Computers*, Invited Talk in the High-Performance Computing Seminar Series, National Institute for Standards and Technology, April 1995.

11. Presentation: *Studies of Electron-Molecule Collisions on Highly Parallel Computers*, Bucy Lecture, Texas Tech University, February 1995.

12. Presentation: *Electron-Molecule Collisions for Modelling Plasmas*, Invited Talk at the Mardi Gras '94 Conference"Toward Teraflop Computing and New Grand Challenge Applications", Baton Rouge, 1994.

13. Presentation: *Electron-Molecule Collisions for Modelling Plasmas*, Invited Talk at the High-Performance Computing Symposium, 1994, Simulation MultiConference, La Jolla, 1994.

14. Presentation: *Studies of Electron-Molecule Collisions on Highly Parallel Computers*, Joint Chemical Physics-Mechanical Engineering Seminar, Ohio State University, May 1994.

15. Presentation: *Data for Modelling Materials-Processing Plasmas: The Impact of Parallel Computers*, Invited Talk at the Defense Science Study Group Symposium on Applications of Advanced and Innovative Computational Methods to Defense Science and Engineering, Institute for Defense Analyses, October 1994.

Inventions: None

Honors

B.V. McKoy: Speaker, Distinguished Lecture Series, Louisiana State University, Baton Rouge, LA, 1997; B.V. McKoy: Fellow, American Physical Society, 1986 -

IV.3 NONEQUILIBRIUM LEEWARD SHOCK-VORTEX AERODYNAMICS

The objectives of this research were to study the hypervelocity flow at enthalpy sufficient to activate dissociation/recombination chemistry about blunt-nosed delta-wings and cones at large incidence, with particular reference to the effect of dissociation/recombination chemistry on the structure of the windward and leeward flow regimes. Frozen flows about a blunt nosed delta-wing at large incidence and hypervelocity flows with active equilibrium and non-equilibrium chemistry about a cone at 30^o incidence were computed. These flows included inviscid flow and laminar viscous flows at Reynolds numbers up to $Re = 4.6 \times 10^5$.

IV.3.1 Finite-Volume Solution of Navier-Stokes Equations

Computations were done with the finite volume code PGP3D (Mallett *et al.* 1995) utilizing the EFM (Pullin 1980) and EFMO (Moschetta and Pullin 1997) patch integrators. EFM is a finite volume technique for solving the inviscid Euler equations of compressible ideal gas flow. It is a kinetic-based flux-split method which is extremely robust, can handle very strong shocks well, and does not exhibit some well-known spurious behaviors (e.g. the carbuncle phenomenon, Quirk 1994). It has no fixes or tunable parameters and is entropy-satisfying and positivity-preserving. The EFMO method (for EFM-Osher) is an extension of EFM, developed under the URI program to be a hybrid method incorporating features of both flux-vector schemes and flux-difference schemes. EFMO employs a correction to EFM's tangential momentum flux, yielding a flux-split method with much reduced numerical viscosity.

Computations were done using both implicit and explicit time-marching versions of PGP3D (Mallett et al 1995), the former based on a linearization of the fluxes using an approximate analytical evaluation of the Jacobian. This technique provided a rate of convergence with EFMO comparable to that obtained with EFM, for which the Jacobian is exact. For three-dimensional flow this procedure results in a block hepta-diagonal system of linear equations which must be solved at each time-step, which was done by factorization into tridiagonal systems that are solved by standard methods. The extension of EFM-EFMO to high order of accuracy was achieved using the usual MUSCL technique (see van Leer, 1974), which consists of reconstructing the primitive variables on each side of a given interface where the flux is calculated.

The Lighthill (1957) Ideal Dissociating Gas (IDG) model for pure nitrogen with the Freeman (1958) reaction rate extension was used to represent the chemical dynamics of the flow. This model was chosen because of the desire to assess the first-order effects of chemistry in a complex three-dimensional flow field using an adequate, but computationally tractable, chemistry model. The use of a simple one-temperature model allowed flexibility and multiple runs with available computational resource. The present implementation is described in Shariff and Pullin (1998).

IV.3.2 Hypersonic frozen flows

The PG3D/EFMO code was subject to extensive testing for a variety of supersonic and hypervelocity frozen flows. These flows include viscous flow over a flat plate at zero incidence at at various Mach numbers, the flow over a flat-plate ramp combination at $M = 14.2$ and at a ramp angle of 24^0, and hypersonic viscous cone-flow at zero and at finite incidence (Moshetta and Pullin 1997). In addition extensive calculations were performed for frozen flow about a blunt-nosed delta wing at 30^o in hypersonic flow. These calculations were described briefly in previous reports and in Mallett *et al* (1995).

There is a difficulty in computing viscous cone-flow associated with the presence of a singularity at the cone apex. Several techniques were used to deal with this problem. In the first, the grid is extended to the cone apex ('full grid'). This grid has the disadvantage that cells tend to be very small near the apex. A second method is to perform a prior calculation using the so-called 'step-back' technique, which assumes locally conical flow for all fluid properties, applied at a streamwise station very near the cone apex (i.e. at small Reynolds number), to provide upstream boundary conditions in the region between the bow shock wave and the cone surface. This calculation is followed by a fully three-dimensional time-marched (TM) calculation using an implicit time-stepping method with zone-varying CFL numbers. This 'partial-grid' method is exact for inviscid frozen or equilibrium cone flow and works very well for nonequilibrium inviscid flow past a cone at incidence. A third method is the quasi-conical stepback method applied at several cone stations.

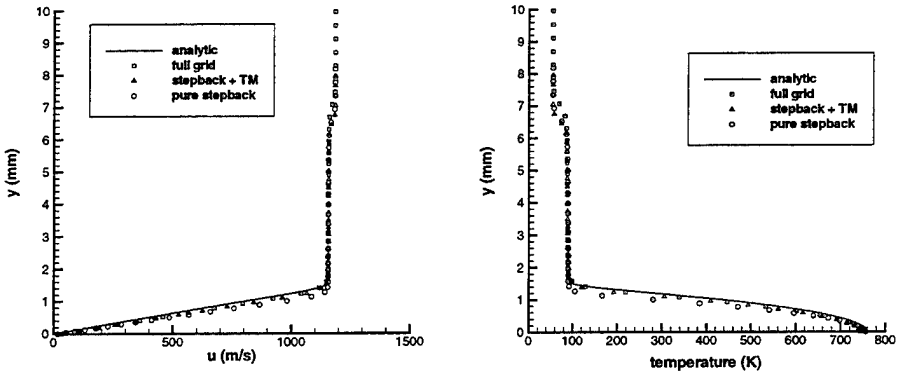

Figure IV.3. Velocity and temperature profiles for a 10^o degree cone at zero incidence, $Re = 4.2 \times 10^5$, freestream $M = 7.95$, $T_\infty = 55.4K$, $U_\infty = 1186.1m/s$, adiabatic wall, $Pr = 1.0$

Fig. IV.3 shows a test of these techniques for frozen flow past a 10^o-half angle cone at zero angle of attack. The freestream Mach number is 7.95. Results are shown for velocity and temperature versus distance from the wall at a station at which the Reynolds number based on distance from the apex is 4.2×10^5. The Prandtl number was $Pr = 1$, and an adiabatic wall boundary condition was used. For comparison purposes, profiles obtained from a separate

numerical integration of the exact flat-plate similarity boundary-layer equations ('analytic') and subsequent application of the Mangler transformation are also displayed. In the near wall boundary layer region the full grid and the 'partial-grid' calculations agree well with the similarity calculation. A calculation based on the stepback method applied directly at the downstream station somewhat underpredicts the boundary layer thickness.

Figures IV.4–IV.6 show results for laminar frozen flow past a 10^o-half angle cone at incidence 24^0, $Pr = 0.72$. The other flow conditions are as above. This case was chosen to match the experimental conditions of Tracy (1964). These calculations were done in high resolution on the Caltech *Delta* parallel machine using the step-back method applied at $x = 0.86\,L$ where L is the cone length. Fig. IV.4 shows Mach number contours compared to results from the pitot-tube survey of Tracy (1964). The angular position of separation can be estimated from the sectional stream-line pattern and is found to be at 26^0 from the leeward symmetry plane compared to 24^0 found by Tracy (1964) from surface stream-line patterns. The thickness of the separated and expanding shear layer is well postdicted, as is the placement and geometry of the leeward flow lambda shock-wave system which sits above the separated shear layer. In Fig. IV.5 we compare surface normalized surface pressure and surface heat transfer with Tracy's data. The results of several different calculations are displayed, including those at two slightly different Mach numbers. All methods give satisfactory agreement with the pressure measurements of Tracy(1964). Surprisingly, the EFM method gives somewhat better comparison to Tracy's experimental results than do the EFMO results.

IV.3.3 EFMO and IDG Chemistry

Computations were performed for comparison with experimental nitrogen data from Krek (1992). These experiments were performed in the T4 shock tunnel at the University of Queensland. The test model was a 15° half-angle cone at 30° incidence in nitrogen. Its length $L = 0.18$ m, and the Reynolds number (based on cone length) for this test was 6.9×10^4. The flow at the end of the shock tube of the T4 tunnel is expanded through a hypersonic nozzle. When the gas enters the nozzle, it is in chemical equilibrium, with a high degree of dissociation. As the gas expands through the nozzle, the species composition departs from equilibrium, with the recombination reaction "freezing". The dissociation rate is highly dependent on the temperature, but the recombination rate depends on density and can be turned off or "quenched" by the expansion. This quenching leaves the gas with a large degree of dissociation, far from equilibrium. When the gas crosses the bow shock of the model, the gas can further dissociate, but the compression of the shock wave reactivates the recombination term of the rate equation, and the chemistry then proceeds as the gas expands toward the leeward plane of symmetry.

This renewed chemical activity presents a problem in terms of utilizing the stepback method (or the partial grid method, since it must start from a stepback solution). Stepback solutions must be either in chemical equilibrium or frozen. In order to apply the stepback method, an equivalent equilibrium flow must be chosen for the freestream. In order to choose these conditions, the non-equilibrium conditions were relaxed by maintaining constant mass, momentum, and enthalpy, while enforcing the law of mass action. Table 1 shows the Krek (1992)

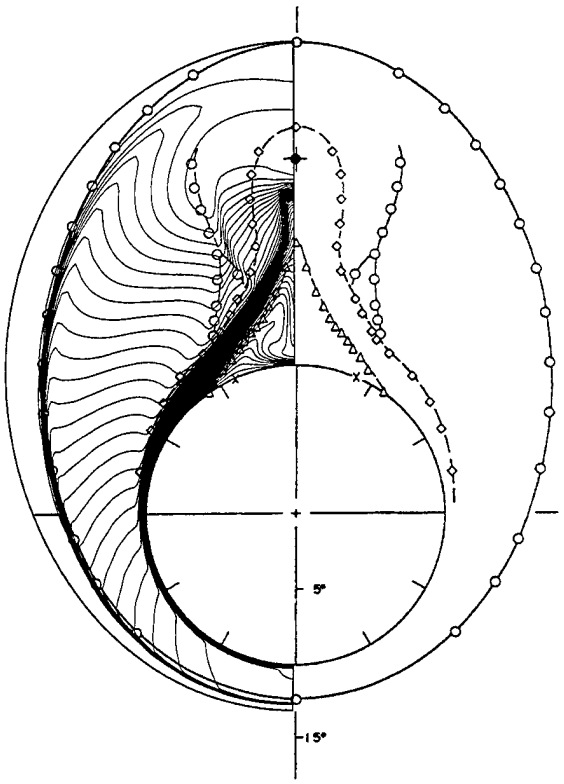

Figure IV.4. Laminar frozen flow past a 10^o degree cone at 24^o incidence, $Re = 3.6 \times 10^5$, $T_\infty = 55.4K$, isothermal wall at $T_w = 317K$, $Pr = 0.72$. Comparison of Mach number contours with pitot-tube survey results of Tracy (1964)

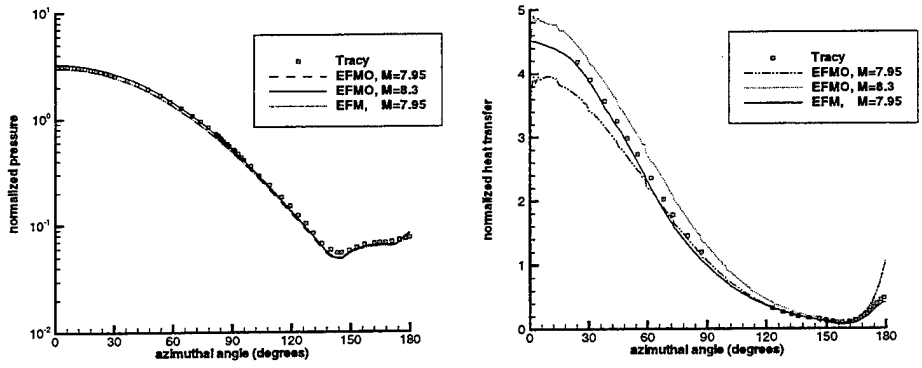

Figure IV.5. Normalized surface pressure and temperature on a 10^o degree cone at 24^o incidence. Tracy(1964) conditions. Tracy normalized pressure is surface pressure times 1000 divided by freestream total pressure . Tracy normalized heat transfer is heat transfer divided by heat transfer for zero incidence cone.

conditions and the calculated equivalent equilibrium conditions.

	Krek conditions	Equiv Equilib. conditions
M_∞	4.57	4.99
ρ (g/m^3)	9.33	9.33
u (m/s)	5683	5683
T (K)	3273	3273
p (kPa)	10.43	9.071
H_0 (MJ/kg)	27.17	20.04
α	0.150	1.15×10^{-4}
Ω	1.23	1.15

Table IV.1. Krek (1992) freestream conditions. $\mathbf{H_0}$ is the stagnation enthalpy, and $\mathbf{\Omega}$ is the Damkohler number.

The non-dimensional Damkohler number Ω is

$$\Omega = \frac{L}{L_s}, \qquad L_s = \frac{1}{U_\infty}\left(\frac{d\alpha}{dt}\right)_f$$

where L is the body length, U_∞ is the freestream velocity and L_s is the chemical relaxation length. $\left(\frac{d\alpha}{dt}\right)_f$ is the reaction rate behind a frozen shock wave, and for this case it is appropriate to use a 45° oblique shock, which is the sum of the cone half-angle and the angle of incidence. This parameter is comparable for the Krek conditions and the equivalent equilibrium conditions, as is seen in Table 1.

Frozen and equilibrium stepback solutions were obtained for each station of Krek's data. An isothermal boundary condition was assumed, with $T_w = 300$ K, since the test time is too short for a rise in the surface temperature to occur. Because of this boundary condition, the temperature gradients in the boundary layer are very large. Several adiabatic simulations were also performed. It was found that having 12-15 cells in the adiabatic boundary layer was sufficient to resolve it, in contrast to the isothermal case, where 25-28 cells in the boundary layer were required for adequate resolution. The isothermal grids were stretched dramatically towards the cone surface, and the bow shock is rather coarsely resolved. However, our main present interest is in the cold-wall, near-surface flow, where the boundary layer is extremely thin, and the thickened shock will still provide appropriate edge conditions. The stepback grids used for these simulations had 45 cells normal to the cone's surface and 100 cells around the cone's surface (and 2 cells in the axial direction). Some of Krek's heat transfer data were normalized by the heat transfer on the cone at zero incidence. These solutions were calculated using the stepback method on grids of resolution (100×2×2). In examining the boundary layers, it was noted that the zero incidence flow is not self-similar at $(x/L) = 0.34$ but has become self-similar by $(x/L) = 0.46$. The equilibrium chemistry has a pronounced effect on the windward shock standoff distance, which is consistent with results for inviscid cone flow (Macrossan and Pullin 1994). Fig. IV.6 shows a comparison of Mach number contours for the same Reynolds number, where $(x/L) = 0.10$, for frozen and equilibrium flows.

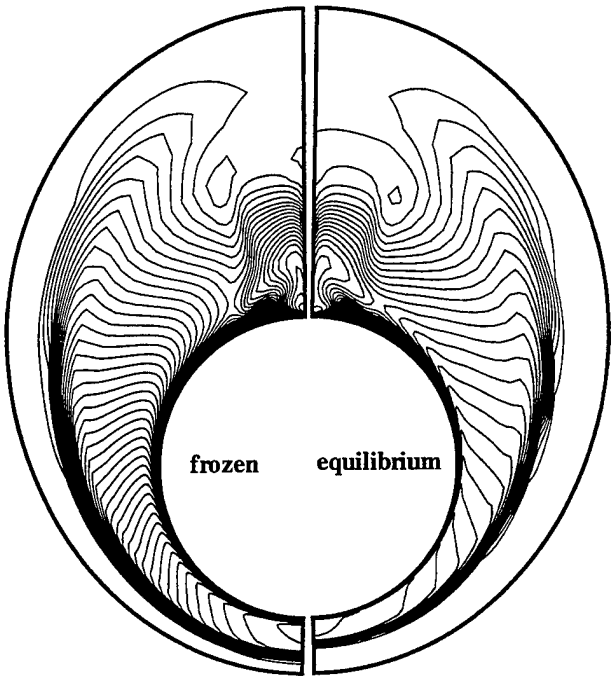

Figure IV.6. Mach number contours for frozen and equilibrium flow past a 15° isothermal cone (T_w=300 K) in N_2, 30° incidence, Re=39800, x/L=0.58. Conditions as in Table 1. Left; Frozen flow. Right; equilibrium flow.

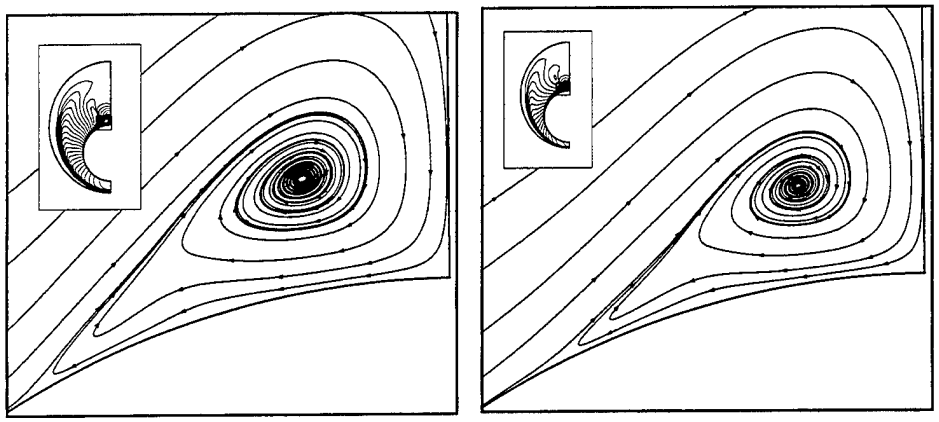

Figure IV.7. Leeward projected streamlines for a 15° isothermal cone (T_w=300 K) in N_2, 30° incidence, Re=22300, r/L=0.34. Left, frozen flow. Right, chemically equilibrium flow. Conditions as in Table 1. Inset shows computational domain.

Fig IV.7 shows closeup views of the leeward vortex for frozen and for equilibrium flow at the conditions of Table 1. It can also be seen that the shape and size of the vortices is slightly

different. This difference is also consistent with inviscid results although the separation mechanisms are somewhat different. In Fig. IV.8 we show plots of heat transfer and surface

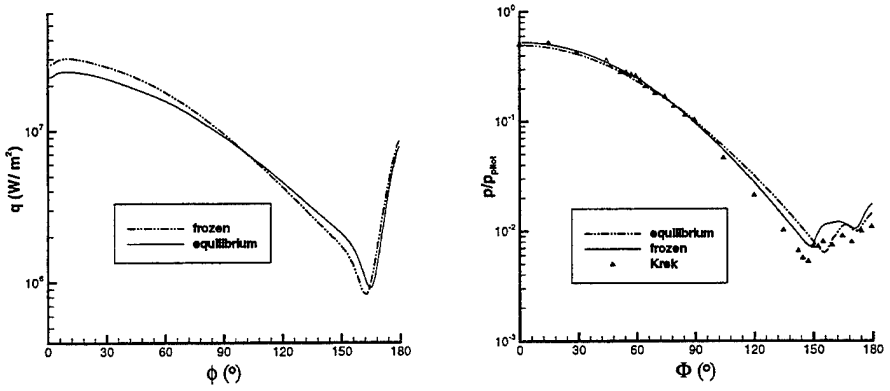

Figure IV.8. Flow past isothermal cone. Frozen and chemically equilibrium flow. Left; surface heat transfer. Right; Surface pressure compared with data of Krek (1992)

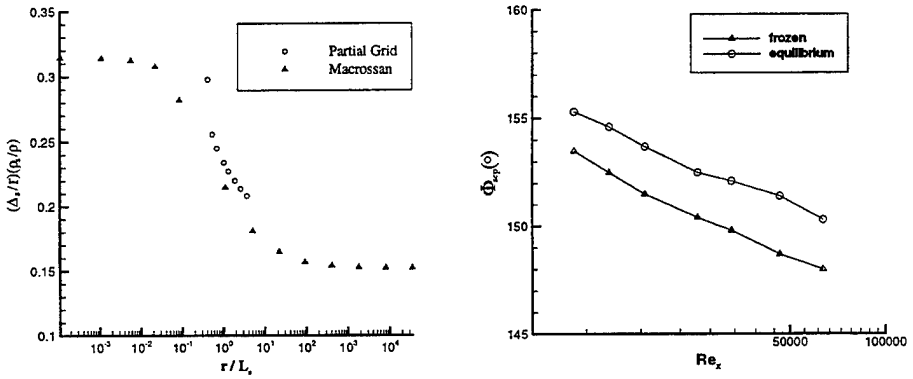

Figure IV.9. Flow past isothermal cone. Left; shock standoff distance Δ_s/r_c plotted against x/L_s, where r is the distance from the cone apex and r_c is the local cone radius. Right; Separation angle versus Reynolds number.

pressure at a station $x/L = 0.8$ The heat transfer over much of the windward cone surface is rather lower for flow with equilibrium than for chemically frozen flow. For both cases the heat transfer shows a very substantial recovery following a sharp minimum. This may be partially related to the effect of the leeward vortex in sweeping hot outer fluid towards the cone surface between the separatrix and the leeward plane of symmetry. There is good agreement with the Krek data for the pressure, when normalized against free-stream pitot pressure, over the windward cone surface. The surface pressure is insensitive to the effects of active chemistry on the windward side. In Fig. IV.9 (left side) the shock standoff distance is plotted versus x/L_s, where r is the local cone radius. Two sets of results are shown, the inviscid calculations of Macrossan and Pullin (1994) (triangles) and the present results

for chemically non-equilibrium viscous flow (open circles). The latter were obtained using a partial-grid calculation starting from a frozen stepback calculation at $x = 0.1\,L$. The comparison is satisfactory except for the smallest x/L for the viscous flow, which may have been affected by the upstream boundary condition. The transition from frozen flow at small x/L to equilibrium flow at large x/L is little affected by the presence of the very thin boundary layer. The trend is similar to that found for chemically active flow past cones and spheres (see Wen & Hornung 1995).

The position of the boundary-layer separation point at a given station along the cone was determined from the local minimum in the azimuthal heat transfer distribution. The separation angle Φ_{sep} is plotted versus Re_x in Fig. IV.9 (right side) for both frozen and chemically equilibrium flow. The effect of chemistry is to delay separation by about 2^o uniformly along the length of the cone. This delay is consistent with the slightly smaller leeward vortex produced by the chemically active flow, as shown in Fig IV.7.

IV.3.4 Conclusions

Both frozen and chemically active viscous hypersonic flows about cones at incidence were found to display a complex shock-vortex system in the region near the leeward plane of symmetry. The shock-standoff distance on the windward side was found to show similar features to those found for inviscid flow, with the standoff distance being substantially reduced by the action of dissociation chemistry downstream of the bow shock. The leeward shock-vortex system for viscous flow is somewhat different in structure than that found for inviscid flow, the former showing a large separated shear layer which modifies the structure of the leeward lambda-shock system. Active chemistry was found to increase the azimuthal position of the separation point and to slightly decrease the size of the leeward vortex compared to a nearly equivalent frozen flow. The heat transfer on the windward cone surface was reduced by a factor of about 1.5 due to active equilibrium chemistry, consistent with the lowered shock-layer temperature produced by dissociation chemistry. The heat transfer was found to exhibit a substantial recovery near the windward plane of symmetry for both chemically frozen and chemically active flows.

References

Lighthill, M.J., 1957, Dynamics of a dissociating gas. Part 1. Equilibrium flow, *J.Fluid Mech.*, **2** 1.

Freeman, 1958, N.C.Non-equilibrium flow of an ideal dissociating gas, *J.Fluid Mech.*, **4**, 407.

Osher, S., Solomon, F., 1982, Upwind Difference Schemes for Hyperbolic Systems of Conservation Laws, *Mathematics of Computation*, **38**, 339-374.

Pullin, D.I, 1980 Direct simulation methods for compressible inviscid ideal-gas flow, *J. Comp. Phys.*, **34**, 231.

Quirk, J.J. 1994, A contribution to the great Riemann solver debate, *Int.J. Num. Meth.*

Fluids, **18**, 555.

van Leer, B. 1974, Toward the ultimate conservative difference scheme II. Monotonicity and conservation combined in a second–order scheme. *J. Comput. Phys.*, **14**, 361–376.

Kewley, 1974, D.J.& Hornung, H.G., Free-piston shock-tube study of nitrogen dissociation, *Chem. Phys. Lett.*, **25**, 531.

Krek, R.M. 1992, Ph.D. thesis, University of Queensland, Australia.

Tracy, R.R., 1964, Hypersonic Flow Over a Yawed Circular Cone, Hypersonic Research Project Memorandum No. 69, Graduate Aeronautical Laboratories, California Institute of Technology, Pasadena, California

Wen, C.Y., Hornung, H.G. 1995, Nonequilibrium dissociating flow over spheres. *J.Fluid Mech.*, **299**, 389.

Publications Resulting from Research

Macrossan, M.N and Pullin, 1994, D.I., A computational investigation of inviscid, hypervelocity flow of a dissociating gas past a cone at incidence. *J.F.M.* **266** 69-92 .

Mallett, E.R. Pullin, D.I. and Macrossan, M.N., 1995, A numerical study of hypersonic leeward flow over a blunt nosed delta wing. *AIAA J.* **33**, 1626-1633, 1995.

Moschetta, J-M. & Pullin, D.I, 1996. Computation of hypersonic viscous flows: are robustness and accuracy compatible?, AIAA paper 96-2087. 1996a.

Moschetta, J-M. & Pullin, D.I, 1997. A robust low diffusive kinetic schme for thr Navier-Stokes/Euler Equations. Subjudice *J.Comp. Phys.* **133**, 193.

Shariff, S. 1998. Computation of hypervelocity viscous flows past cones at incidence with active dissociation/recombination chemistry. Phd Thesis, Caltech. In preparation.

Shariff, S. and Pullin, D.I, 1998. Numerical simulation of viscous reacting hypervelocity cone flows with the stepback method. AIAA paper 98-2360.

Personnel Associated with Research

D. Pullin, Professor of Aeronautics.

Dr R. Mallett, Postdoctoral Scholar.

Dr Jean-Marc Moshetta, Associate Professor of Aeronautics, SUP'AERO, Toulouse France. Visiting Associate Professor of Aeronautics at Caltech.

Shaun Shariff, Postgraduate student.

Interactions/Transitions

(a) Participations/presentations at meetings etc.

Moschetta, J-M. & Pullin, D.I, "Computation of hypersonic viscous flows: are robustness and accuracy compatible?" Presented at 27th AIAA Fluid Dynamics Conference, New Orleans, June 1996.

Shariff, S. and Pullin, D.I, 1998. Numerical simulation of viscous reacting hypervelocity cone flows with the stepback method. Presented at 29th AIAA Fluid Dynamics Conference, June 1998.

(b) Consultative and advisory functions etc.

None.

(c) Transitions

None.

New discoveries, inventions, patents

None.

Honors/Awards etc.

None.

Chapter V: DIAGNOSTICS

V.1 DIAGNOSTICS WITH LASER-INDUCED THERMAL ACOUSTICS, (LITA)

Accomplishments

During the course of this sub–project, the development of LITA into a sophisticated new laser diagnostics scheme proceeded via the following steps:

1. Development of theoretical basis of the technique, involving the derivation of the expressions that explicitly describe the LITA signal in terms of the optical properties and geometry of the laser beams and the physical and spectroscopic properties of the gas.
2. Experimental demonstration of the technique as a very accurate non–intrusive method for determining the sound speed of a gas at a point and as a less accurate, but unique, method for determining transport properties of a gas non–intrusively.
3. Demonstration of LITA in single–shot mode at temperatures up to 4000 K in the reflected–shock region of a shock tunnel, automation of the calibration, and analysis of the LITA signal.
4. Improvements in signal analysis software, extension of the analysis of LITA signals, and experiments to probe the parameters that dictate single-shot repeatability.

To illustrate the results of this work, a few examples are presented in the form of plots. The theory of the LITA derived in the early phase of the project gives the form of the signal explicitly in terms of the properties of the gas in the measuring volume interrogated. The dominant properties are sound speed and thermal diffusivity. A number of other variables influence the signal in minor ways. These variables also include such instrument functions as beam misalignment. To demonstrate the quality of the theory, Fig V.1 shows a comparison of theory and experiment for a LITA signal in carbon dioxide at room conditions.

Applying LITA to the measurement of the speed of sound in air results in the data presented in Fig V.2, taken with very weak NO_2 seeding. The real–gas effect of high pressure on the speed of sound can be seen to be very accurately obtained by LITA measurements. The scatter of the data at lower pressures is a result of the deterioration of the accuracy when the thermal grating has a wavelength comparable with the mean free path.

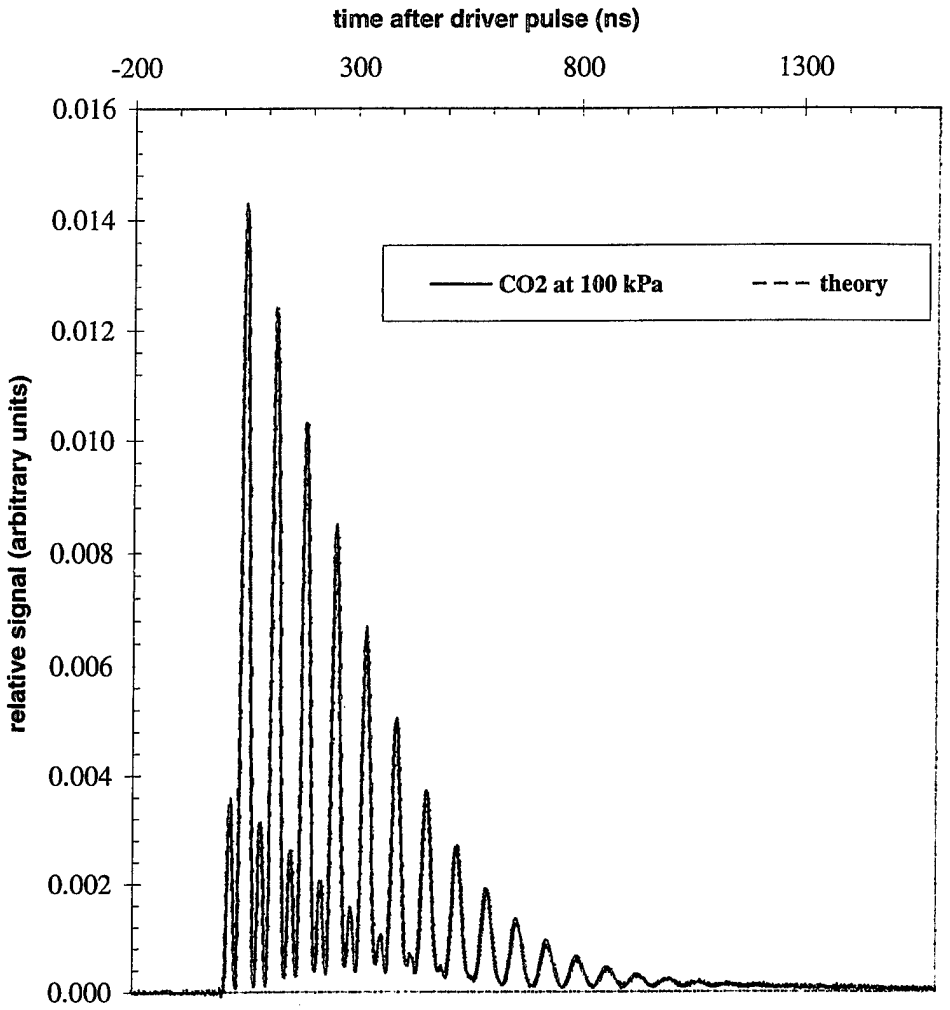

Figure V.1. Experimental and theoretical LITA signals from electrostriction and thermalization in unseeded carbon dioxide at room conditions. The secondary peaks in this signal arise from electrostriction.

The dependence of the LITA signal on signal–to–noise ratio was studied by deliberately degrading S/N through laser power reduction and other methods. Measurements were conducted for NO_2–seeded air and helium for pressures ranging from 10 kPa to 2 MPa. The following expression was used to calculate the signal-to-noise ratio with respect to the peak signal amplitude

$$S/N = \frac{\max_i y_i}{\sqrt{1/n \sum_{i=1}^{n} (x_i - y_i)^2}} \tag{1}$$

where the x_i are the discretized measured signal intensities, the y_i are the theoretical values at corresponding times, and n is the number of sampled points. An example of the results is shown for the case of thermal diffusivity measurements in Fig. V.3

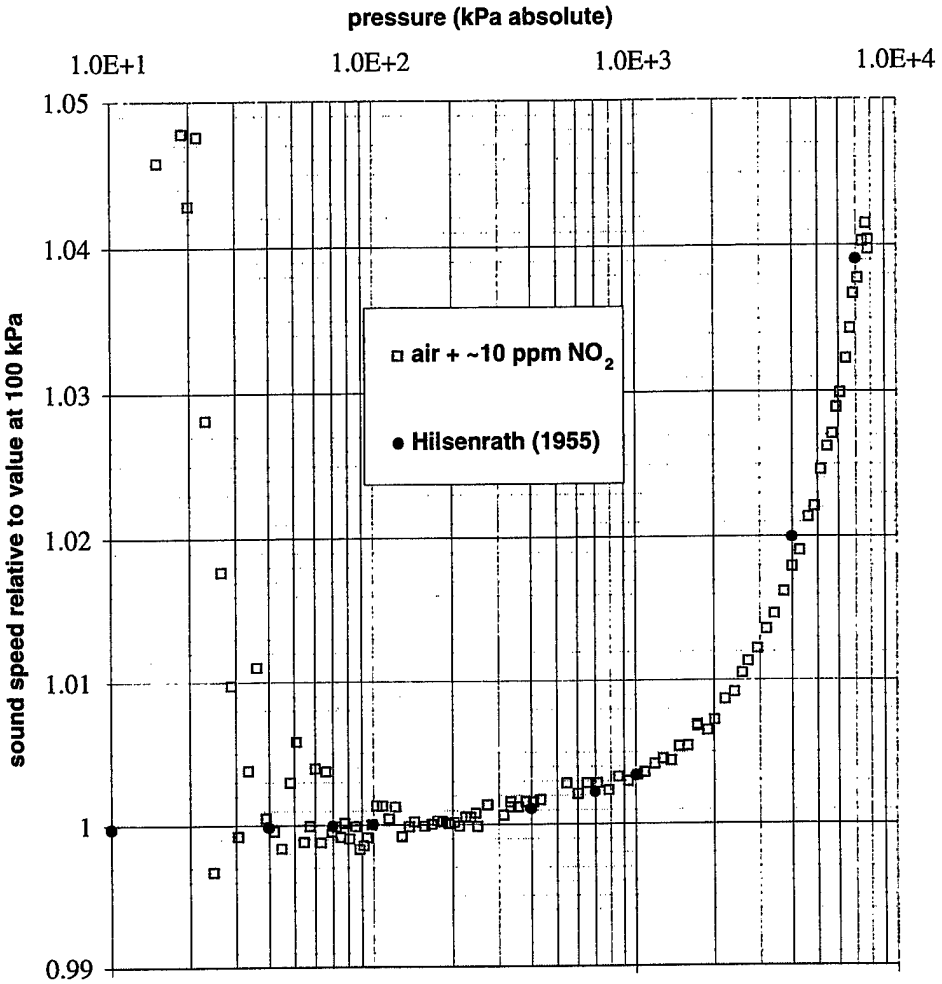

Figure V.2. Sound speed of air *vs.* pressure normalized to the value at atmospheric pressure and 300 K. The solid symbols are data from National Bureau of Standards measurements by Hilsenrath (1955). Note that one major division corresponds to 1%.

Reference

Hilsenrath, J., 1955, "Tables of thermal properties of gases", NBS Circular 564.

Personnel Supported

1. Hans G. Hornung, Kelly Johnson Professor of Aeronautics, GALCIT Director.
2. Eric B. Cummings, Graduate Research Assistant, Ph. D. 1995, Staff Scientist
3. Bonifacio Calayag, Graduate Research Assistant
4. Stefan Schlamp, Graduate Research Assistant
5. Bahram Valiferdowsi, Associate Engineer

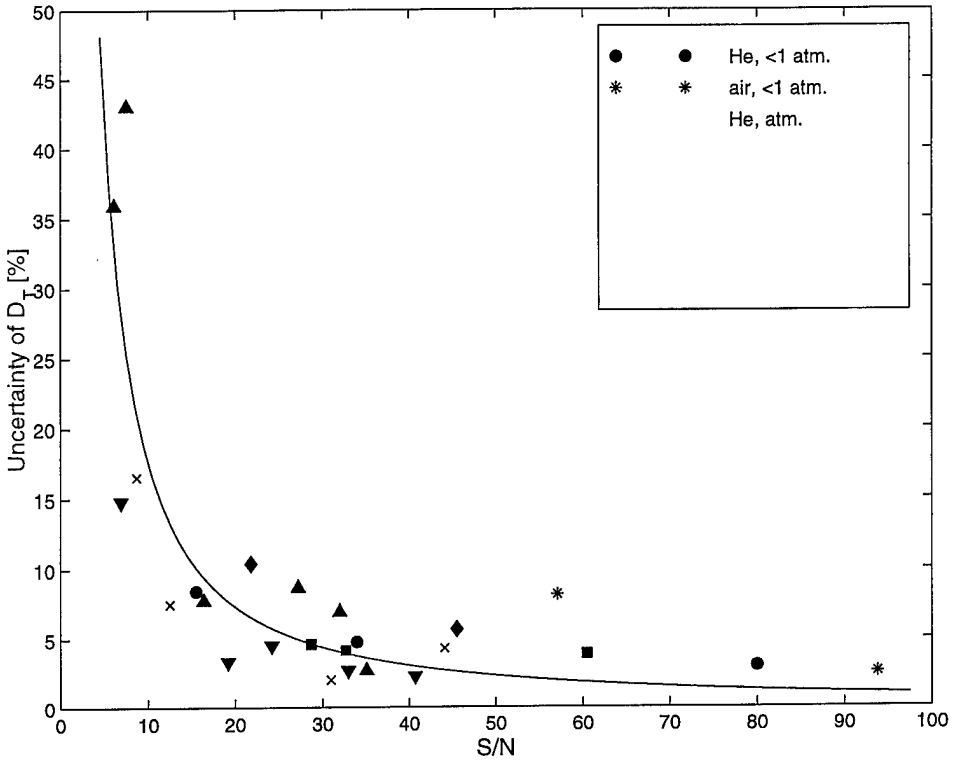

Figure V.3. Uncertainty of thermal diffusivity vs. S/N in percent of average value. Power law fit: $\sigma_D = 320 \cdot x^{-1.26}$.

Publications Resulting from the Research

Cummings, E. B. (1994a) "Laser-induced Thermal Acoustics (LITA): Simple, Accurate Single-shot Gas Measurements," 1994 Technical Digest Series, Vol 5, Optical Society of America, Washington, DC.

Cummings, E. B. (1994b) "Laser-induced Thermal Acoustics (LITA): Simple Accurate Gas Measurements," *Opt. Lett.***19**, pp 1361–1363.

Cummings, E. B., Leyva, I. A. and Hornung, H. G. (1995a) "An expression for laser-induced thermal acoustic signals from finite beams," *Appl. Opt.*, to be published in May 1995.

Cummings, E. B., (1995b) *Laser-Induced Thermal Acoustics*, Ph.D. Thesis, Calif. Inst. of Technology, Pasadena, CA.

Cummings, E. B., Hornung, H. G., Brown, M. S., and DeBarber, P. A. (1995c) "Measurement of Gas-Phase Sound Speed and Thermal Diffusivity Over a Broad Pressure Range Using LITA," *Opt. Lett.* **20**:1577–1579

Interactions, Transitions

The optical diagnostic research that this URI has supported has spun off a collaborative venture with an industrial partner to develop a commercial, turn-key LITA system. The collaboration between Caltech, Advanced Projects Research, Incorporated (APRI) of La Verne, CA, and LabSmith of Livermore, CA will produce a prototypical LITA system that demonstrates critical automatic data analysis and auto-alignment features. This project is being funded through a Phase I SBIR program at the Air Force Research Laboratory Propulsion Directorate. In Phase II of this project we will produce a fully computer–controlled, robust, LITA system featuring homodyne detection and heterodyne detection (for velocimetry).

The analysis software that was developed at Caltech under the URI is being extended and modified under this partnership to provide real-time LITA signal analysis at 10 Hz and higher frequencies. The software will interface with system-control software, which will use misalignment information extracted from the signals to control beam actuators to correct for static or slowly changing beam misalignments (such as those from thermal drift) and analytically account for dynamic or rapid beam misalignments (such as those caused by turbulence). Our understanding of beam misalignment effects and schemes for implementing the LITA system are direct results of the URI-sponsored research.

In addition:

1. Presentation of seminar at Princeton University (Cummings)
2. Presentation of nominated talk at session on Experimental Methods in Fluid Mechanics, International Congress of Theoretical and Applied Mechanics, Kyoto, August 25-31, 1996 (Hornung and Cummings)
3. Attendance at Workshop on Radiatively Driven Hypersonic Wind Tunnel Concept, Air Force Research Laboratory Air Vehicles Directorate, Dayton, April 25-26, 1996 (Hornung).
4. Attendance and presentation at Workshop on Plasma-Based Hypersonic Drag Reduction, Major Scott Schreck, Air Force Research Laboratory Air Vehicles Directorate, May 10, 1996 (Hornung).
5. Transfer of LITA technology to MetroLaser personnel (M. Brown) in preparation for their NASA funded research.

Honors/Awards

Milton and Francis Clauser Prize for Caltech Ph. D. Thesis: E. B. Cummings, 1995

Ballhaus Prize for GALCIT Ph. D. Thesis: E. B. Cummings, 1995, shared.